TOWARDS IMPROVED DEVICE DESIGN AND CLINICAL MANAGEMENT: THE THROMBOGENIC EFFECT OF THE FLUID DYNAMICS AND MATERIAL SURFACE RELATIONSHIP

A Dissertation
Presented to
The Academic Faculty

By

Susan M. Hastings

In Partial Fulfillment
of the Requirements for the Degree
Doctor of Philosophy in Bioengineering

Georgia Institute of Technology

May 2017

TOWARDS IMPROVED DEVICE DESIGN AND CLINICAL MANAGEMENT: THE THROMBOGENIC EFFECT OF THE FLUID DYNAMICS AND MATERIAL SURFACE RELATIONSHIP

Approved by:

Dr. David Ku, Advisor
School of Mechanical Engineering
Georgia Institute of Technology

Dr. Julia Babensee
Department of Biomedical Engineering
Georgia Institute of Technology

Dr. Wilbur Lam
Department of Biomedical Engineering
Georgia Institute of Technology

Dr. Lakshmi Sankar
School of Aerospace Engineering
Georgia Institute of Technology

Dr. Kevin Maher
School of Medicine
Emory University

Dr. Shriprasad Deshpande
School of Medicine
Emory University

Date Approved: April 5, 2017

The road to wisdom? – Well it's plain and simple to express:

Err and err and err again, but less and less and less.

Piet Hein

To my parents - they are my pillars, without whom I could not stand.

ACKNOWLEDGEMENTS

This document would simply not exist without the support, guidance, and direct help of many wonderful people, and I am deeply grateful to each and every one of them. I will do my best to put my gratitude into words and thank those at the top of the list.

First I would like to thank my advisor, Dr. David Ku. I joined Dr. Ku's lab as an undergraduate, and am so fortunate to grow under his tutelage. I am proud to say that he has shaped the way I think, and therefore who I am.

I am also grateful to my committee. I would like to thank my committee member, Dr. Kevin Maher, for being the first catalyst for the ECMO project, which launched the inspiration for my doctoral work. Thanks also to my committee members Dr. Shriprasad Deshpande, Dr. Julia Babensee, Dr. Wilbur Lam, and Dr. Laskshmi Sankar for their invaluable time, resources, and input.

I would next like to thank past and present members of the Ku Lab, for both tehcnical input and friendship (as well as sharing the special burden of early a.m. trips to the slaughterhouse). Thank you specifically to my original mentor Dr. Andrea Para, and I would also like to thank and acknowledge Dr. Marmar Mehrabadi, Dr. Lauren Casa, (soon to be Dr.) Joav Birjiniuk, Sumit Khetarpal, Michael Griffin, Hao Yue, and Matthieu Seimandi. I would also like to thank my team of undergraduate researchers, who helped both with design and running experiments: Timothy Arleo, Ryan Rudy, Joshua Qian, and Aaron Burtz. I would like to especially thank Ku Lab member Dongjune Kim for his contributions of CFD analysis.

I would also like to thank the staff of Holifield Farms for accommodating myself and other Ku Lab members and the inconvenience we caused during blood collection.

Funding for my research was provided through grants from the Center for Pediatric Innovation, and CHOA support for ECMO research. I additionally received support from the Georgia Tech President's Fellowship, the ARCS Scholars Award, and the ASAIO Graduate

Fellowship.

I would like to also express my deep and heartfelt gratitude to my parents, Dr. Mardi Hastings and Dr. Gordon Hastings. They have together encouraged me to pursue any and every dream that I could come up with. My mom is an absolute inspriation as a woman and as an engineer and I can only aspire to be like her. They have raised me in their image and I am proud to be their daughter. I love you both.

My love and thanks also goes to my fiance, Matthew Shea. He has known me only as a student and has seen me through the course of my PhD, and for some crazy reason still wants to stick around. I am looking forward to a lifetime of adventures with this amazing, endlessly supportive, fabulously tall, selflessly kind, and wonderfully fun future husband.

Finally, as an only child, my friends are my siblings. I could not have kept myself sane throughout the course of my graduate work without the amazing group of girls I am lucky enough to call best friends. I love you all.

TABLE OF CONTENTS

LIST OF TABLES

LIST OF FIGURES

SUMMARY

Medical devices are burdened with complications of thrombosis and hemorrhage. The combined interaction of material surface, local hemodynamics (in particular shear rate), and large-scale thrombosis is poorly understood.

First, basic science studies elucidated the relative importance of material surface and shear rate for large-scale bulk thrombus formation in an *in vitro* setup. We then used the results from these studies to develop a thrombogenicity ranking.

Next we assessed thromogenicity issues with current blood-contacting devices and worked to develop understanding of the contributing mechanisms. We then simulated the device thrombosis *in vitro* and validated our results against the clinical results.

Finally, we proposed two novel devices to correct current thrombogenicity issues, and tested our prototypes *in vitro*.

The results of these studies are summarized below:

· Development of a relative thrombogenicity comparison for current device materials

· Histological analysis of bulk thrombi revealing mixed platelet and fibrinous composition regardless of shear rate

· Analysis of clinical thrombosis in 1) ECMO circuits, 2) the Sorin Revolution centrifugal pump and 3) Berlin Heart EXCOR pediatric VAD on the basis of macroscopic thrombus formation

· CFD anaylsis of areas of thrombotic germination in ECMO circuits and the Sorin Revolution

· Development of a system for *in vitro* simulation of device thrombosis validated against clinical samples

· Proposal and prototyping of novel devices validated *in vitro*

The contributions from the results of this thesis are as follows:

- Demonstration of differences in bulk thrombosis formation of materials across shear regimes
- Recommendations for device design and clinical management from a thrombogenicity ranking
- Evidence of material surfaces overriding classical “red” and “white” clot mechanisms
- Identification of specific thrombogenic areas and elucidation of thrombotic behavior in ECMO circuits, the Sorin Revolution, and the Berlin Heart EXCOR
- Hypothesis and validation of thrombotic mechanisms in ECMO circuits and the Sorin Revolution
- Validated *in vitro* simulation of device thrombosis
- Device design and *in vitro* validation

CHAPTER 1
BACKGROUND AND MOTIVATION

Blood-contacting medical devices, such as stents, grafts, catheters, extracorporeal circuits, and ventricular assist devices (VADs), are used to treat a variety of cardiovascular and cardiopulmonary diseases. Complications resulting from thrombus formation in these devices are a frequent source of failure [1], and thrombosis and hemorrhage are the two dominant clinical issues for mechanical circulatory support patients [2]. The aforementioned complications not only impede the function of the device, but pose direct risk to the patient. To reduce the risk of occurrence of thrombosis, patients are subjected to anticoagulation regimens for the duration of the treatment, which can be long-term. Such treatments reduce the overall quality of life of these patients, and pose additional risks, such as hemorrhage. There is a gap in understanding the relationship of how the thrombotic outcome is related to the initial processes that occur when blood contacts material surfaces. This relationship is the central to the prevention of device thrombosis, and its quantification will benefit design, troubleshooting, and patient treatment.

The material surface field is vast and much work has been done to elucidate the blood-surface interactions and their effects for decades. Material pathways are complex and have lots of crosstalk, further increasing the difficulty of study.

When blood contacts a material surface, a series of complicated systems initiate that ultimately potentiate thrombosis (Figure 1). The enacted mechanisms include protein adsorption, platelet adhesion, platelet activation, coagulation activation, leukocyte activation, and complement activation. The immediate adsorption of blood proteins is the initial event in the material-thrombosis pathway [1, 3, 4]. Protein adsorption is initially controlled by diffusion, but is dominated by protein-surface affinity over time (the Vroman Effect) [5]. Surface adsorption subsequently triggers events such as fibrin polymerization and/or

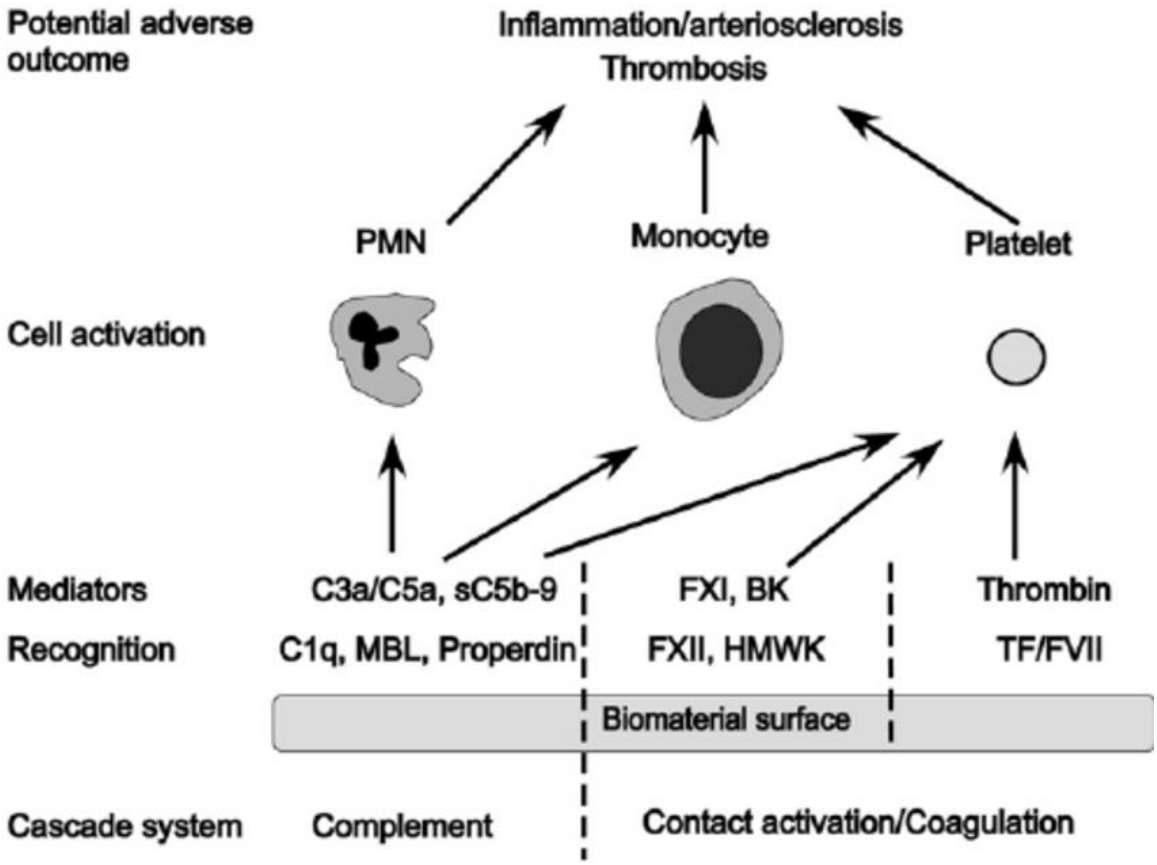

Figure 1.1: Initiation and interaction of response cascades by a biomaterial surface from Ekdahl et al. [8].

platelet activation and adhesion, which potentially lead to thrombus formation [6, 7].

The coagulation cascade occurs through a series of positive feedback zymogen-enzyme conversions that ultimately result in thrombin production and subsequent fibrin polymerization [9]. The cascade is separated into two branches (extrinsic and intrinsic) that are potentiated separately but come together in a common pathway that leads to thrombin. The extrinsic cascade is activated by vascular injury *in vivo*. The intrinsic cascade is activated by circulating high molecular weight kininogen and prekallikrein. The first step in intrinsic potentiation is the activation of FXII which is referred to as "autoactivation" [9]. The initiation of this cascade is also mediated by contact with artificial surfaces [10]. It is generally accepted that anionic surfaces are the strongest activators of the intrinsic cascade [9, 10]. A diagram of the cascade is shown in Figure 2 [9]. The intrinsic cascade is a part of the

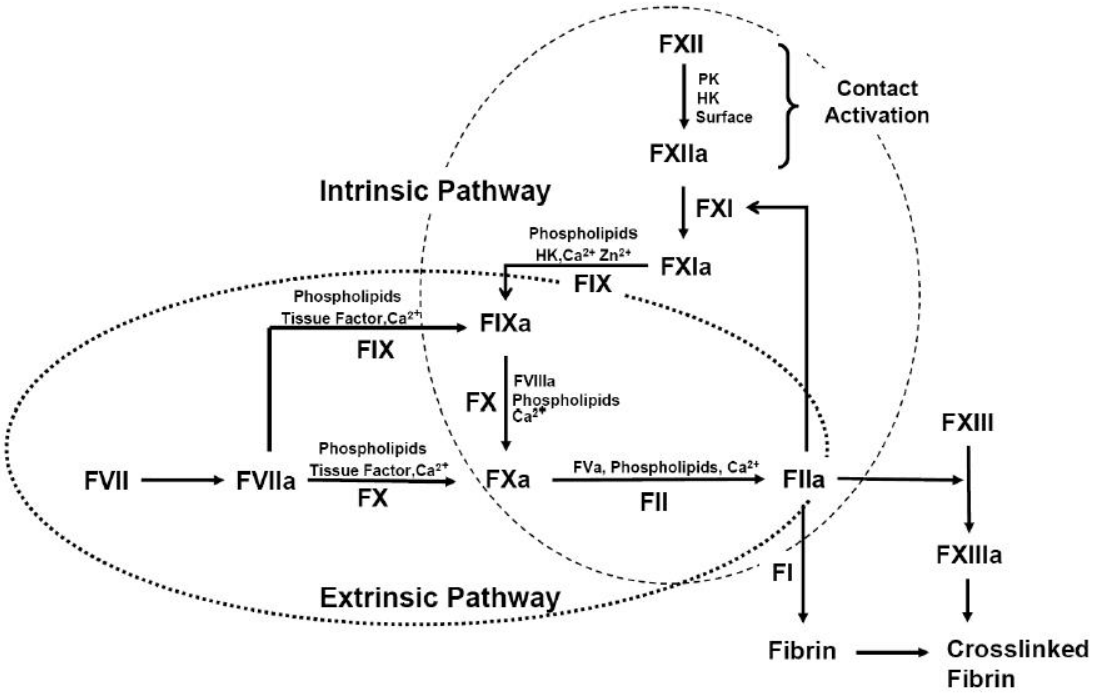

Figure 1.2: Coagulation cascade diagram from Vogler and Siedlecki's 2009 review [10].

immediate protein adsorption process and thus occurs during the first seconds to minutes of material surface contact with blood [10]. Tissue factor expression on monocytes requires synthesis and therefore up to an hour must elapse before this pathway would contribute to thrombin generation [10]. Thrombin generation by activated FXII is flow dependent and therefore timescales of the coagulation cascade will depend on the flow situation, which contributes to the complex problem of understanding mechanisms in the blood-contacting device setting [10, 11].

The materials most often used in devices are typically hydrophobic and have affinity with many proteins [12]. The most commonly adsorbed plasma proteins are albumin, fibrinogen, IgG, fibronectin, and vWF [12, 13, 14, 15]. VWF and fibrinogen appear to be the most important mediators of procoagulant platelet activity [16]. These proteins undergo conformational changes to expose hydrophobic domains and therefore become adsorbed to the hydrophobic surface [12, 17, 18, 19]. It is these conformational changes that expose receptor cites that cause subsequent immune reactions and initiate thrombosis [12, 20, 21].

The concentrations and conformations of adsorbed proteins are dependent on the material surface [12, 22, 23, 24].

The complement system, platelets, and leukocytes all play important roles in material compatibility and ultimately together lead to a surface-induced immune response [10]. The complement system is made up of numerous plasma proteins that cascade to produce complement produces that then bind foreign particles, surfaces, bacteria, and immune system complexes which allows uptake into inflammatory cells [10, 25]. Complement activation is initiated by either a classical or alterative pathway, and both join in the terminal pathway. Both begin with an enzyme that causes C3 convertase formation. C3 convertase then generates C5 convertase which allows the creation of the terminal complement complex (TOC). Complement activation and inhibition pathways are shown in Figure 3 [10]. Complement and intrinsic activation are intertwined [10, 26, 27]. Complement activation also induces cellular responses and activation of the immune system, and has been shown to do so specifically in the presence of artificial materials [28, 29]. Platelet activation at surfaces can also induce an immune response and has been shown to induce neutrophil activity in this setting [30]. Leukocytes can then make procoagulant contributions in conjunction with platelets, such as surface-mediated tissue factor production [31].

Many groups have made significant contributions to the field. Horbett has demonstrated various effects of pre-adsorbed proteins on platelet adhesion, activation, and procoagulant activity. In 1999 Grunkemeier et al. showed that different polymer materials had different propensities for fibrinogen and vWF adsorption, and that the vWF trends were similar to procoagulant activity trends [32]. A series of studies from this group then also showed that fibrinogen and vWF are the most important proteins to mediate platelet procoagulant activity [16, 33], and in addition that the adsorbed conformation of fibrinogen, not the concentration, is the determining factor for procoagulant activity [34]. Shen and Horbett also show that the immune response is dependent on surface chemistry even post protein adsorption [35, 36].

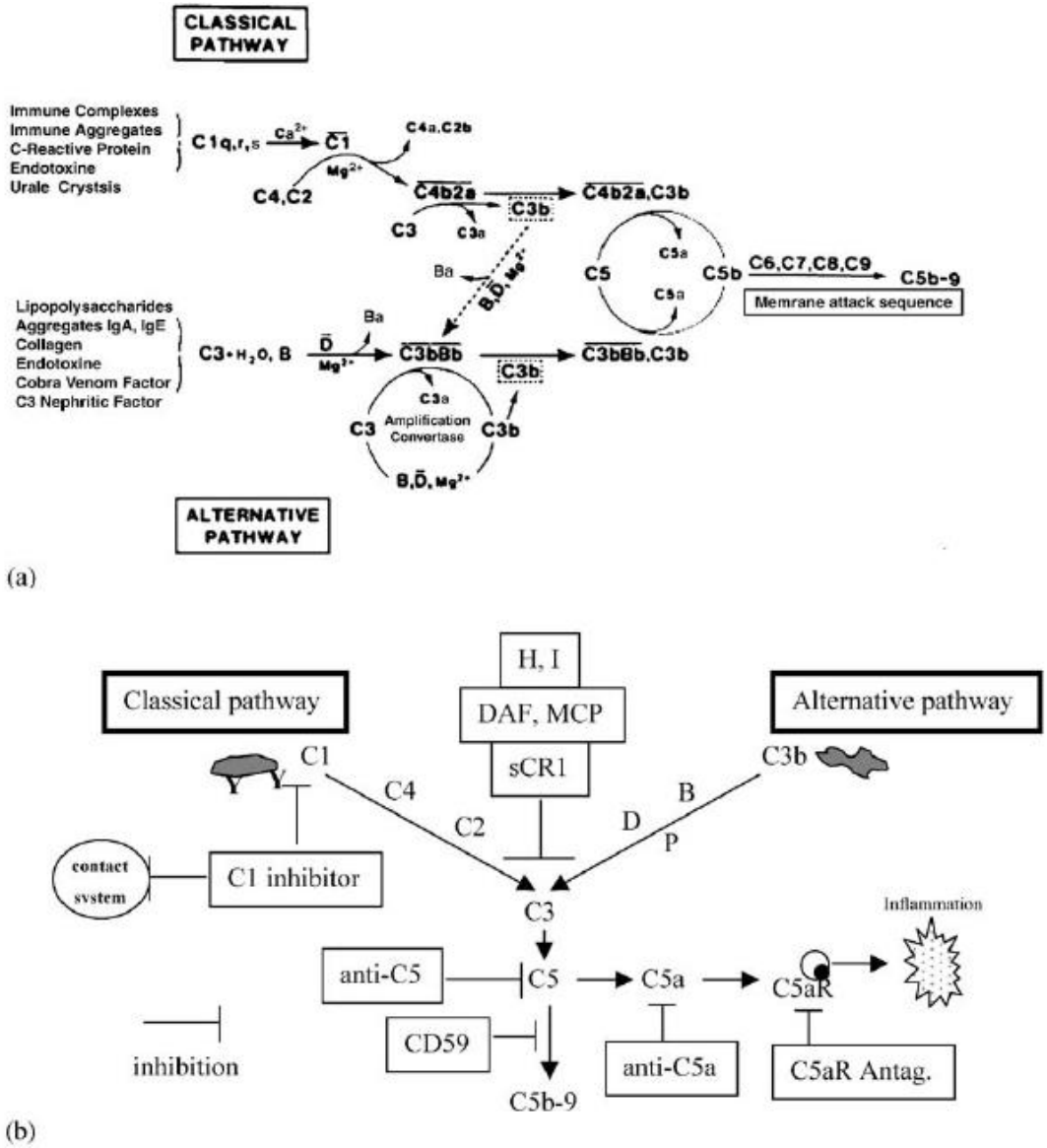

Figure 1.3: Complement activation (a) and inhibition (b) from Sefton and Gorbett [10].

Sefton has also made substantial contributions. In 2001 they showed that bulk behaviors for leukocyte activation differed from surface behaviors, and that bulk activation of leukocytes was independent of platelet activation [37]. That study also demonstrated initiation of the extrinsic pathway by tissue factor and resulting fibrin formation [37]. In a 2003 study they showed that platelet activation was necessary for material-induced tissue factor expression [31]. In their 2000 review they discuss the need to redefine thrombogenicity as clotting times and platelet deposition have proven insufficient to predict thrombogenicity [38]. In another 2005 review they highlight the importance of the consideration of the immune response when discussing thrombosis, as these two mechanisms are largely intertwined [10]. It is also important to note that many device materials cause significant compatibility issues [39].

Ekdahl has done lots of recent work regarding complement activation. In a 2010 polymer surface study, Engberg et al. found that uncharged hydrophobic surfaces are best to resist complement activation [40]. In 2014 Engberg et al. looked for complement markers and found C4/C4BP as a possible predictor of biocompatibility [29]. In 2016 Huang et al. found an inverse relationship between contact activation and complement activation after half an hour of incubation [41]. In a 2015 review, Ekdahl highlighted evidence for a platelet role in innate immunity via crosstalk with the complement cascade, but that under normal physiological conditions, platelets defend themselves from complement attack [42].

A few materials studies have tested effects of shear. Otto et al. showed that platelet adsorption on material surfaces is influenced both by pre-adsorbed proteins and flow, and that materials ranked differently for platelet adhesion under varied shear regimes [43]. Balasubramanian and Slack demonstrate varied platelet adhesion to fibrinogen-adsorbed surfaces by shear after 5 minutes of single-pass perfusion, as well as varied abilities for surfaces to retain fibrin under varied shear, and came to the conclusion that shear must be considered when discussing thrombogenicity [44]. Wagner's group found an inverse shear-platelet adhesion relationship on device-relevant surfaces after 5 minutes of perfusion [M29]. Flow

has otherwise been acknowledged as a parameter of importance yet is still rarely incorporated into material evaluation [38, 45].

There has so far been a failure of *in vitro* thrombogenicity results to predict *in vivo* and clinical outcomes [1, 10]. For example, while studies on poly-(ethylene oxide) (PEO) modified surfaces demonstrated protein and cell resistance*in vitro*, the *in vivo* results are contradictory [1, 10]. Another study on albumin coatings showed reduced platelet and leukocyte adhesion *in vitro*, but the coating failed to ameliorate outcomes*in vivo* [1, 46, 47]. Heparin coatings have also been unable to achieve clinical improvements [10]. And again, even though reduced platelet adhesion was demonstrated with carbon coatings *in vitro*, carbon coatings texitin vivo did not improve long-term performance [1, 48, 49, 50]. Surfaces incorporating phosphatidylcholine were also thought to be promising after reduced adhesion of platelets both *in vitro* and *in vivo* is some animal models, the results in humans did not demonstrate any improvement [1, 51, 52]. Design of these devices relied primarily on adsorption studies without blood flow, which so far has proven insufficient to directly predict *in vivo* behavior.

The thrombotic behavior of blood depends on the shear rate regime [53, 54, 55]. Gross thrombus can be millimeters in thickness and the growing surface is expected to be far away from the material surface and therefore largely independent of surface interactions and processes. Thus, the initial adhesion mechanisms are likely to be quite different from the growth of gross thrombus. Under low shear regimes, red, fibrin-rich clot is potentiated with a distinct absence of platelets. Under high shear regimes, white, platelet-rich thrombosis occurs [53, 55]. Platelet adhesion is preferential to fibrinogen at low shear, but requires von Willebrand factor (vWF) at high shear depending on the shear rate [54, 56]. vWF undergoes shear-induced stretching at critical shear rates that have been reported as $\geq 3000\ s^{-1}$ and $\geq 5000 s^{-1}$, which exposes many additional platelet binding sites required for high shear capture of unactivated circulating platelets [57, 58, 59]. Platelet thrombosis studies, as well as coagulation studies, typically adsorb the surface with a protein (e.g. fibrinogen

or collagen) prior to blood exposure in order to provide an active surface for thrombus formation [60, 61, 53, 55] skipping the step of adsorption, and eliminating material surface effects as a parameter for modulation of thrombosis.

As an alternative to the aforementioned thrombosis studies, some groups have used recirculating loops to study devices directly in a true-to-life model without pre-activation of the surface. Stents are a common choice due to the natural vessel analog of the flexible tubing used to construct such loops. However, exposure times are typically $\leq$ 10 mins and endpoints are therefore only initial adhesion [62, 63]. Krajewski et al. investigated the thrombogenicity of neurovascular stents and used a perfusion time of 60 mins with endpoints of endothelialization, and platelet activation, adhesion, and consumption [64]. Grove et al. studied cannula thrombogenicity in an *in vitro* ovine loop with a perfusion time of approximately 4 hrs, and were able to demonstrate some differences in macroscopic thrombus formation between positive and negative controls [65].

Despite much study of the biocompatibility of artifical materials, the field is still at a loss to understand, predict, and therefore prevent device thrombosis. There is a need to innovate thrombogenicity studies. Device thrombosis *in vivo* can occur in days, weeks, months, or even years. Catastrophic device thrombosis is macroscale and likely occlusive. It is unclear whether the material-dependent blood interactions or the shear regime determine the final gross thrombotic outcome. If this relationship can be determined reproducibly, then device design and material selection may eliminate clots on the medical device, ultimately improving patient treatment.

In an effort to study thrombogenicity in a clinically relevant way, we therefore propose the need for longer timescales ($\geq$ 24 hours), the inclusion of flow and surface, adsorption and thrombus formation from whole blood, and macroscale endpoints. It is also of utmost importance to learn from clinical thrombosis examples and to use clinical information to inform basic science studies.

We will therefore attack this problem with a combination of the aforementioned con-

siderations.

First, basic science studies will attempt to measure the relative importance of material surface and shear rate for large-scale bulk thrombus formation in an *in vitro* setup. We will then use the results from these studies to compare and contrast the thrombogenic performance of materials in our setup.

Next we will assess thromogenicity issues with current blood-contacting devices and work to develop understanding of the contributing mechanisms. We will then simulate the device thrombosis *in vitro* and validate our results against the clinical results.

Finally, we will propose two novel devices to correct current thrombogenicity issues, and test our prototypes *in vitro*.

CHAPTER 2

LONG TERM PERFUSION OF ARTIFICIAL SURFACES AT VARIOUS SHEAR RATES TO ELUCIDATE THE SURFACE-SHEAR RELATIONSHIP

2.1 Introduction

Thrombotic complications in blood-contacting medical devices are a frequent source of failure. Confusion reigns as to the cause, mechanism, and treatment of this device related thrombosis. Predicting thrombogenicity based on protein surface adsorption has not been successful, despite being the most commonly accepted method to assess thrombosis potential for materials. We hypothesize that there is sequential requirement of a) absorption of blood proteins; then b) extrema of blood shear rate, and further that thrombotic outcomes can we predicted based on material surface and shear rate.

To investigate these hypotheses, we set out to develop an *in vitro* study with the goal of ultimately addressing two major needs for study and understanding of device thrombogenicity: (1) the elucidation of the material-flow relationship and (2) the incorporation of both adsorption and thrombus formation. To accomplish this challenge we designed long-term ($>$ 24 hours) recirculating blood loops and created flow chambers to modulate both the shear rate and material surface. The chambers created three distinct shear rate environments: low shear (LS) ($<$ 100 s^{-1}), physiologic shear (PS) (500 s^{-1}), and high shear (HS) (5000 s^{-1}). The chambers also allowed for insertion of a surface of interest. The materials included in the present study are summarized in Table 1.

Table 2.1: Biomaterials in blood-contacting medical devices.

Material	Examples of Clinical Use
Acrylic	Extracorporeal Membrane Oxygenation (ECMO) connectors
PVC	Flexible tubing in ECMO and pediatric ventricular assist device (VAD) circuits
Stainless Steel	Centrifugal pumps, stents
Silicone	Pacemaker leads, peristaltic tubing, catheters
Dacron	Vascular grafts
PTFE	Vascular grafts

2.2 Methods

2.2.1 Chamber Design and Fabrication

In order to control for shear rate and material surface in the loop, the modulation of the shear rate resulted only from the change in geometry of the chambers. The tubing was setup in the same configuration and measurement each time so that the surface exposure in each experiment was constant. The flow rate was set to 1.5 lpm so that the shear rate in the loop outside of the chamber was constant and physiologic across experimental runs The chambers are an assembly of three parts to facilitate insertion and integration of various material surfaces (Fig 2.1).

The chambers have a top piece and bottom piece encapsulating the flow field, as well as a third material insert piece. The bottom flow surface has a square hole, and the third piece fits into this opening. The pieces are 3D printed acrylic, which was treated post-printing to achieve medical-grade standing. The material insert is 1 cm square, and the chamber is 3 cm wide total at the point of interest. The tubing to supply the circuit is 1/4" in (0.635 cm) diameter, and the chamber allows for a gradual size change to and from the 3 cm width over 4 cm, and is 10 cm in total length. For the acrylic and stainless steel studies, bottom pieces were printed and machined, respectively, to fit into the opening. PTFE and Dacron fabrics were secured around an acrylic insert. Likewise, a PVC film was secured around an

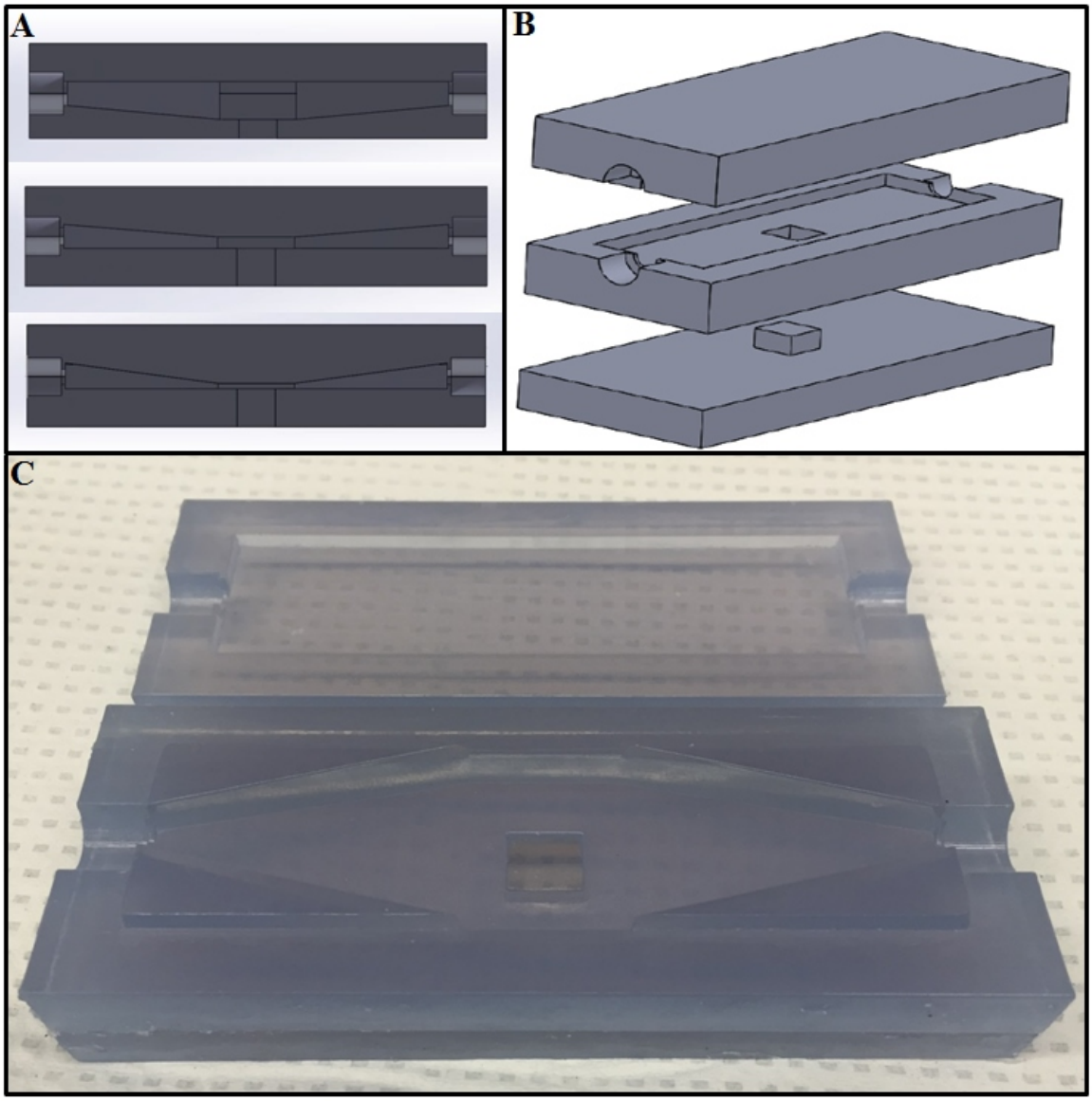

Figure 2.1: Chamber design. A: Cross sectional views of low shear (top), physiological shear (middle) and high shear (bottom) chambers. B: Chamber assembly. C: Printed chamber.

acrylic insert. Silicone was cured directly into the insert.

Vaccuum grease was used to ensure sealing between chamber layers but care was taken so that no grease contacted flowing blood. Clear silicone caulk was used to seal the chambers from the outside, and again care was taken to ensure no caulk-blood contact.

The chambers were perfused via roller pump (COBE Century) and the flow rate was set at 1.5 L/min. The heights of the chambers were (X, Y, Z) to achieve shear rates of 50 s^{-1}, 500 s^{-1}, and 5000 s^{-1} based on the shear rate equation for flow between two infinite parallel stationary plates:

$$\dot{\gamma} = \frac{6\dot{Q}}{wh^2}$$

Where $\dot{\gamma}$ is the shear rate, $\dot{Q}$ is the flow rate, and w and h are the width and height of the channel, respectively. This equation assumes 1-dimensional laminar flow. Under this assumption, the shear rate equation is accurate for 95% of the channel for an aspect ratio (w:h) of 5:1 [66].

2.2.2 Chamber CFD

CFD was done in the chambers to evaluate the flow field. The simulation was Newtonian and steady state and viscosity was set to 4 cP. Input fow was 1.5 lpm and the outflow boundary condidtion was a pressure outlet. CFD was performed in ANSYS with a mesh size of 254234-268099 cells and convergence criteria of 1e-4.

2.2.3 96-Hour Perfusion

The experiment was run for a total of 96 hours, which consists of two 48 hour sections. Whole porcine blood was collected at a local abattoir into light heparinization (7 U/mL). Upon arrival at the laboratory, the blood was dosed with 2.2 mM glucose (Sigma), 2 mM L-glutamine (Sigma), and 10 mL/L antibiotic antimycotic solution (Gibco), and the

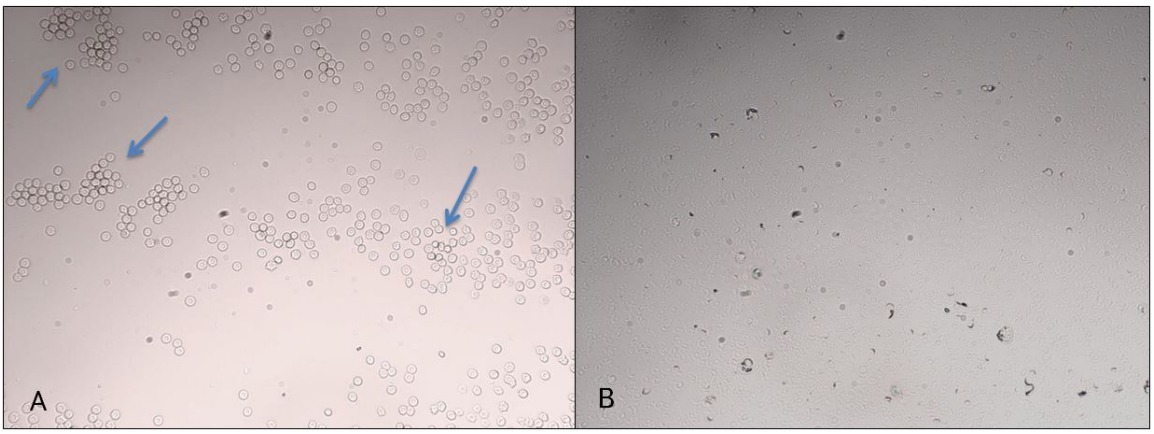

Figure 2.2: Blood smears. A: A perfused loop with no chamber treated with glucose, L-glutamine, antibiotic/antimycotic, and temperature has presence of RBCs after 48 hours of perfusion. B: The untreated perfused counterpart has no cell presence after 48 hours.

loops were filled. The glucose, glutamine, and antibiotic/antimycotic cocktail has been previously used to maintain survival of arteries in a flow loop [67]. Portions of circuit tubing were submerged in a water bath at 37 °C to maintain body temperature of the blood. The blood was dosed with heparin at 12 hour intervals post collection.To establish these methods, comparison circuits with and without temperature and treatment with glucose, glutamine, and the antibiotic/antimycotic solution were run on simple loops. The inclusion of all treatments was determined to be the best for RBC maintenance (Fig 2.2).

2.2.4 Blood Assays

Assays were performed throughout the experiment to ensure the health of the blood as a baseline at the start of the experiment and to compare changes across materials.

Hemoglobin

The hemoglobin (Hgb) assay was performed daily using a kit (Sigma). Three replicates per sample were averaged for each concentration calculation.

Platelet Assays

Light transmission aggregometry (LTA) was used to establish functionality of the platelets upon arrival to the laboratory. Platelet rich plasma (PRP) was dosed with agonists in suspension and the absorbance was recorded for 10 minutes. The agonists used were ADP (2 uM), adrenaline (2 uM), collagen (3 ug/mL), and ristocetin (1.5 mg/mL).

Platelet counts were performed initially and then subsequently every 24 hours of loop perfusion. Whole blood was incubated in 5% ammonium oxalate (1:20 dilution) for 5 minutes to lyse RBCs. The solution was loaded into a disposable hemacytometer(INCYTO C-Chip, Neubauer improved) which was then manually counted.

Coagulation Assays

The activated clotting time (ACTs) and activated partial thromboplastin time (APTT) were both performed initially and then subsequently every 24 hours of loop perfusion. The ACT was done manually with 6 mg kaolin per mL blood in a 5 mL centrifuge tube and a water bath. The APTT was also performed manually using a kit (Fisher Scientific).

2.2.5 Histology

Post perfusion, the loops were disassembled and the chambers were photographed with any adherent thrombus undisturbed. Any thrombus of interest was preserved in 10% formalin. Samples were embedded, sectioned, and stained with Carstairs' stain for fibrin and platelets and Hemotoxylin and Eosin (H&E).

2.2.6 Endpoints

Circuit occlusion was detected by visual inspection of the chamber and the loop. If a thrombus was observed covering the width of the chamber the circuit was determined occluded. If a circuit occluded prior to 96 hours, the occlusion time (OT) was recorded, and the circuit was dismantled and samples recorded and preserved as described above.

Photographs of circuit chamber thrombus were analyzed in GIMP 2. Thrombus was selected for by pixel differentiation by color and area and a thrombus surface area was calculated using a given reference area.

2.2.7 Model Development

The materials were sorted sorted by surface area for both low shear and physiological shear cases. For the high shear case, materials were sorted by occlusion time first and surface area second. Thrombogenicity rankings were therefore unique to shear regimes. A total thrombogenicity ranking was calculated by summing the ranking across shear regimes. Surface areas and occlusion times were tested for stasticially significant differences across materials using a Student's t-Test (α=0.05).

2.3 Results

2.3.1 CFD

Skewing was observed in the flow field in the low and physiological chambers (Fig 2.3). The high shear chamber did not exhibit any skewing (Fig 2.3). In the low and physiological cases, the material insert was subjected to a shear minimum in the field. The values of the minimum shear rates are shown in Figure 2.3.

2.3.2 Assays

Hgb concentrations of whole blood were 23650 +/- 14517 mg/dL. Hgb concentrations throughout perfusion were not significantly different across materials nor across shear regimes.

ACTs and APTTs rarely clotted within 10 minutes. There was no significant difference across materials nor across shear regimes.

Platelet counts were 140312 +/- 68953 plts/uL. Platelet counts were not significantly different across materials nor across shear regimes.

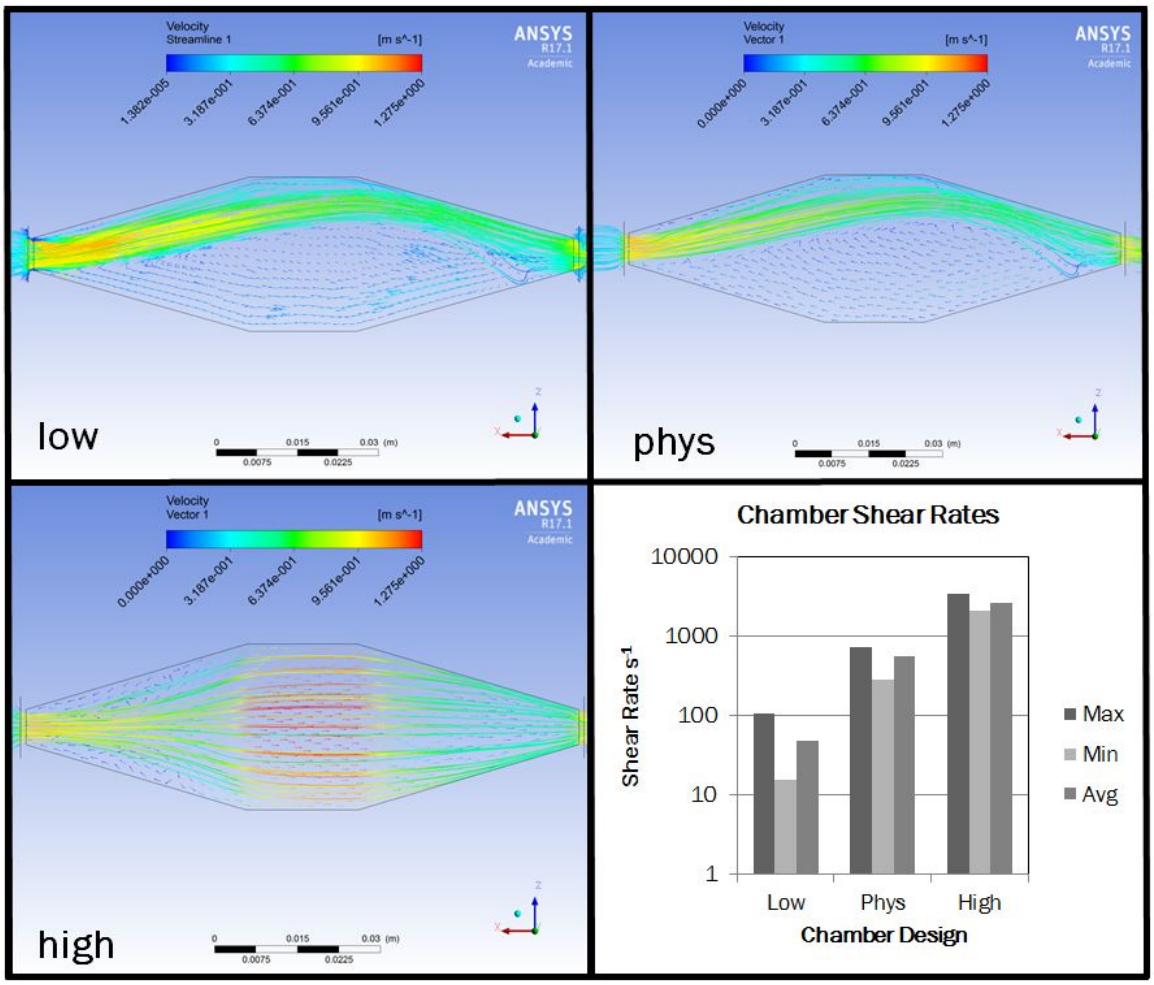

Figure 2.3: Chamber CFD. Top left: low shear chamber. Top right: physiological shear chamber. Bottom left: high shear chamber. Bottom right: Min, max, and average shear rate values for the chambers.

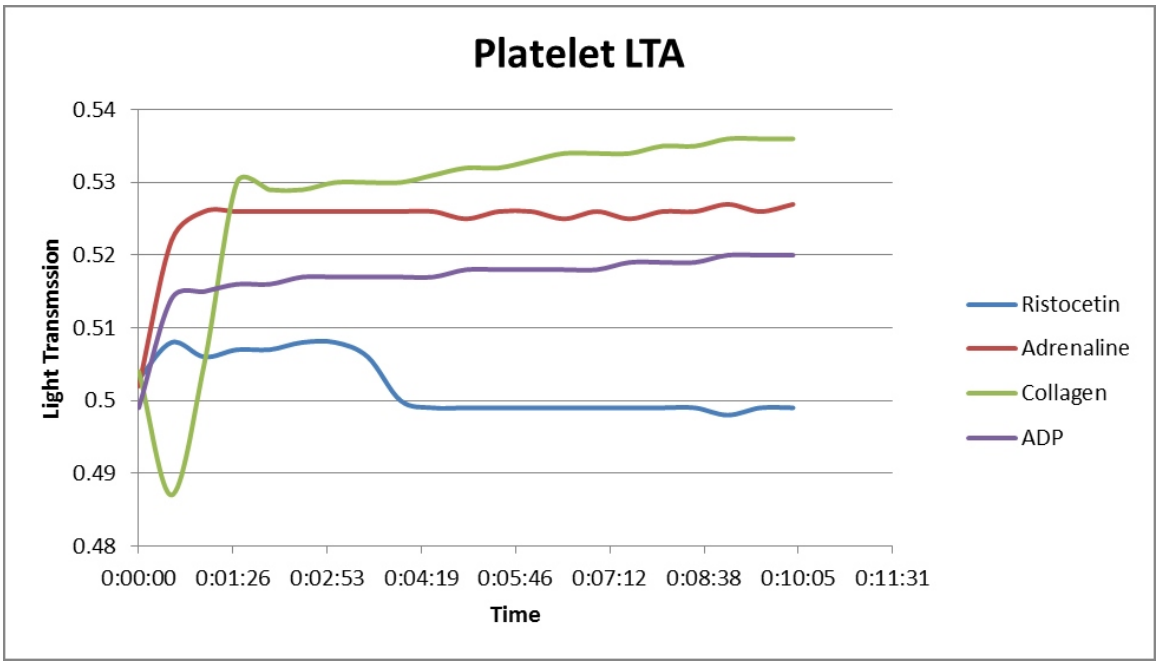

Figure 2.4: Platelet light transmission aggregometry (LTA). LTA was performed with four agonists (ADP (2 uM), adrenaline (2 uM), collagen (3 ug/mL), and ristocetin (1.5 mg/mL)) and absorbance readings were caputred over 10 minutes.

LTA confirmed platelet activity. An example is shown in Fig 2.4.

2.3.3 Thrombogenicity Assessment and Ranking Model

When the circuits were drained and refilled with fresh blood on Wednesday, the chambers were clean in every case. It was only after the second half of the experiment began that thrombus formed. A sample of chamber results for acrylic and silicone chambers are shown in Fig 2.5.

Thrombogenicity results are shown by shear reate in Fig 2.6. The resulting rankings are shown in Table 2.2.

2.3.4 Histologogical Analysis

Across all shear rates and materials, the Carstairs' stain revealed a mixed presence of platelets, fibrin, and red blood cells (Fig 2.7). Materials differed in morphology and relative presence of platelets, fibrin, and red blood cells (Fig 2.7). H&E revealed the presence of

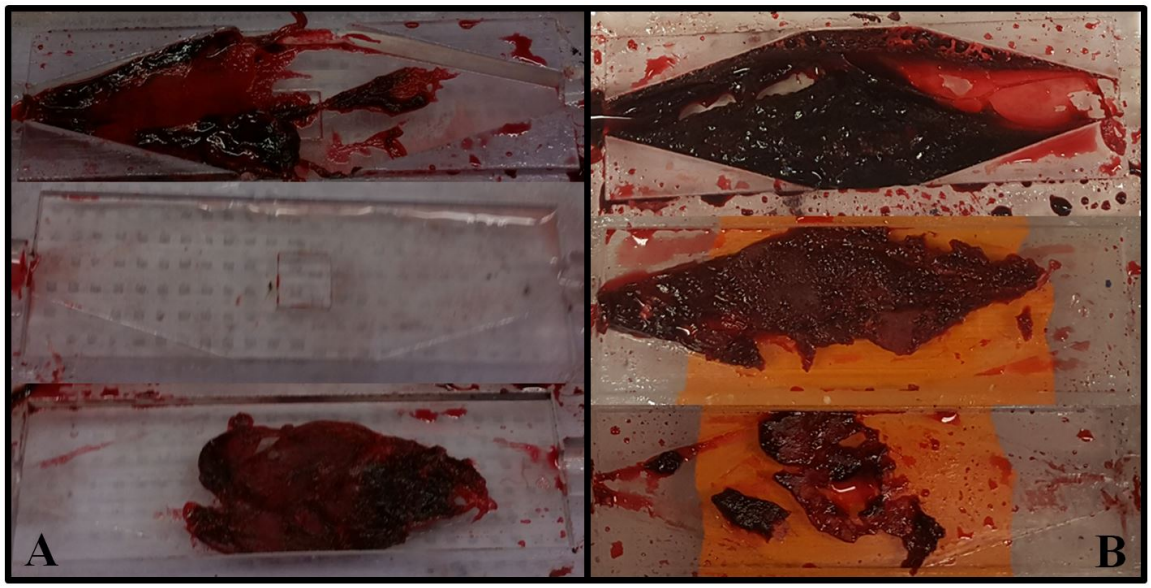

Figure 2.5: Examples of chamber thrombus. A: Acrylic chambers after 96 hours of perfusion under low shear (top), physiological shear (middle), and high shear (bottom). B: Silicone chambers after 96 hours of perfusion under low shear (top), physiological shear (middle), and high shear (bottom).

Table 2.2: Thrombogenicity ranking by shear rate.

	Low Shear	Physiologic Shear	High Shear
1 (Best)	PTFE	PVC	Acrylic
2	Stainless	Acrylic	Silicone
3	Acrylic	Stainless	PVC
4	Dacron	Dacron	Dacron
5	PVC	PTFE	PTFE
6 (Worst)	Silicone	Silicone	Stainless Steel

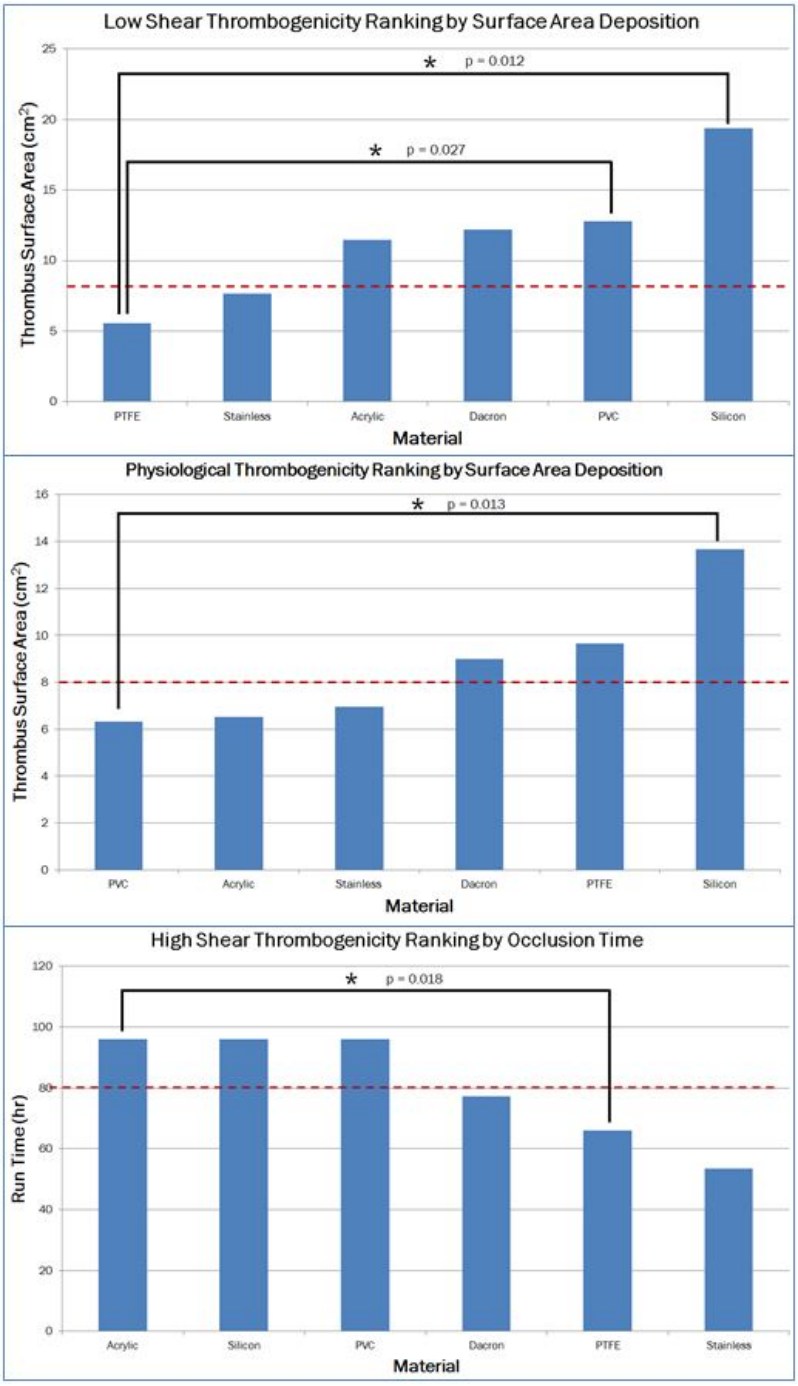

Figure 2.6: Thrombogenicity results by surface area (low and physiological shear) and occlusion time (high shear). Best performers are on the right, worst performers are on the left. Stars indicate significant differences from the best performing material. Bars and asterisks indicate significance and p-values are displayed for each case. Red dashed lines indicate thresholds assigned for discussion of "acceptable" thrombogenicity level.

cells in some thrombus samples due to hematoxylin staining of nuclei (Fig 2.7). Across shear rates, platelts were always present, yet shear appeared to modulated morphology (Fig 2.8). H&E and Carstairs' were applied to sections from the same sample. In some cases, orientation of cross-sections was preserved (Fig 2.9).

2.4 Discussion

Using a 96-hr, two-stage, perfusion setup, and endpoints of bulk thrombus formation and occlusion time, we have determined a relative thrombogenicity comparison for five materials currently used in blood-contacting medical devices.

The material ranking differed under varying shear regimes. For example, PTFE was the least thrombogenic under low shear perfusion, but second to worst under physiological and high shear perfusion. Conversely, silicone was the worst performer under low and physiological perfusion, but second best under high shear perfusion. Material surface therefore dictates thrombogenicity in a flow-dependent manner, and thrombogenicity rankings thus necessitate the inclusion of flow considerations.

These rankings lend themselves to basic recommendations for device design, that still must be considered in context of this system. We set thresholds of 8 cm^2 and 80 hours of perfusion time to facilitate discussion and consideration of low and physiological and high shear thrombogenicity (respecitvely) acceptance levels. When considering a low shear flow environment for a novel device design, these results suggest PTFE and stainless steel as a low thrombogenic choice. This is supported by clinical success of large-diameter synthetic PTFE grafts. Stainless steel would be another good option. For physiological shear applications, Acrylic, PVC, and stainless steel are choices with low thrombogenicity. This is also supported by ECMO circuits lacking thrombus in the bulk of the tubing and connector lumens, as we will present discuss in further detail in the next chapter. For low and physiological shear, it is surprising that stainless steel performed well, as this contrasts with the clinical notions of metals having high thrombogenicity. However, stainless steel is

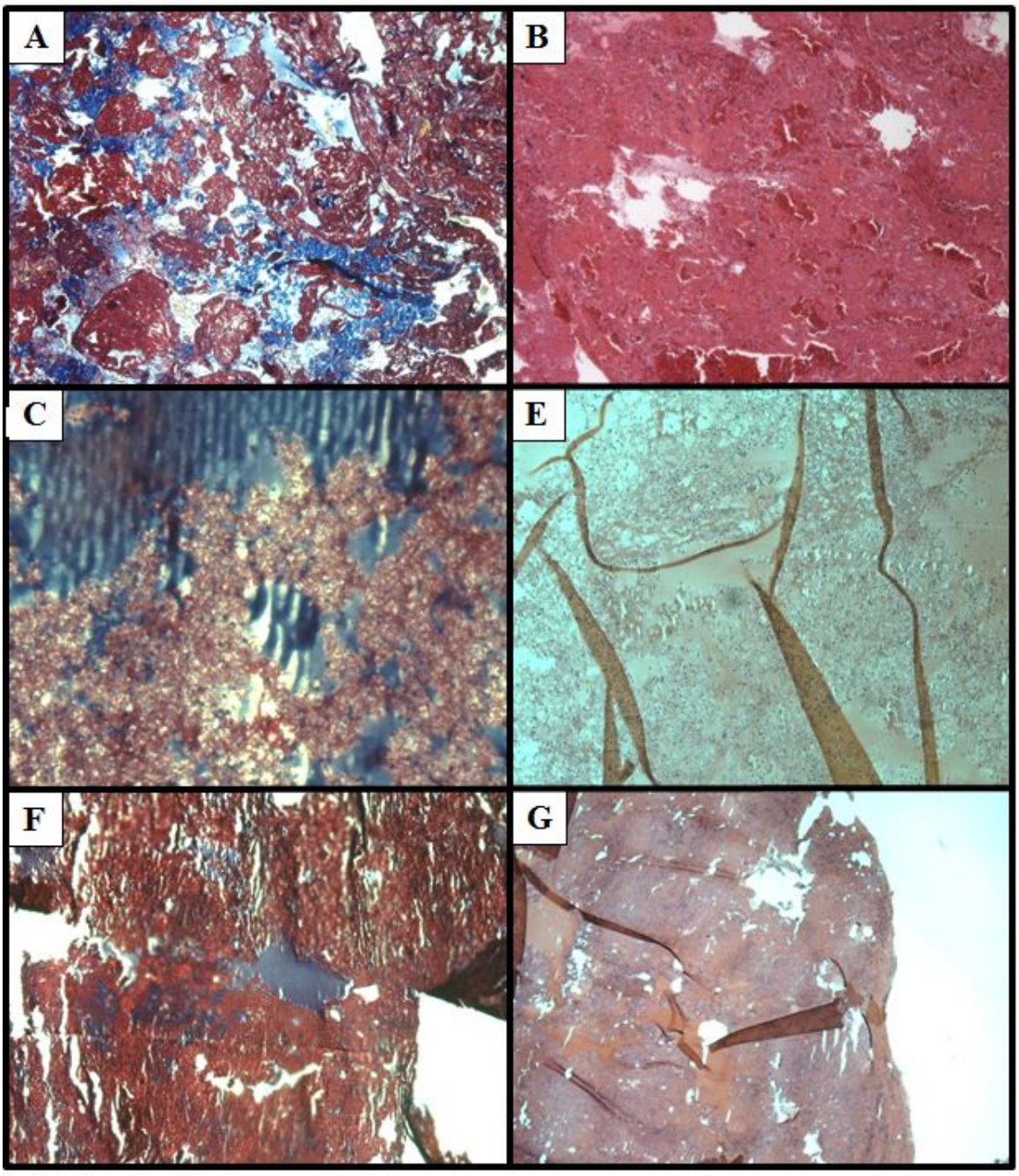

Figure 2.7: Examples of stained sections from thrombus samples (10x). A: Carstairs' stain of a low shear PVC thrombus exhbiting mixed platelet-rich and fibrinous sections. B: H&E stain of the same low shear PVC thrombus. The purple dots are cell nuclei. C: Carstairs' stain of a low shear stainless steel thrombus exhibiting mixed platelet-rich and fibrinous sections. D: H&E stain of the same low shear stainless steel thrombus. The dots are cell nuclei. E: Carstairs' stain of a high shear acrylic thrombus sample. This thrombus is of mixed platelet-rich and fibinrous, RBC-rich sections. F: H&E stain of the same high shear acrylic thrombus sample. Small purple dots are cell nuclei.

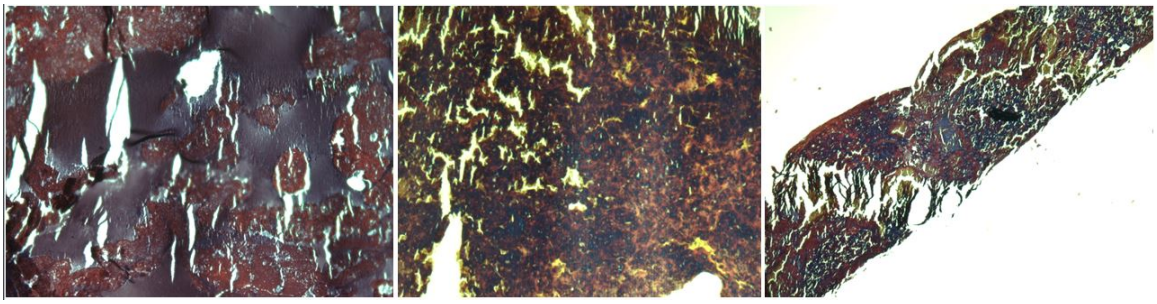

Figure 2.8: Silicone samples across all shear regmies. At left, low shear silicone sample (10x). Middle, physiological shear sample (4x). At right, high shear silicone sample (4x). Samples are stained with Carstairs' stain.

typically chosen for its high mechanical strength, which would often subject it to systems and settings with extreme high flow requirements. For high shear applications, acrylic and silicone are good choices, and stainless steel is highly thrombogenic. VADs and centrifugal pumps have known clotting problems and often incorporate stainless steel and/or other metals, and as just mentioned this may account for the general attribution of thrombogenic to this class of materials. We will also explore these comparison rankings further with clinical data and discussion in the following chapter.

The histological analysis revealed clots of mixed composition with Carstairs staining, which implies that material surfaces overrule the classical thrombosis divisions of red and white clot [53, 55]. H&E staining is of course unable to differentiate platelet presence, but did reveal the presence of cell nuclei that were undetectable with Carstairs as they likely blended in with blue staining of platelets. These cells are most likely immune cells that were recruited to the material surface. Staining of thrombus cross sections with Carstairs also revealed a presence of platelets at the clot-material interface, and a transition to a more fibrinous-RBC composition away from the surface. This again could imply the platelet-material interaction initiating the thrombotic mechanism. However, at high shear this may be due to platelet thrombus growth changing the surrounding shear regime and thus subsequently causing red fibrinous thrombus to form. Due to the mixed composition of thrombi it is no surprise that clinical management of device thrombosis is a huge challenge. These results suggest both antiplatelet and anticoagulant agents are necessary for the management

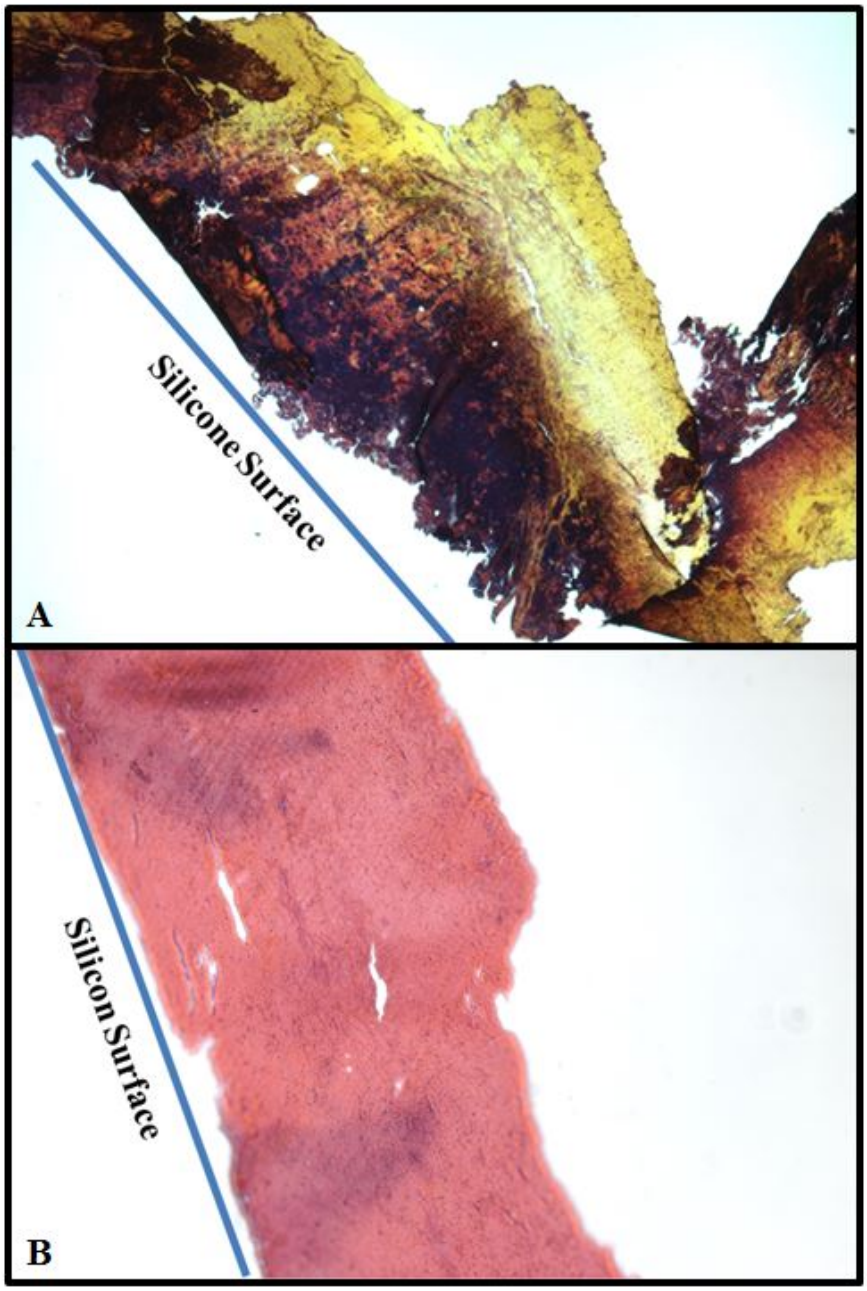

Figure 2.9: High shear silicone thrombus cross section with orientation preserved (10x). A: Carstairs' stain reveals platelet presence at the side of the material surface. RBC presence is seen away from the surface. B: H&E stain does not show such obvious differences. Darker areas are possibly cell nuclei.

of the majority of material surface thrombi.

The assays typically used to differentiate material thrombogenicity (platelet count, Hgb concentration) showed no significant differences across materials nor shear rates. These results confirm the need for endpoints of macroscopic bulk thrombus formation to elucidate material thrombogenicity.

At the halfway point of the experiment, the chambers were free of thrombus. It was only after addition of fresh blood that bulk thrombus formation occurred, and sometimes quickly enough to occlude the chamber later that day. We therefore deduce that material adsorption was occurring for the first 48 hours, and upon addition of fresh blood with physiologic concentrations of coagulation proteins and platelets, thrombus formation was potentiated on the activated surface.

There are some limitations in this study. Real-time thrombus visualization is not recorded, and therefore parameters such as growth rate are not available to us. The blood samples used to perfuse the loops came from different animals, and therefor there may be blood type incompatibility. Additionally, only adhered thrombus in the chamber was accounted for, and therefore any emboli were not included in the thrombogenicity assessment.

This study has demonstrated the time-delay of the bulk-adsorption-thrombosis relationship, and has shown modulation of thrombogenicity by shear regime. These methods also open doors for *in vitro* device assessment, troubleshooting, and design.

CHAPTER 3
COLLECTION AND ANALYSIS OF EXAMPLES OF THROMBUS FORMATION IN CURRENT CLINICAL DEVICES

3.1 Extracorporeal Membrane Oxygenation Circuits

3.1.1 Background

The use of extracorporeal membrane oxygenation (ECMO) as a form of extracorporeal life support (ECLS) is now a well-established therapy for cardiorespiratory failure. Currently the use of ECLS is dominated by neonatal and pediatric patients over adult patients, and use of ECLS is increasing for both adults and pediatric patients. The ELSO registry currently documents use of ECMO in $>$ 55,886 pediatric and neonatal patients since 1990. Neonatal patients ($<$30 days old) account for 47% of all ECLS cases, pediatric pateints (30 days - 16 years old) account for 24% of total cases, and adult patients account for the remaining 29% [68]. However, in the face of ever increasing experience, there continues to be significant morbidity and mortality related to clotting and bleeding related complications, especially in the neonatal and pediatric population [69, 68]. Overall hospital to discahrge survival of ECLS cases is 58% for adules, and 41% for both children and neonates [68]. In addition to the events captured on the patient side, issues related to clotting contribute significantly to equipment malfunctioning necessitating interventions such as circuit and oxygenator changes. For respiratory ECLS patients, adverse events relating to mechanical malfunctions, bleeding, and infarction occurred in 404%, 62.4%, and 46.3% of neonate, pediatric, and adult patients respectively [68]. The incidence of these events was higher in cardiac pateints, and occurred in 67.5%, 69.1%, and 62.4% of neonate, pediatric and adulte patients respectively [68]. In the neonatal and pediatric population, management and appropriate balancing of the anticoagulation to counteract clotting is a tremendous challenge.

A reduction in the inherent generation of clots in an ECMO circuit would reduce the need for anti-coagulation with its concomitant bleeding complications.

There is very limited data on the clot composition, contributing factors, or mechanism of clot generation within the ECMO circuit. The goals of this study were to characterize clot formation and location within the circuit, to understand the basic histologic composition of the clot, and to ascertain the relation between clot location and the local hemodynamic conditions in the extracorporeal circuit.

3.1.2 Methods

According to Emory IRB policies, this study is not subject to IRB approval as it did not involve the acquisition of data via interaction or intervention with the patient, and there was not identifiable private information obtained.

ECMO Circuits

ECMO circuits were prospectively collected from Childrens Healthcare of Atlanta (CHOA), Emory University (Atlanta, GA) between 2012 and 2014. Every patient supported with ECMO during this period was considered eligible for inclusion in the study. No circuits were excluded based on patient or ECMO characteristics and the study population was representative of the overall ECMO supported group in terms of age, diagnosis, type of ECMO and duration of ECMO. During the ECMO support, all of these patients were managed by using the institutional protocol for anticoagulation and blood product administration. The anticoagulation is achieved using unfractionated heparin, with target anti-Xa levels between 0.3 to 0.7 as well as bedside activated clotting time (ACT) measurements using an i-STAT device (Abbott Laboratories, Abbott Park, Illinois) with a Kaolin ACT cartridge. The ACT target ranges were adjusted based on patient anti-Xa levels as well as clinical scenario of bleeding or clotting problems. Blood component therapies were administered as needed to maintain hematocrit between 35% and 45%, platelet count of greater than 100,000/cmm,

and fibrinogen count of greater than 200 mg/dl.

Following removal of a patient from ECMO support, the circuits were immediately drained of blood and gently flushed and filled with normal saline. The circuits were refrigerated (4 °C) at Georgia Tech 24-48 hours until inspection.

Each circuit was inspected for gross clots easily visible through the saline. The location of adhered clots was recorded and regions of interest were photographed. To determine if clots were adherent, saline was perfused lightly in the direction of flow. A clot was deemed adherent if it remained completely or partially attached during perfusion. Tubing sections of interest were cut from the circuit, then labeled and photographed. Clots were then excised from the sections and were immediately fixed in 10% formalin (VWR International, Radnor, PA) until histological analysis. Oxygenator clots were removed by either flushing clots out of the oxygenator with saline or with forceps if a sample was in reach of the entry. Patient parameters of interest while on ECMO were also collected.

A single connector has two TCJs, one upstream and one downstream, and the TCJ was cataloged according to its internal diameter. A typical expansion connector, for example, would have one 1/4 inch TCJ upstream and one 3/8 inch TCJ downstream.

Histological Analysis

The dissected clots were embedded in paraffin and 5-micron thick slices were cut using a microtome (Thermo Fisher Scientific, Waltham, MA). The slices were then mounted on glass slides and dried.

Prior to staining, the slides were first deparaffinized and rehydrated. Carstairs stain for fibrin and platelets was used for staining [70]. After staining, the slides were dehydrated via ethanol, cleared via xylene, and mounted. The Carstairs method stains platelets grey blue to navy, fibrin red, muscle bright red, collagen bright blue, and red blood cells yellow to clear. Images of the slides of the stained clots were analyzed using a pixel count by color in Adobe Photoshop CC 2015 in order to quantify the clot composition.

Computational Anaylsis

In order to identify the regions of extreme shear rate, flow separation, and other flow profiles of interest, computational fluid mechanics was used to analyze the flow through a segment of tubing with a connector.

The tubing connector junction geometry was represented as a 2-D, axisymmetric cylinder in COMSOL Multiphysics. Representative ECMO flow rates (300 mL/min - 5000 mL/min, Re = 500 1014) were used to generate streamlines, velocity profiles, and shear rate profiles. The mesh is smaller at the boundary layer and expands in size in the lumen. The mesh contains 49,923 elements and has an area of 33,940 mm^2. The dynamic whole blood viscosity was assumed to be 0.0004 Pa·s. Convergence was calculated with relative tolerance of 0.001.

Statistical Analysis

An unpaired Students t-test was used for significant differences among TCJ clotting incidences ($p < 0.05$).

3.1.3 Results

Patients and Parameters

Basic patient characteristics and relevant ECMO parameters are described in Table 3.1. The study cohort is representative of the ECMO population at this hospital, with 64% (32/50) of the patients having a cardiac etiology and 36% (18/50) with a non-cardiac etiology for the support. The majority of the cardiac patients (70%) were post-cardiotomy. There was a wide range of age represented from newborn to 16 years of age, with corresponding weight range of 2.2 to 80 kgs. Mean duration of ECMO was 166.5 hours (range of 12 hours to 878 hours (36.6 days). Management of ECMO during the course was based on the basic strategy described in the methods section. Goal directed anticoagulation was

Table 3.1: Summary of ECMO patient parameters

Parameter	Mean	Median	Range
Weight (kg)	15.68	5.16	2.2-80
Age (months)	38.17	1	0.16-195
ECMO duration (hours)	166.52	132	12-878
Flow rate (mL/min)	464	N/A	328-4081
Hemoglobin (g/dL)	13.6	N/A	9.4-13.8
Platelet count (plts/cmm)	115.7e3	N/A	67e3-270e3
Prothrombin time (s)	17.7	N/A	14.1-25.2
APTT (s)	110.1	N/A	38-200
ACT (s)	162	N/A	130-190
Mean heparin dose (IU/kg/hr)	32	N/A	22-114.4

maintained with target anti-Factor Xa levels as well as point of care ACT testing. This resulted in maintenance of target ACTs in all of the patients with a range of 130-190 seconds. ACT range was lower for immediate post-operative patients with significant bleeding (130-160 seconds) while a range of 160-190 seconds was expected for the rest of the patients.

Circuit Analysis

A total of 50 ECMO circuits were collected after separation from patients at removal from the patient. These circuits were then processed and analyzed as described.

The recovered circuits were composed of S-97-E Tygon tubing (Saint-Gobain Corporation, Courbevoie, France) for the roller pump raceway (in the case of circuits with roller head pumps) and Class 6 bypass tubing (Medtronic, Minneapolis, MN) for the rest of the circuit. Oxygenators used were either an adult or pediatric Quadrox D Oxygenator (Maquet, Rastatt, Germany). The circuit also included an arterial filter (Medtronic) as well as a bladder system the majority of the circuits (39/50) with the Better- Bladder (Circulatory Technologies, Inc., New York, USA). The circuits used either a SIII roller pump (Stockert-Shiley SIII, LivaNova, Munich Germany) (68% of circuits) or a centrifugal pump (Sorin Revolution, LivaNova, Munich, Germany) in (32% of the circuits). A system-wide change over for the institute from a roller to centrifugal technology occurred 2/3 of the way through

Figure 3.1: Typical TCJ Thrombus. Clot at downstream TCJ identified by green arrow.

the collection time period. ECMO circuits at CHOA were primed with packed red blood cells immediately prior to use.

Visual documentation of gross clots was performed for all circuit components. Overall, 94% of circuits exhibited thrombus formation. Clots were not evenly distributed within the various components of the ECMO circuit. Although the tubing accounts for over 90% of the surface area exposed to blood, no clots were present on the free tubing surface. Instead, thrombi were focused at two locations: the tubing-connector junctions (TCJs) and the oxygenator. The clots found at the TCJs were adherent and typically axisymmetric (Fig 3.1). The clots that were found in the oxygenator were not adherent to the membrane and were found loose on the deoxygenated or pre-membrane side. In some cases, clots from TCJs grew downstream and formed large masses greater than 2 cm^2 (Fig 3.2). The clots were only adherent to the TCJ attachment point, and under perfusion, the portion downstream of the TCJ was mobile. It is likely that these large clots would eventually break off and migrate to the oxygenator.

The ECMO circuits were comprised of approximately 5 m of tubing, with 6-12 connectors that were used to control flow and insert devices (oxygenator, filters, vascular access, etc.). Depending on the entry size of the circuit components, circuits were either a single diameter throughout or sized up and down between two diameters. Overall, the connectors accounted for about 10% of the exposed surface area, yet exhibited 99% of the clots. The

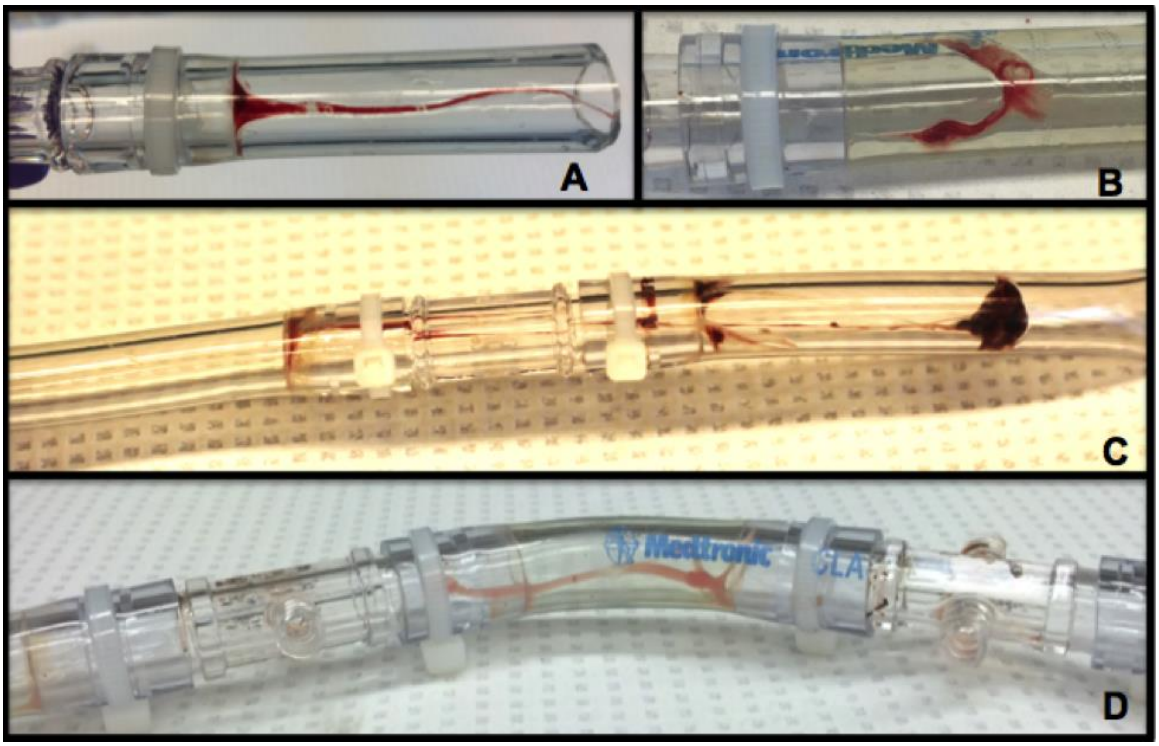

Figure 3.2: Examples of growth from TCJs. A: A clot attached with a wide base at a downstream TCJ and a long, thin extending tail. B: A clot with two attachment points at a downstream TCJ. C: A large, nearly occlusive clot in the tubing lumen attached by multiple tethers to both upstream and downstream TCJs at the nearest upstream connector. D: A clot attached to both downstream and upstream TCJs of adjacent connectors.

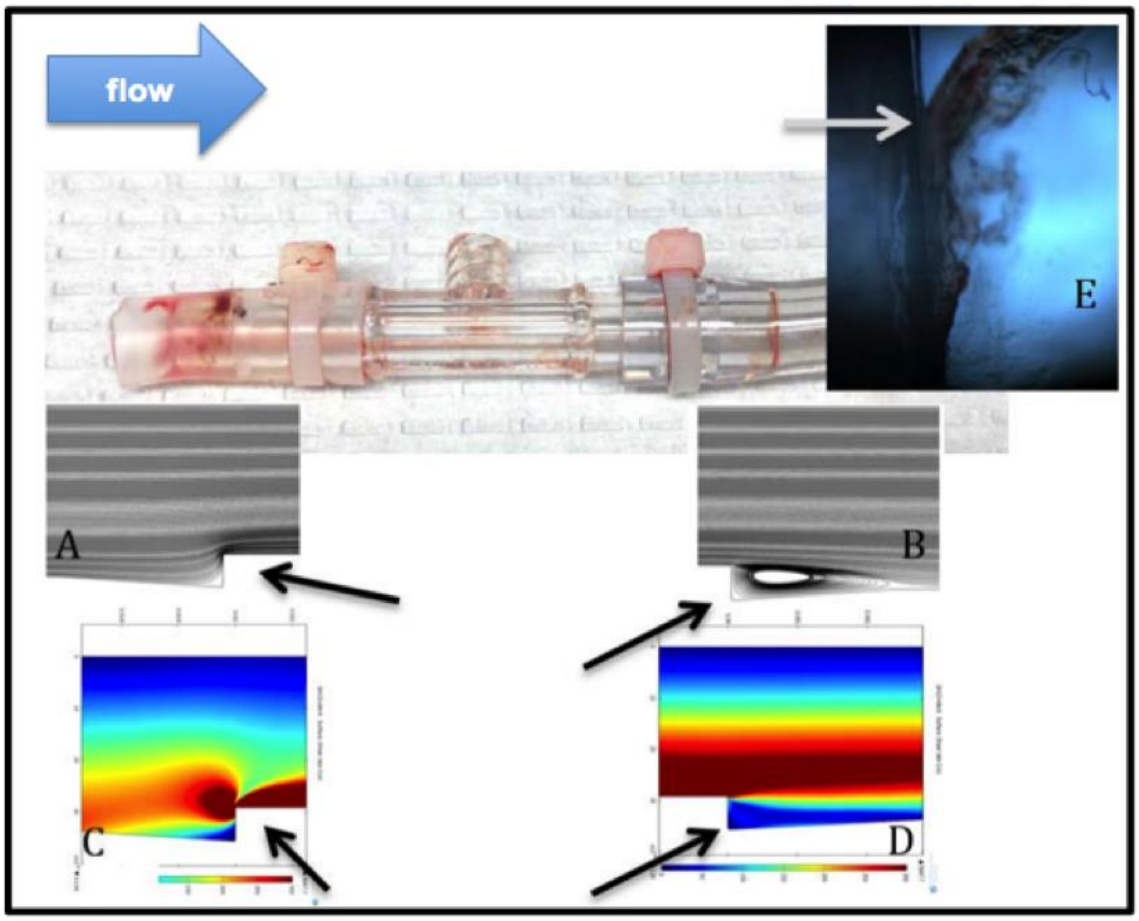

Figure 3.3: Connector CFD. A: The upstream connector edge (arrow) causes a point of stasis. B: The downstream step of the connector edge (arrow) creates a recirculation zone. C: The upstream connector edge creates a point of stasis in the corner (shear rate $<<50$ s^{-1}). D: The downstream connector edge creates an extended period of low shear (shear rate <100 s^{-1}). E: A low-power microscopy view of a downstream clot shows the attachment point to the connector edge (arrow).

majority of ECMO circuit tubing diameter was 1/4 inch (0.635 cm), and a typical circuit sized up and down between 1/4 in and 3/8 in (0.953 cm) tubing. A few larger roller pump circuits sized up and down between 3/8 in and 1/2 in (1.27 cm) tubing, which accounted for only 8% of the circuits in this study.

The TCJ is formed by the thickness of the connector wall and the region of tubing that is expanded to fit over the outer diameter of the connector until it returns to the relaxed diameter (Fig 2). Clots were found in the step right at the junction in the lumen expansion zone on both the inlet and outlet ends of the connectors.

The incidence of clotting was high at certain connectors and regions of the ECMO circuit, and is correlated with areas of low shear ($p << 0.05$) (Fig 2). The downstream end of expansion connectors was the most thrombogenic region in the ECMO circuits, with a 74% incidence rate, while its upstream counterpart had a thrombi incidence rate of only 13%. The 3/8 in diameter TCJs in general had a higher incidence of thrombosis of 45% overall vs. the 1/4 in TCJs which were at 22%. In general, a downstream TCJ was significantly more likely to be thrombogenic than its upstream counterpart (33% vs 25.2%, $p = 0.00297$).

Clot Histology

Histological analysis revealed the TCJ clots to be fibrin-rich and full of red blood cells (RBC) (Fig 3.4). The oxygenator clots were coiled, and when expanded reached a length of > 5 cm (Fig 3.5). Oxygenator clots were present on the upstream pre-membrane side, and these clots were non-adherent. Under light perfusion of water, the clots dislodged and became mobile. With changes in oxygenator orientation (tipping), clots would slide in the direction of gravity. The composition of oxygenator clots is similar to the axisymmetric TCJ clots (Fig 3.5). The clots were on average 54% fibrin, 45% RBCs, and approximately 1% platelets. These red clots had a paucity of platelets.

Computational Fluid Dynamics Analysis

Based on the frequency distribution for the localization of adherent clots, we identified the TCJ as the highest priority site for potentiation of thrombosis. We then characterized the hemodynamics of the TCJ zones. CFD analysis of the TCJ region revealed distinct regions of low shear and a recirculation region on the downstream side of the TCJ. A figure of the streamlines and shear rates is shown in Figure 3.3. For the inlet to the connector, a zone of very low shear rates less than 50 s^{-1} is present in the corner. At the outlet, the zone of very low shear rates is even larger and directly located in the corner of the junction. Note

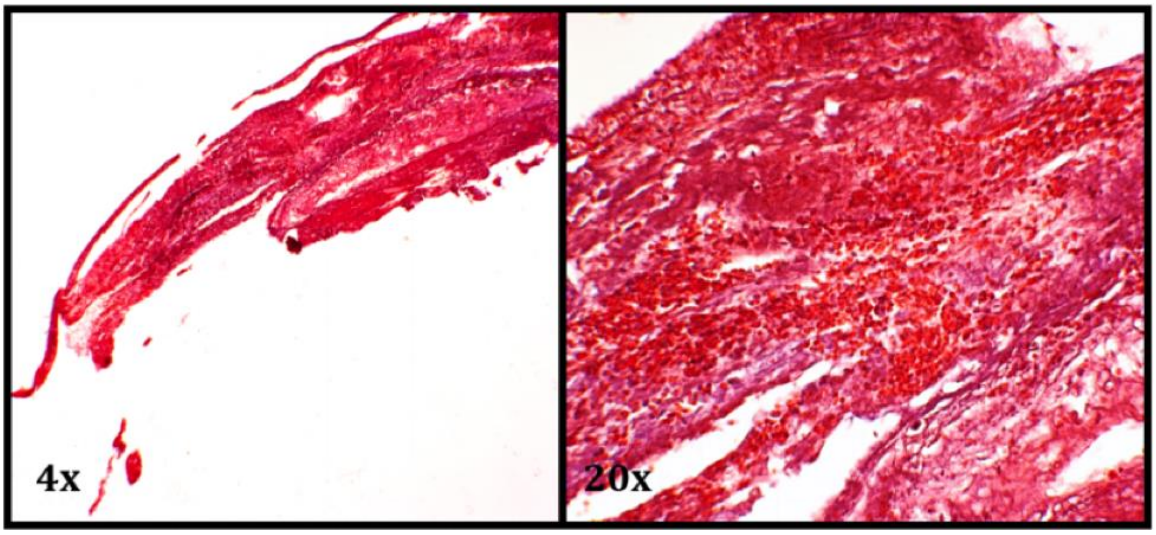

Figure 3.4: ECMO TCJ clot histology. Carstairs stains red blood cells yellow to clear, fibrin red, muscle deep red, collagen bright blue, and platelets blue-gray to navy.

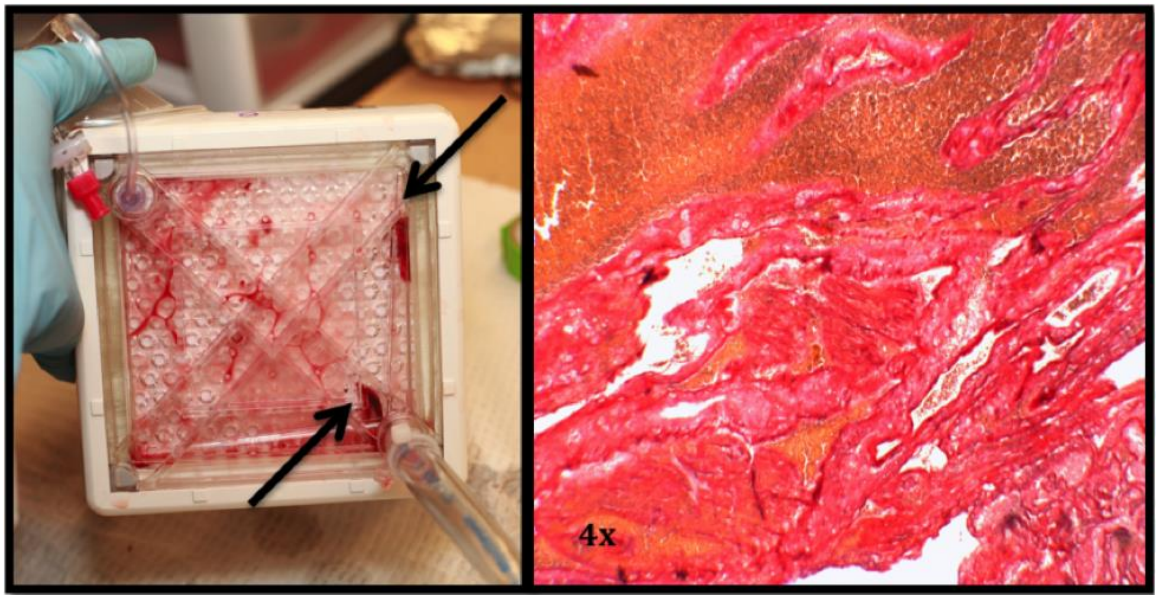

Figure 3.5: ECMO oxygenator clot example (left) and histology (right). Arrows point to clots caught in the entrance side of the oxygenator. Carstairs stains red blood cells yellow to clear, fibrin red, muscle deep red, collagen bright blue, and platelets blue-gray to navy.

that the shear rates outside of the corners return to a normal shear rate range from 450-1000 s^{-1}. Thus, the clots co-locate directly at the site where blood is virtually stagnant with shear rates less than 50 s^{-1}, or a shear stress of less than 0.2 Pa ($p << 0.05$).

3.1.4 Discussion

This is one of the first studies to examine in detail the location and histologic composition of thrombosis within the ECMO circuit. The analysis was extended to examine the statistical relationship of thrombosis with hemodynamics in the clinical circuits.

Analyses of clinical ECMO circuits revealed that thrombosis occurs consistently in nearly all of ECMO circuits at specific sites. The ECLS Registry collects information on clot formation at certain ECMO circuit components, however clots are typically recorded when large enough to be seen from outside the circuit while blood is still flowing, or when large enough to be detrimental. There is some variation in frequencies of these clot related complications. For example, in neonatal cardiac ECMO patients, 11.6% reported oxygenator clots, 3.9% reported bridge clots, 5.9% reported bladder clots, 4.3% reported hemofilter clots while 13.6% reported clots at other locations[69]. For pediatric cardiac ECMO patients, the frequencies were as follows: oxygenator 8.4%, bridge 3.0%, bladder 4.0%, hemofilter 3.5% and other locations 10.2% reported clots [69] However, the ECMO circuits vary from facility to facility and the methods for recording clots are inconsistent. The development of a consistent method for identifying and reporting clots at specific sites in ECMO circuits would be of benefit to the patient population. In general, our data suggests that there is significant under-recognition and therefore under-reporting of circuit thrombosis.

The blood clots are found at specific locations within the circuit, primarily at the junctions made by the tubing and connectors (TCJs). It is noteworthy that although the tubing of the circuit constitutes a large portion of the surface area, there were no clots detected on the tubing surface. This is remarkable given that the standard circuit tubing (Medtronic

Class VI) is not coated. This TCJ clot location corresponds directly to zones of very low shear rates less than 50 s^{-1}. Conversely, almost no clotting occurs with tubing material where shear rates are greater than 450 s^{-1} ($p << 0.05$) based on the CFD analysis. These conditions correspond to a Virchows Triad requirements for foreign surface, blood coagulation proteins, and zones of virtually stagnant blood. The fibrin clots are also consistent with previous studies that have looked at the behavior of blood components in relation to differences in shear rates. Using rabbit aorta with endothelial disruption, Weis et al. showed that the degree of fibrin deposition inversely correlated with the shear rates; high fibrin content at low shear rates of 50 s^{-1} versus low fibrin content at high shear rates of $>$ 650 s^{-1} [71]. Similarly, Guy et al have showed that low shear rates correspond directly to a higher degree of fibrin gel deposition on an injured blood vessel surface, using mathematical modeling [72]. The height of the fibrin gel achieved was highest at shear rates less than 100 s^{-1} yet was minimal at shear rates above 1000 s^{-1}. In the current study, we find concordance with these studies. The areas of TCJs with shear rates < 50 s^{-1} exhibited with high fibrin deposition and clot formation. The contribution of the local hemodynamics to local clot formation within the clinical ECMO system is critical.

Growing clots with small attachment points at TCJs are particularly worrisome, as they imply the possibility of large emboli which could cause devastating patient complications. These large clots would be subject to large drag forces and may be the source of the large, loose thrombi seen in the oxygenator.

The histologic appearance of clots in the ECMO circuits were fibrin-rich with few platelets. Thus fibrin coagulation is the dominant problem for ECMO circuits rather than platelet thrombosis. The observation that ECMO clots are fibrin-rich is also consistent with reports of fibrinogen consumption in these patients [73, 74]. These red clots form in the setting of adequate anti-coagulation with heparin and with therapeutic ACTs, illustrating the criticality of shear rate as a new factor. Currently, there are no universally established guidelines for ECMO anticoagulation, though unfractionated heparin is used at most

ECMO centers, and very few centers (6 in a recent 119 center survey) use antiplatelet agents (acetylsalicylic acid, prostacyclin) [75]. Unfractionated heparin is effective at binding with antithrombin III (AT III) and causing a conformational change that leads to acceleration of AT III mediated inactivation of various coagulation factors including thrombin, factors IX, X, and XI [76]. However, one of the major limitations of heparin in the setting of biomaterials is its inability to inactivate thrombin bound to fibrin or to biomaterial surfaces [77]. Hence, we can speculate that once fibrin deposition is initiated within the circuit, further propagation at low shear rate zones may not be sufficiently prevented by heparin use.

Our data also indicate that circuits with centrifugal pumps have more incidence of thrombus than the roller pumps. The circuit thrombi may be due to the size of tubing to fit the centrifugal pump, which typically sizes up and down between diameters to go through the pump and the oxygenator. Our data show these connectors of diameter increase and subsequent larger diameter regions to be highly thrombotic. Redesign of the circuit to avoid such step size changes may reduce the thrombogenecity of the circuit by reducing the amount of regions with extreme low shear rates. Indeed, elimination of just 4 TCJs could reduce circuit thrombus by 80%.

This study is methodologically limited in some ways. The inspection of ECMO circuits was done macroscopically, and microscopic examination of the entire tubing was not performed. This may have excluded smaller, subclinical clots. Circuit components such as the oxygenator and arterial filter were not dismantled for investigation, and thus assessment of these components was limited to outer visual inspection. Though the morphological and histological similarity of clots found in the oxygenator entry and the TCJs suggest that these mechanisms are linked, it is also possible that low shear in the oxygenator could also potentiate thrombosis. Our results are also in agreement with other oxygenator findings, i.e. that the thrombi accumulate in the venous side of the oxygenator [78]. The histological analysis performed was used only to ascertain whether the clot was predominately composed of fibrin or of platelets, neglecting further details of clot morphology. The circuits

were gently irrigated with saline prior to refrigeration. So it is possible that some lightly adherent clots may have washed out. However, the overall clot burden noted in our study is far more extensive than the visual inspection methodology used for registry reporting. We anticipate the overall analysis including histology is not affected by the procedure, based on staining and microscopic examination of the various sections. We did not evaluate the circuits at successive time intervals and cannot comment on the growth rate of clots. This is also a single-center study, which may limit applicabilitygeneralizations.

A better understanding of clot formation in ECMO may allow for targeted preventive treatments and thus better patient outcomes. Current anticoagulation regimens alone are not sufficient to eliminate thrombosis, and modification of the circuit itself may be necessary to minimize thromboembolic events. Identification of the areas of the circuit that are thrombogenic allows for improved circuit design. Our results demonstrate that the local hemodynamics, which create small zones of low shear rate, are strongly related to thrombus formation in extracorporeal circuits. We recommend that circuits be designed to reduce the zones of low shear rate ($< 100 s^{-1}$) such as occurs at expansions and connectors. However, it is also still important to circuit design to exclude pathologically high shear rates that may induce hemolysis ($> 40{,}000\ s^{-1}$) and/or platelet thrombosis ($> 10{,}000\ s^{-1}$) [53, 79]. Our data also suggest that on the basis on thrombogenecity, roller pumps appear to produce less thrombosis than centrifugal pumps. We conclude that blood clotting in ECMO circuits may be reduced through an understanding of the induction of coagulation combined with fluid mechanic design to eliminate zones of stagnation.

This was published in the ASAIO Journal [80].

3.2 Sorin Revolution Centrifugal Pump

3.2.1 Background

While we were collecting ECMO circuits from CHOA as discussed above, the center made a change from roller pumps (COBE Century) to centrifugal pumps (Sorin Revolution)

for ECMO circuit perfusion. As previously described, ECMO continues to be burdened by both thrombotic and hemorrhagic complications [47, 81, 82].

Original concerns centrifugal pump induced hemolysis kept the roller pump in use over the past couple of decades. Recently, there has been a nationwide clinical shift to centrifugal pumps in the US due to improvements in the technology [82, 83, 84, 85, 86, 87]. Some current centrifugal pumps include the Revolution (Sorin Group), the Rotaflow (Maquet), and the Centrimag (Thoratec) which have small priming volumes and mitigate heat generation [85]. The Centrimag is levitated and has a magnetic bearing. The ECMO center at Childrens Hospital of Atlanta (CHOA) at Egleston recently converted to the Sorin Revolution. The Revolution pump has stainless steel bearings that secure the impeller, as it is not a magnetically levitated centrifugal pump. At the top of the shaft, there is an exposed piece of the stainless steel bearing (Fig 3.6). The steel bearing shaft is unique to the Revolution pump.

Thrombosis, anticoagulation, and bleeding remain clinical problems. Most analyses of these pumps focus on hemolysis and other markers [88]. While hemolysis may contribute to a hypercoagulable state of blood or serve as a marker of thrombosis, analysis based on bulk thrombosis is lacking in the field. We propose that to truly gauge the thrombogenicity of the pumps, it is necessary to use the endpoint of large-scale thrombus formation. Furthermore, there is a need for improved guidance of device design and device testing that incorporates flow, surfaces, and clinically relevant endpoints.

Here we examine neonatal and pediatric ($>$30 days old, $<$18 years old) ECMO circuits after patient use and compare them to roller pump circuits on the basis of bulk thrombogenicity. We will also develop a CFD model of the Revolution to investigate the shear rate in potential thrombogenic areas, and then we will simulate a growing thrombus to explore changes in shear rate.

Figure 3.6: Sorin Revolution Centrifugal Pump. Flow comes in at the top over the cone. The shaft secures the cone and there is an exposed piece of the stainless steel bearing at the top of the cone.

3.2.2 Methods

ECMO Circuit Collection

ECMO circuits with centrifugal pumps were collected from Childrens Healthcare of Atlanta, Emory University (Atlanta, GA). Patient parameters are the same as the previous study and are listed in Table 1 in the first section. Circuits were drained of blood and filled with saline immediately following removal of patient support for transport to our laboratory at Georgia Institute of Technology (Atlanta, GA). The saline was then drained and the circuits were inspected for adherent thrombi. The location of thrombi was recorded, and in some cases, samples were excised gently using a hemostatic clamp and preserved in formalin.

Histological Analysis

Preserved clots were embedded in paraffin and 5-micron thick slices were cut using a microtome (Thermo Fisher Scientific, Waltham, MA). The slices were then mounted on glass slides and dried for 24 hours at 37C.

Prior to staining, the slides were first deparaffinized and rehydrated. Carstairs stain for fibrin and platelets was used for staining [70]. After staining, the slides were dehydrated via ethanol, cleared via xylene, and mounted. The Carstairs method stains platelets grey blue to navy, fibrin red, muscle bright red, collagen bright blue, and red blood cells yellow to clear.

CFD Analysis

A 3D computational model of the pump head was generated from actual pump heads and photographic images available in the public domain. The pixel mesh was scaled and is shown in Figure 3.7. The mesh was composed of 5 million cells and inflation cells were placed on the tip of vanes where high velocity was expected. Ansys CFX and Windows OS

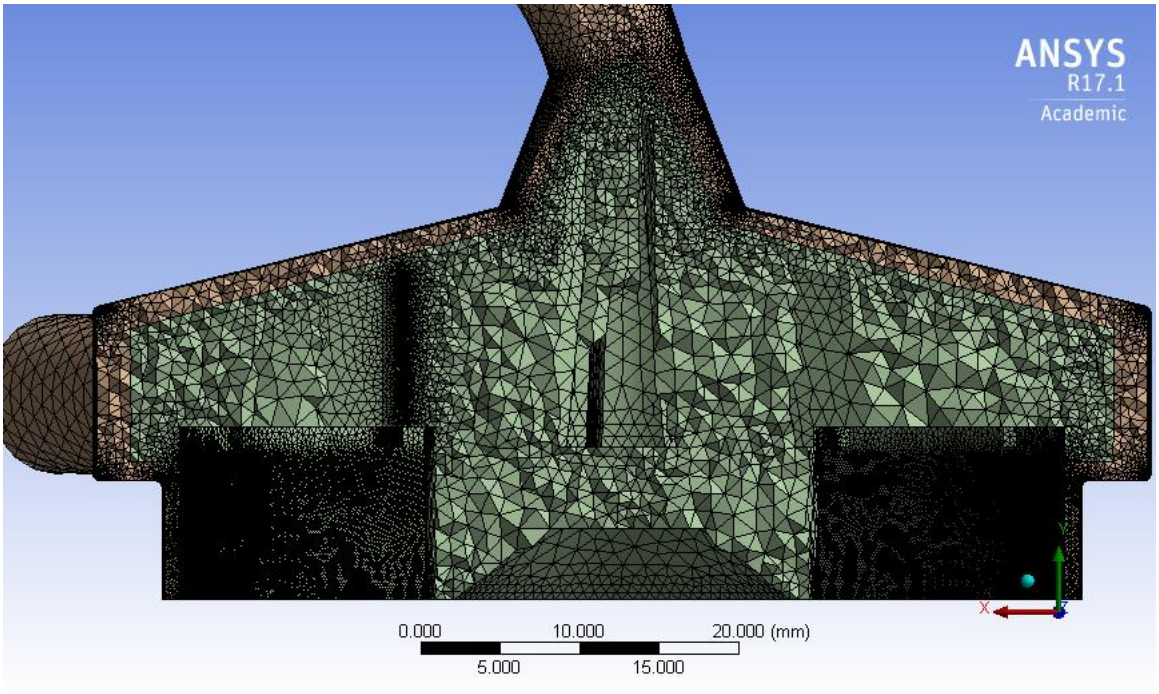

Figure 3.7: CFD mesh. Pump head mesh consisting of 5 million cells.

on a computer with 6 CPUs were used for the computation. Blood was modeled as a Newtonian fluid and boundary conditions were taken from clinical data. A Moving Reference Frame (MRF) method was used to reflect the rotational effect of the vanes. A summary of relevant parameters is shown in Table 3.2.

The endpoint calculated was the wall shear strain rate in the entire pump head. Further investigation was made around the metal shaft with the simulation of an adherent growing

Table 3.2: Summary of CFD parameters

Software:	ANSYS CFX
Hardware:	Dell, 6CPUs
Time dependency:	Steady flow
Turublence:	k-epsilon
Rotation analysis:	MRF
Inlet boundary condition:	85 mmHg
Outlet boundary coniditon:	2.4 L/min
Rotational speed:	2,000 rpm
Blood density:	1,050 kg/m^3
Blood viscosity:	4 cP

thrombus.

3.2.3 Results

Circuit Thrombosis

Of the 16 centrifugal pumps in patient circuits, all pump heads (100%) exhibited macroscopic adherent thrombi. Thrombi consistently formed at the top of the shaft of the pump, covering the exposed stainless steel bearing at the top of the pump cone (Fig 3.8). The thrombi were firmly adherent and cohesive upon extraction. In 5-10% of cases, large thrombi extended from the pin onto the tops of the vanes (Fig 3.9). While the size of the thrombus varied considerably, the location of macroscopic thrombus was consistent at the inlet to the pump head. No macroscopic thrombus was seen in the depths of the vanes or at the tips of the vanes at the periphery.

In addition, centrifugal pump TCJs were compared with roller pump TCJs, and it was found that the centrifugal pump circuits had a higher overall incidence of thrombosis at the connector junctions (41% vs 25%, $p<<0.05$).

Clot Histology

The clinical thrombi were sectioned and stained using Carstairs to distinguish platelets from RBCs. As with most histology, samples varied due to staining intensity, orientation, and area of extraction. Under low power microscopy, the thrombus was recovered as a circular section that surrounded the shaft (Fig 3.10). In most samples, the tissue appeared under medium power to have significant sections of blue stained platelets with sparse red blood cells indicating the predominance of platelet-based thrombus (Fig 3.11).

CFD Analysis

The shear rate was quantified for steady flow in the pump head. Certain pump head areas had pathologically high shear rates ≥ 2000 s^{-1}. Other areas had very low shear rates < 50

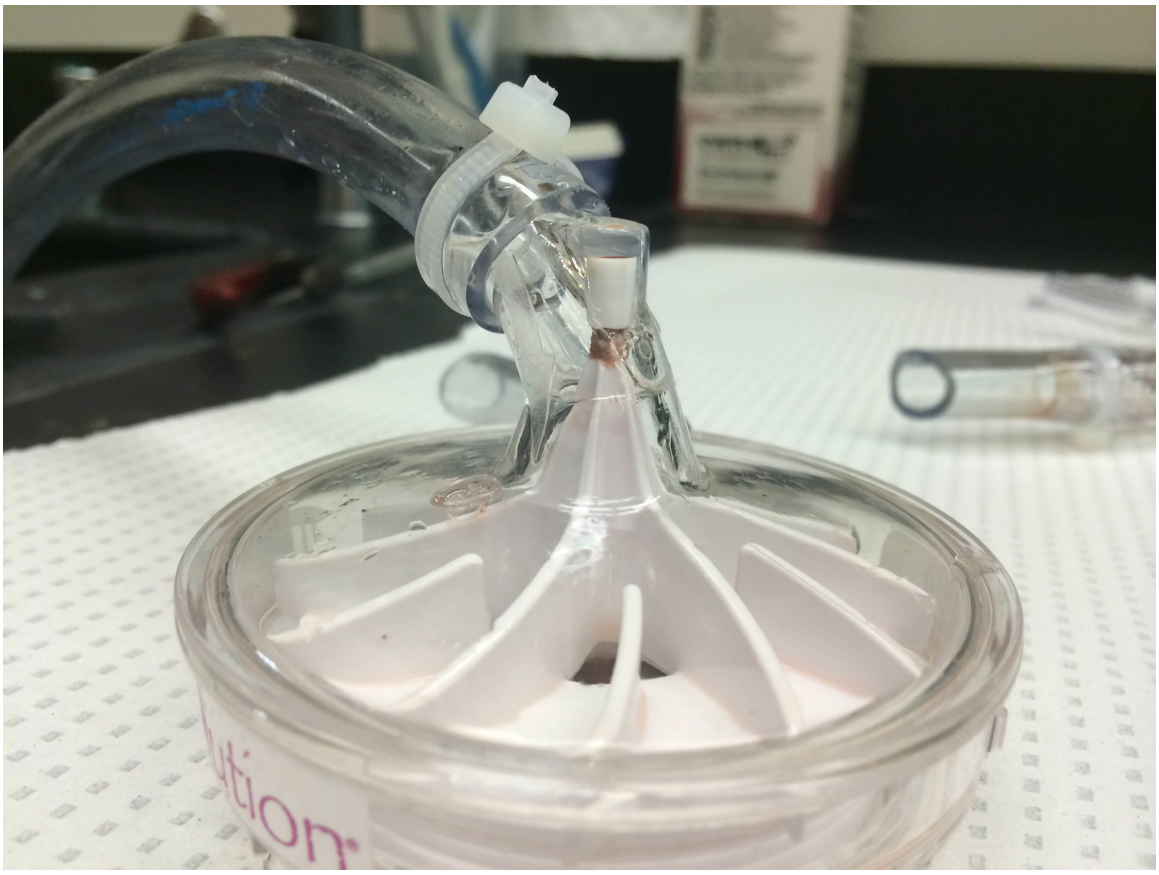

Figure 3.8: Inlet shaft coverage by thrombus was seen in 100% of clinical circuits.

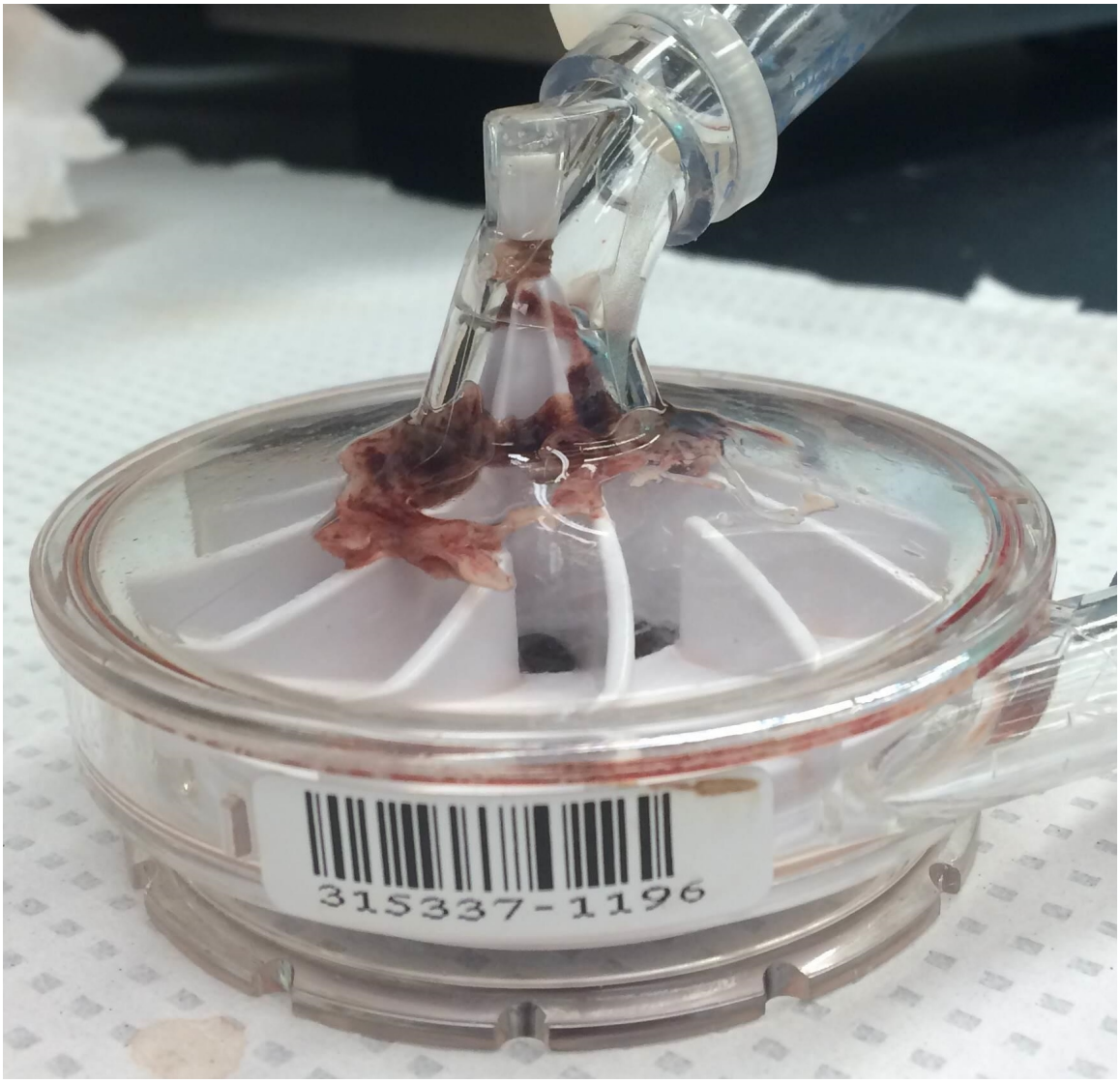

Figure 3.9: Centrifugal pump from a clinical circuit with large-scale thrombus formation at the top of the cone including the shaft.

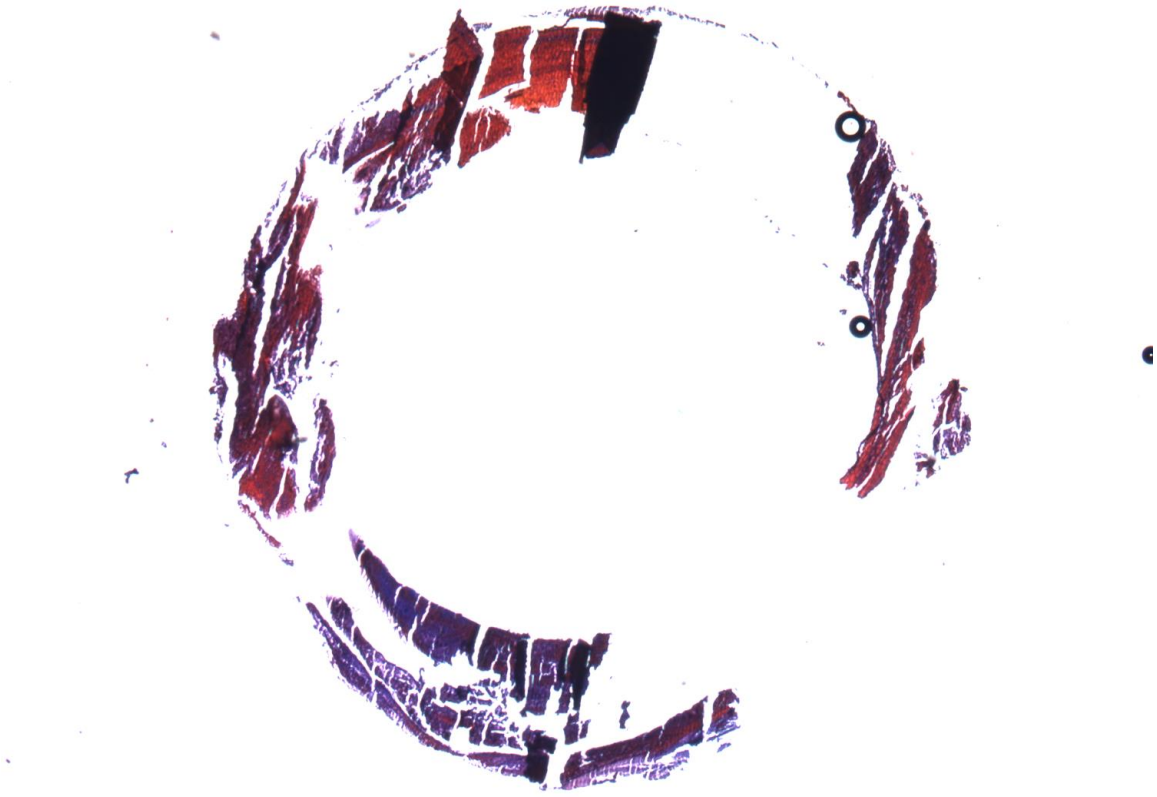

Figure 3.10: Low power (4x) view of thrombus surrounding the shaft. The circular form of the shaft is cisible in the center with a uniform thickness of the sample giving a circular form to the blood surface of the thrombus. Carstairs stains red blood cells yellow to clear, fibrin red, muscle deep red, collagen bright blue, and platelets blue-gray to navy.

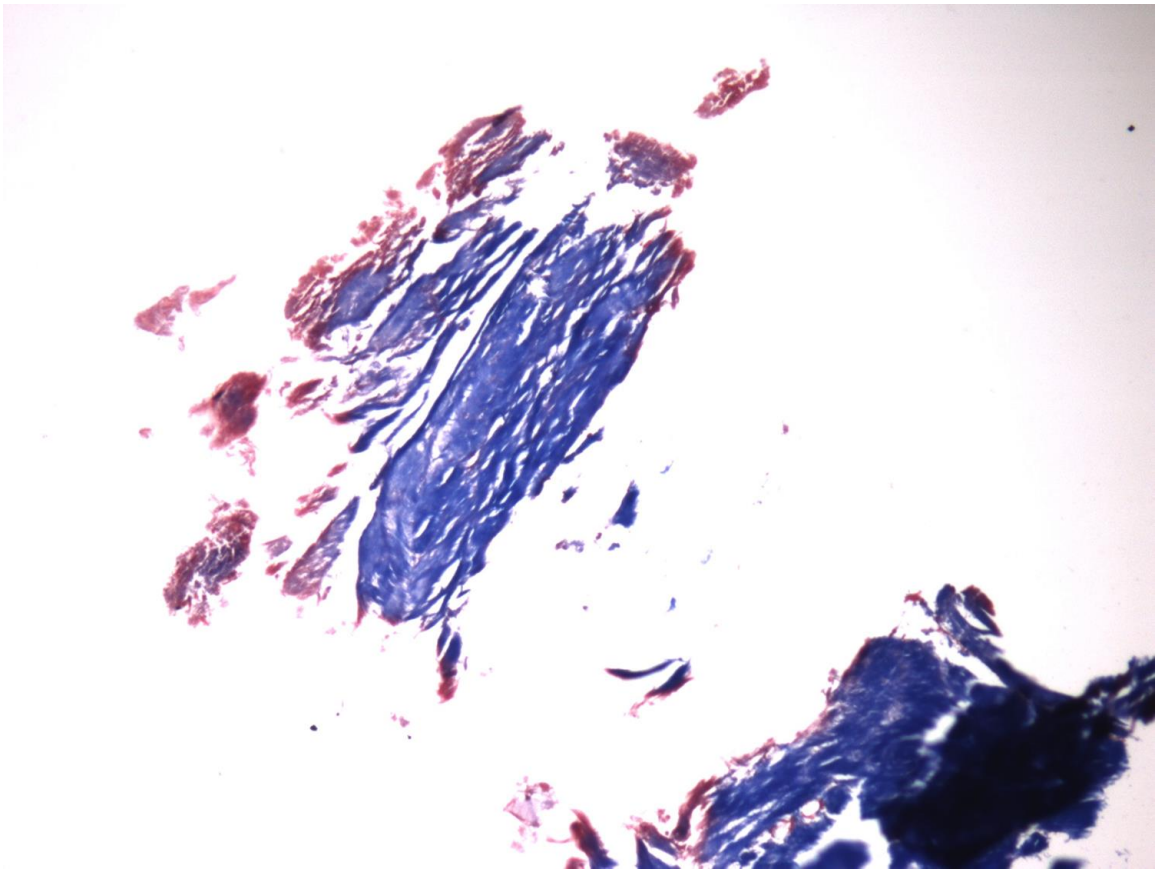

Figure 3.11: Example of medium power (10x) view of a thrombus sample from a clinical centrifugal pump. Carstairs stains red blood cells yellow to clear, fibrin red, muscle deep red, collagen bright blue, and platelets blue-gray to navy. Thrombi were of mixed composition of platelets and fibrin in distinct regions. In this section, 89% of pixels are blue and 11% of pixels are red.

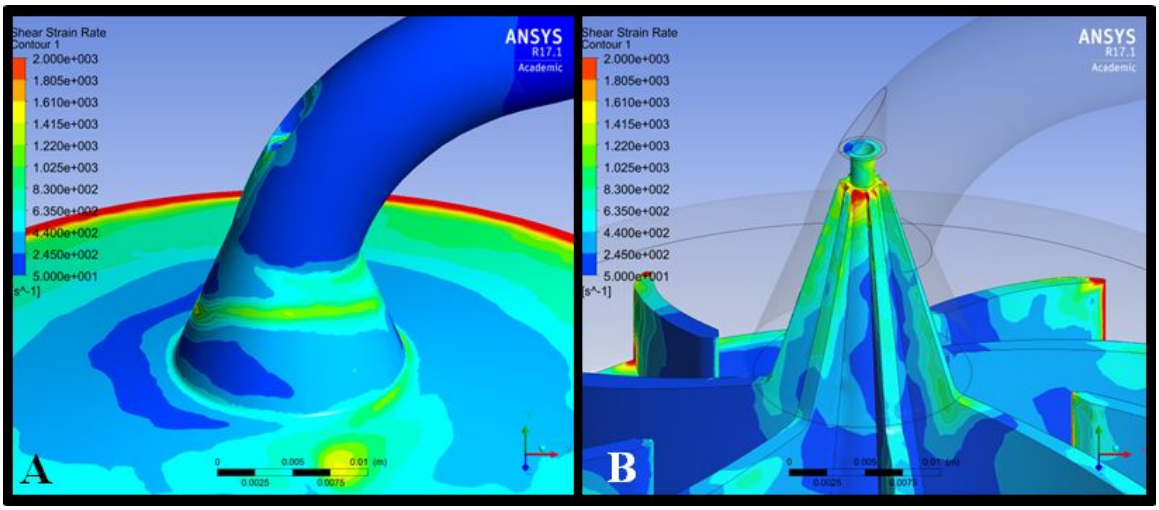

Figure 3.12: Shear strain rate in the pump head. A: Outer housing. B: Inner cone.

s^{-1}. Calculation results of the shear rate in the pump head are shown in Figure 3.12. The shear rates in the curved entrance tube were physiologic with values about $240s^{-1}$. As flow entered the cone shaped entrance to the pump, a band of high shear greater than 1,220 s^{-1} was seen on outer housing in Figure 3.12. Shear rates on the inner cone eached values greater than 2,000 s^{-1} shown in Figure 3.12. Shear rates at the bearing pin exceeded 1,220 s^{-1}. Note that the metal bearing pin is subjected only to high shear stresses without a zone of stagnant blood. Then as the flow exits the vanes, the tips exhibited high shears of $>$ 2,000 s^{-1}.

Figure 3.13 shows an iso-volumetric view of the regions of low shear rate and those of high shear rate. Areas of low shear $<$ 50 s^{-1} form in the valleys of the vanes at the bottom-center of the pump. Conversely, high shear rate regions are concentrated at the vane tips. The high shear rate region occurs on the shaft surface facing inlet blood flow and the cone tip. For scale, the length of the exposed pin is about 1.5 mm. Thus, the pump head subjects the blood to both very high shear rates and very low shear rates at artificial plastic surfaces, while the metal pin is exposed to high shear rate blood flow.

As thrombus accumulates around the bearing pin, the growing thrombus will change the dimensions of the shaft. We modeled the thrombus growth as an increase in shaft diameter. The shaft radius was changed from 1.6 mm to 2 mm and then 3 mm to quantify

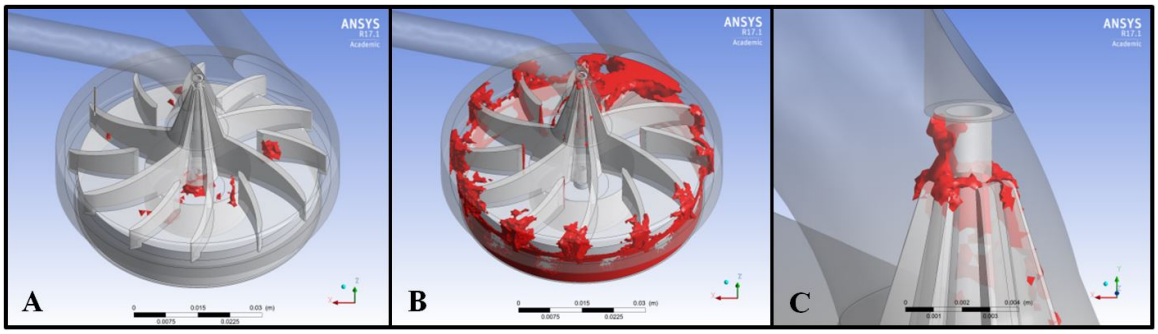

Figure 3.13: Isovolumetric view with shear extrema. A: Under 50 s^{-1}. B: Over 1,000 s^{-1}. C: Zoomed in view of B.

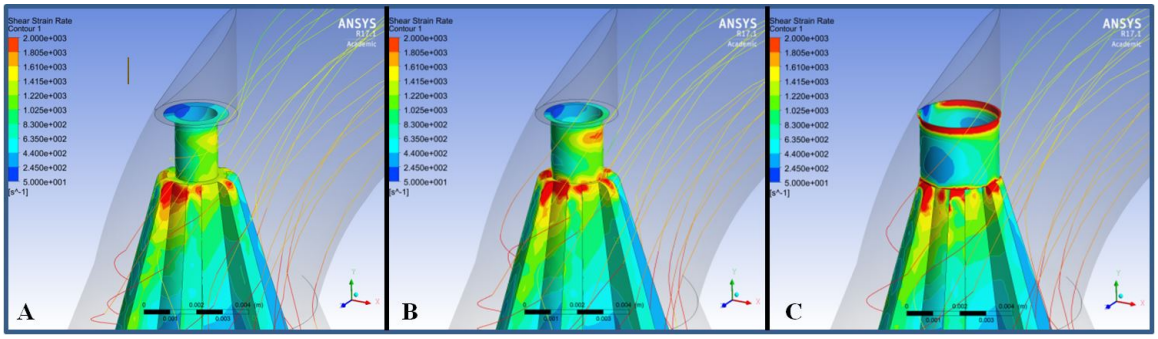

Figure 3.14: Varying shaft radius to simulate growing thrombus. A: Diameter of 1.6 mm. B: Diameter of 2 mm. C: Diameter of 3 mm.

the difference in shear strain rate around the metal shaft and the cone tip. Figure 3.14 shows the simulation result with the legend ranging from 50 s^{-1} to 2,000 s^{-1}. Blood flows from upper right corner to left bottom and path lines are colored with velocity 0 m/s to 1 m/s. The cone tip region shows the highest shear strain rate over 2,000 s^{-1}. With the increase of the axis radius, the surface area of high shear rate around the shaft increases. The maximum shear rate on the shaft appears at the surface facing the blood flow for radius 1.6mm and 2mm, but the maximum area shifts to upper side of the shaft as the radius reaches 3 mm. The shear rate around the metal bearing shaft is 2,500 s^{-1}, but reaches over 5,000 s^{-1} if the shaft becomes thicker.

3.2.4 Discussion

Thrombosis in clinical ECMO circuits is a serious problem affecting patients supported by this life-saving procedure. Large macroscopic thrombus was observed in 100% of clin-

ical centrifugal pumps. The thrombus was adherent to the exposed piece of stainless steel bearing at the top of the shaft. Large thrombus was commonly seen extending from the shaft, covering the inlet portion of the vanes while not being seen at the peripheral tips or depths of the vane channels. Histology reveals the clinical thrombus as having a large platelet component, which suggests platelet thrombosis activity. The use of the centrifugal pump therefore introduces an additional thrombotic mechanism to ECMO circuits, which are otherwise dominated by fibrinous coagulation germinating at the TCJs. In addition, the centrifugal pumps themselves demonstrate adherent thrombus, especially at the pin of the cone. The centrifugal pump also potentially poses other complications such as heat generation due to the high resistance of pediatric and neonatal cannulas. Variation in designs of various available centrifugal pumps and its implication to thrombus generation will be the focus of a future study.

The presence of fibrin within the clot could arise from contact activation initiation of clotting on the exposed stainless-steel shaft. The histological composition of the bulk of the thrombi point to a platelet-rich thrombus, which previous work has linked to pathologically high shear rate conditions by a mechanism mediated by platelet attachment to von Willebrand factor (vWF) [53, 55, 89, 90, 91]. Our interpretation of the sequence of events is that the exposed stainless steel bearing initially absorbs blood proteins to induce fibrin formation at the surface during the first 24 hours. This initial fibrin thrombus then grows by rapid platelet accumulation under the high shear conditions at the entrance to the pump. Further growth of the thrombus to extend over the inlet is then a process stimulated by pathologically high shear away from the surface of contact activation.

Our CFD model predicts high shear rates at the shaft. Our growth model also shows increasing shear rate as the shaft diameter thickens, as in the case of coverage othe shaft by uniform thrombus. This model supports the histology results and our resulting hypothesis of initial protein and fibrinous deposition and subsequent platelet thrombus growth as shear rate increases.

These findings continue to confirm that it is important to consider both the material surface and shear regime while designing a blood contacting medical device, as both contribute to thrombogenicity. The Sorin Revolution pump head relies on a bearing shaft of steel. A levitated pump head without a shaft could potentially mitigate thrombogenicity. We have not gained access to these pumps for comparison. Future studies may examine the relative contribution of the exposed stainless steel surface nidus versus hemodynamic shear rate in the thrombogenic area.

It has also been shown that acquired von Willebrand factor (vWF) disease (avWD) can occur due to centrifugal pumps [3]. This is presumably due to high shear and can lead to bleeding problems. Since we observe platelet-rich thrombi occurring in these pumps and suspect a high shear mechanism, there is the potential for avWD to interact with this pathway.

In this study, we focused on the endpoint of macroscopic thrombus to assess pump thrombogenicity. Direct observation of large-scale thrombosis may be more clinically relevant as an endpoint for blood pumps, as compared to indirect measures of blood damage such as hemolysis or platelet activation, though hemolysis and platelet activation may be interesting markers to include in future studies. Other contributors to thrombus formation, such as heat generation, suspected contributor due to the friction of the bearing, may also be explored in a future study. Comparison studies of different centrifugal pumps designs may point to the relative roles of surface, shear rate, and heat in macroscopic thrombosis.

Portions of this study were published in the International Journal of Artificial Organs [92].

3.3 BerlinHeart

3.3.1 Background

The Berlin Heart EXCOR is a pulsatile pediatric ventricular assist device (VAD) for support of infants and children with end-stage heart failure. This patient group has the

highest waitlist mortality of all patients waiting for a transplant [93, 94]. While adults and larger adolescents have a choice of a wide variety of available VADs currently on the market, children and infants do not. ECMO has thus historically served as a bridge-to-transplant for these patients but survival rates are low [93].

The EXCOR has recently progressed as another option for pediatric bridge-to-transplant [93, 95, 96]. In the EXCOR IDE trial, 75% of all patients survived to transplant or recovery [93]. Thrombosis and management of the anticoagulation-bleeding balance persists as a challenge for clinical patient management, and EXCOR patients are at high risk for stroke. Neurological dysfunction was reported in 29% of children and is the leading cause of death for EXCOR patients [93].

There is a lack of published data on incidence, rate, and distribution of clotting specifically within the VAD itself. Our colleagues at CHOA tabulate incidence of thrombosis but so far the data has not been analyzed. Here we quantify and analyze the thrombosis incidence in pediatric Berlin Heart EXCOR patients.

3.3.2 Methods

Pump records were obtained for CHOA patients without any link to patient information (n=4). The records were tabulated with pen and paper and were first digitized. The log sheets were provided by Berlin Heart. The EXCOR is divided into 11 sections (Fig 3.15). Deposits were noted with a letter in the corresponding section that they were observed, and for analysis purposes the letters were assigned a number (Table 3.3). Increasing value corresponds roughly with increasing surface area. If more than one deposit was noted in an area of the same type, the formula 1+0.1·(incidence) was applied. If more than one deposit of different types were noted in the same area, the values were summed. Notes were taken every couple of hours during support.

Pump performance was also indicated for both eject and fill as being in one of three categories: 80-100%, 50-79%, or $\leq$ 49%.

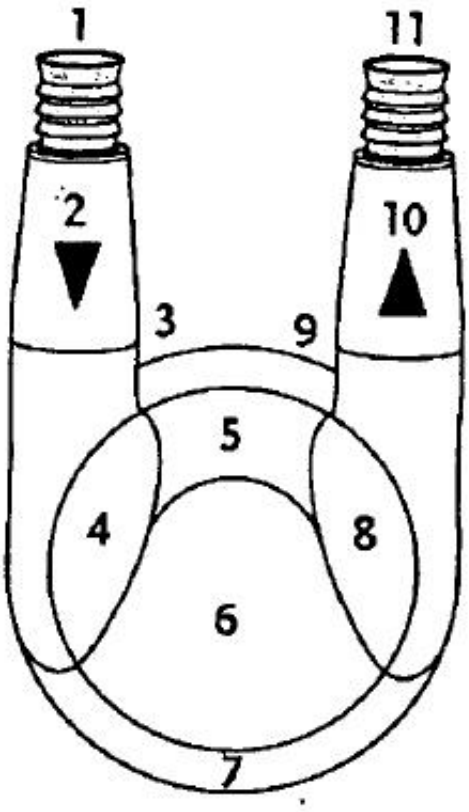

Figure 3.15: EXCOR Pump with labelled sections. The log sheet lists descriptions of each area as follows: 1 transition inflow cannula-inflow connector; 2 only on pumps with PU valves: inflow stub in front of inflow valve; 3 inflow valve; 4 inflow stub behind inflow valve; 5 area between inflow and outflow stubs; 6 remaining area of blood chamber; 7 transition blood chamber-membrane (directly above the reinforcement ring); 8 outflow stub in front of outflow valve; 9 outflow valve; 10 only on pumps with PU valves: outflow stub behind outflow valve; 11 transition outflow connector-outflow cannula.

Table 3.3: Clot cataloging description. Thrombi observed on the EXCOR were categorized by morphology. For analysis, each type was assigned a number, with increasing value corresponding with increasing severity.

Letter	Number	Description
p	1	Small punctual deposit
P	2	Large punctual deposit
a	3	Small area of deposit
A	4	Large area of deposit
f	5	Small strand (often fibrin deposit)
F	6	Large strand (often fibrin deposit)
t	7	Small thrombus
T	8	Large thrombus

One-way ANOVAs were performed in MATLAB to look for significance across pump sections.

3.3.3 Results

Four patients were analyzed. Patients were randomly assigned a number 1-4 and will be subsequently referred to as Pt 1, Pt 2, Pt 3, and Pt 4. The incidence of thrombosis for each patient over the duration of their support is shown in Fig 3.16-3.19 in stacked area plots.

Pt 1 was supported for 87 days. The incidence of thrombosis in Sections 10 and 9 in Pt 1s pump were significantly higher than the rest of the sections (incidence in descending order). Sections 3, 4, 6, and 7 had no incidence of thrombosis.

Pt 2 was supported for 24 days. Sections 3 and 9 had the highest incidence of thrombosis, and were not significantly different from each other, but were significantly different from the rest of the sections. Section 10 had the third highest incidence of thrombosis and was significantly different than the rest of the sections. Section 2 ranked fourth highest and was significantly different than the rest of the sections. Section 5 ranked fifth highest and was significantly different than the rest of the sections. Sections 1, 3, 4, 5, 6, and 11 had no incidence of thrombosis.

Pt 3 was supported for 125 days. The incidence of thrombosis in Sections 10, 9, and 2 in Pt 3s pump were significantly higher than the rest of the sections (incidence in descending order). Section 6 was the only section with no incidence of thrombosis.

Pt 4 was supported for 134 days. The incidence of thrombosis in Sections 6, 3, 9 in Pt 4s pump were significantly higher than the rest of the sections (incidence in descending order). The incidence of thrombosis in Sections 2 and 8 were not significantly different from each other, but were significantly different than the rest of the sections (lower than 6, 3, and 9, and higher than 1, 4, 5, 7, 10 and 11. Section 11 was the only section with no incidence of thrombosis.

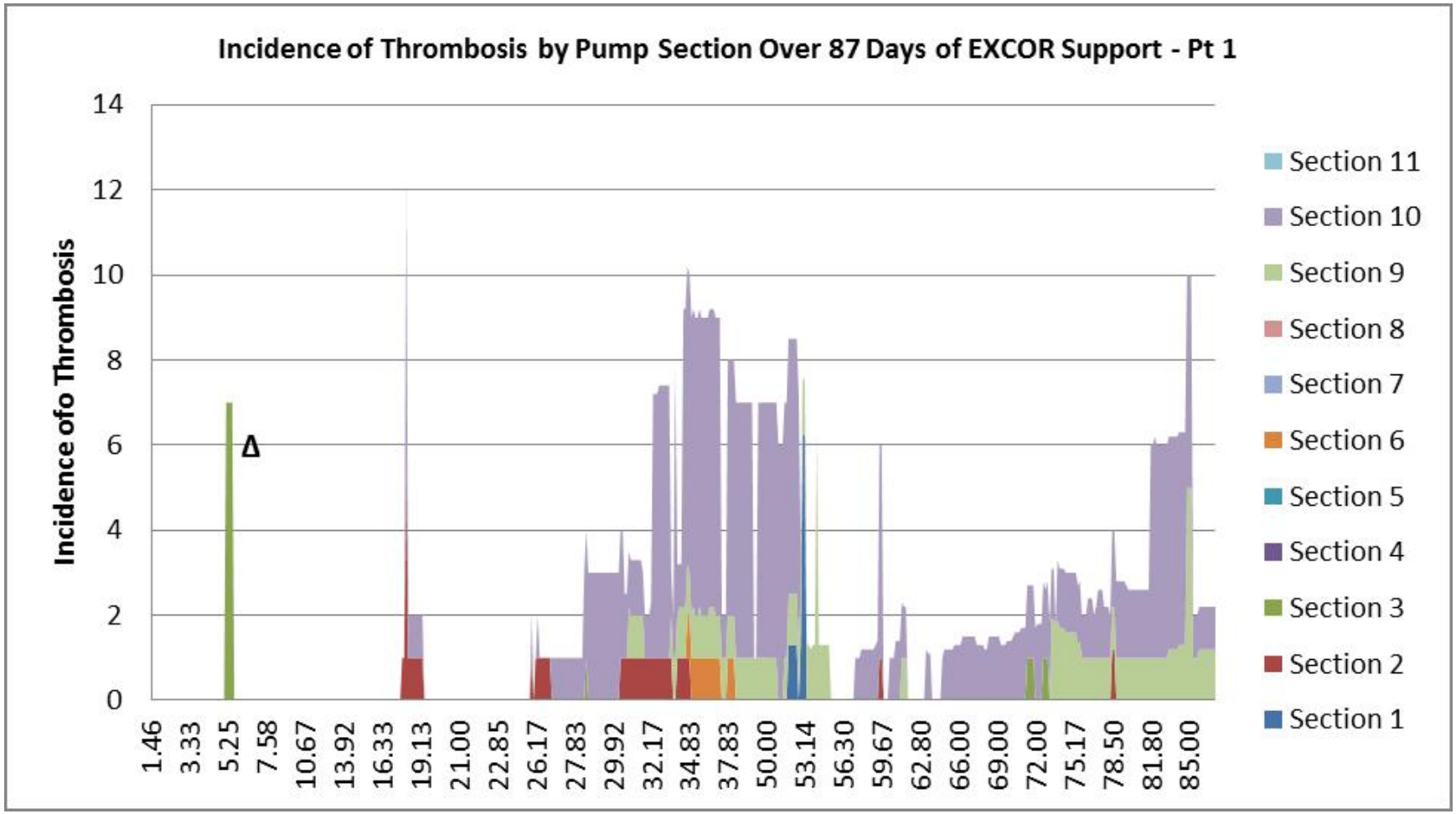

Figure 3.16: Pt 1 incidence of thrombosis. Incidence is represented over time by stacked area. Each pump section is a different color. The δ symbol indicates a pump change.

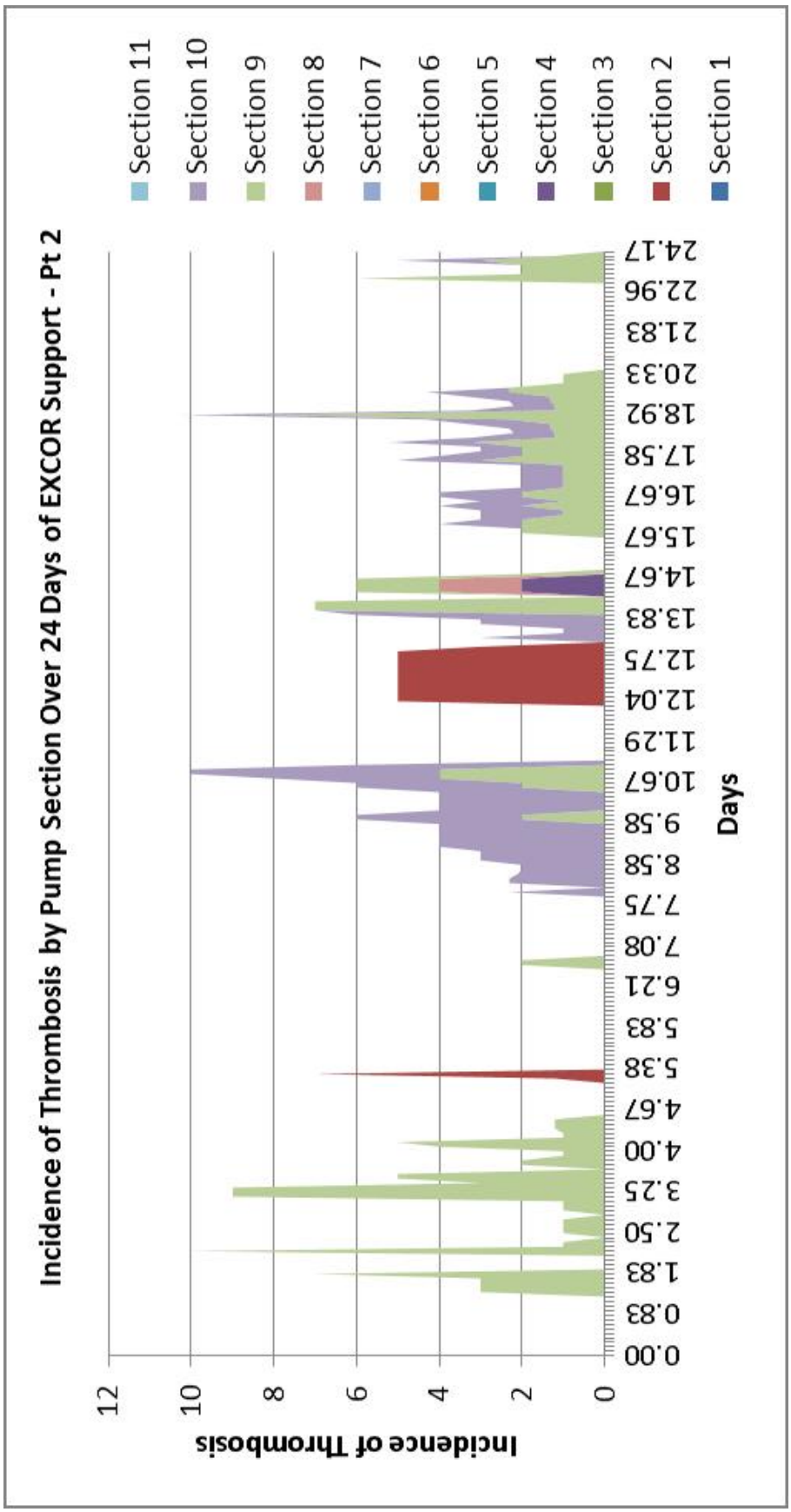

Figure 3.17: Pt 2 incidence of thrombosis. Incidence is represented over time by stacked area. Each pump section is a different color.

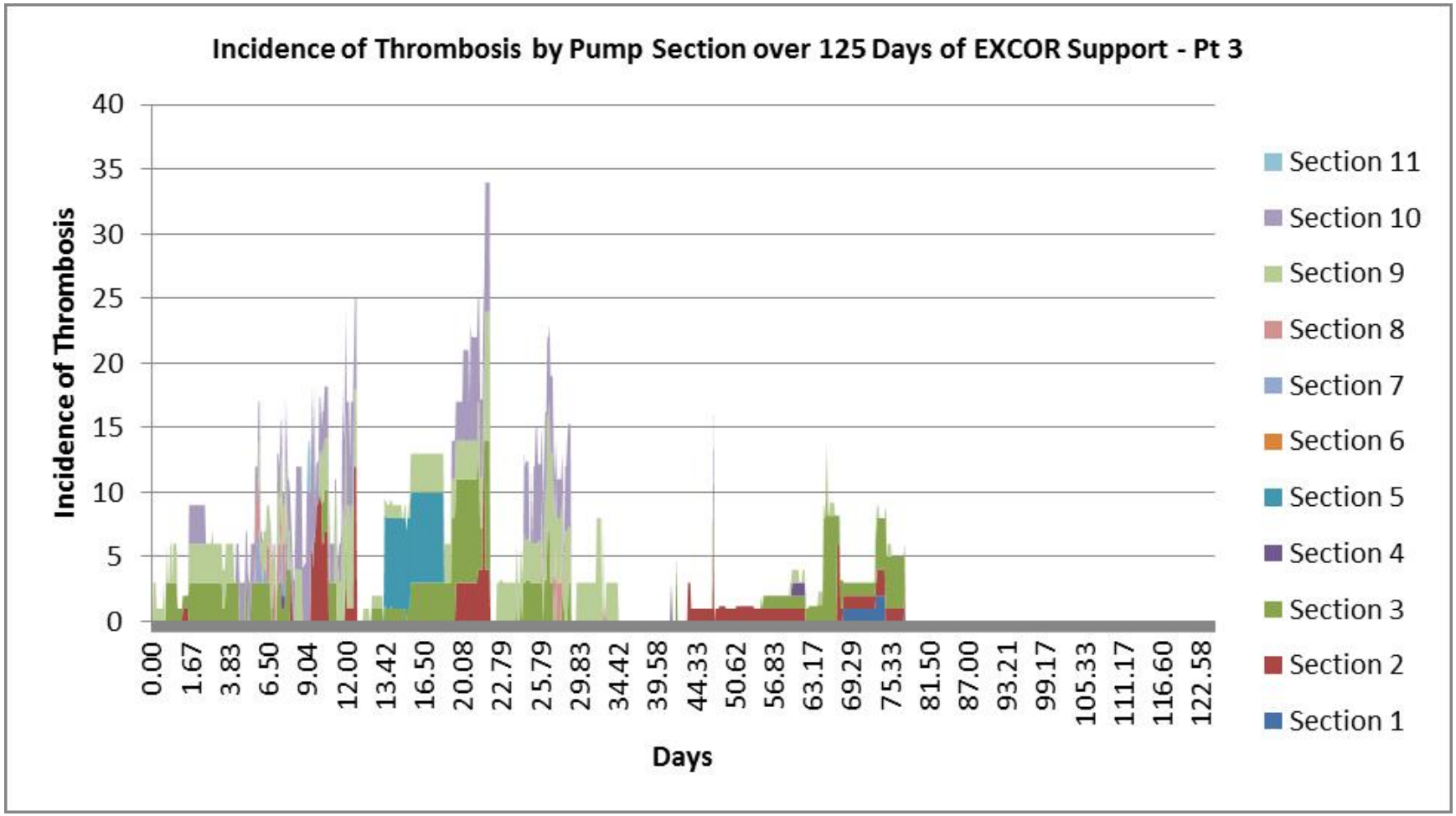

Figure 3.18: Pt 3 incidence of thrombosis. Incidence is represented over time by stacked area. Each pump section is a different color.

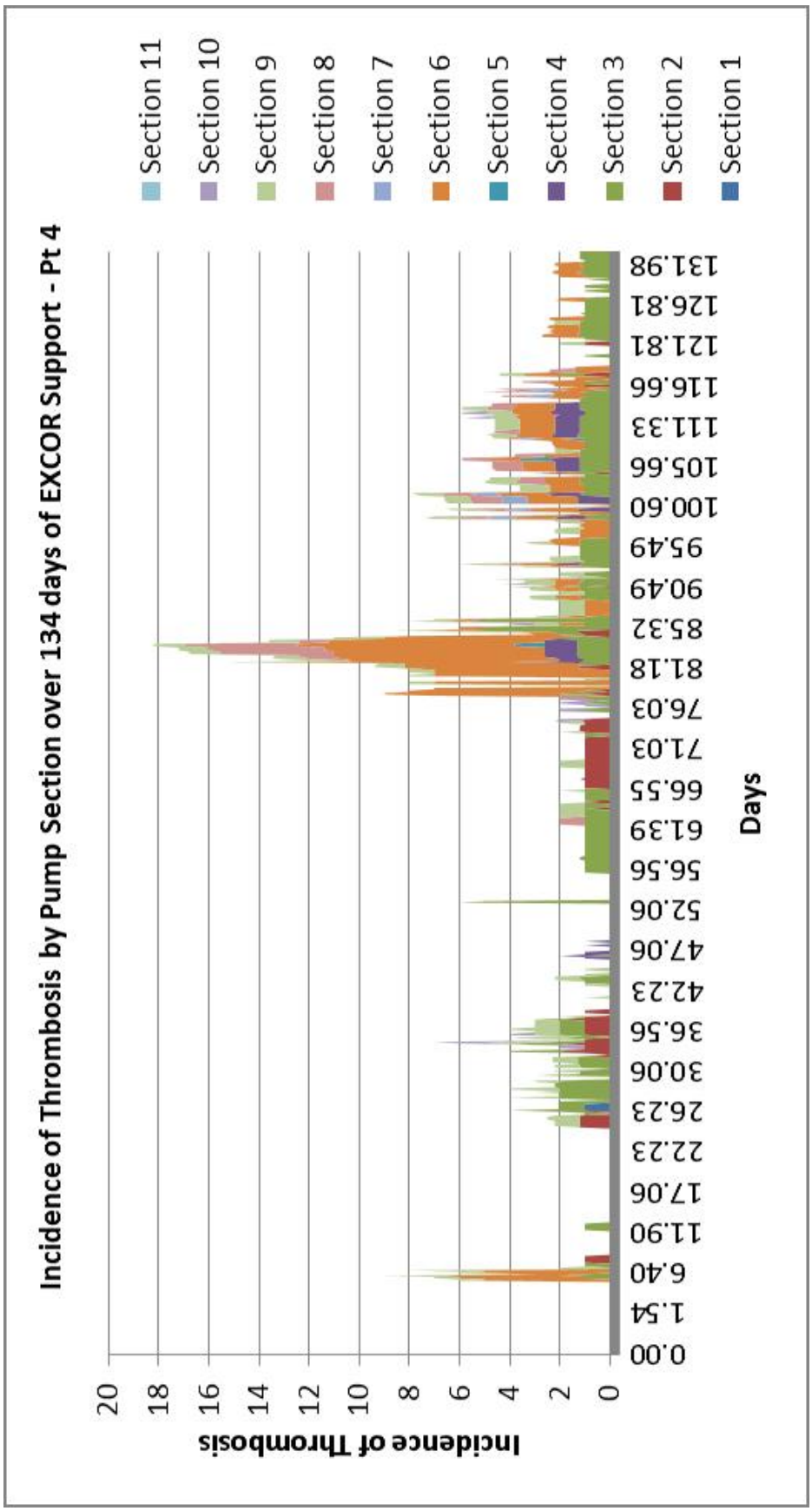

Figure 3.19: Pt 4 incidence of thrombosis. Incidence is represented over time by stacked area. Each pump section is a different color.

3.3.4 Discussion

Here we have analyzed incidence of pump thrombosis by area for four patients supported by the Berlin Heart EXCOR over a range of 24 to 134 days. In 3/4 patients, the pump section 10 was very thrombogenic, and significantly so over the rest of the sections. In the remaining patient, section 6 was the worst, which was surprisingly low in incidence for the others. Sections 1 and 11 were consistently low in thrombosis across all four patients. Sections 9 and 10 are on the outflow valve. The inflow valve sections were not nearly as thrombogenic as the outlow sections, and in some cases did not thrombose at all. This is possibly due to activation of platelets or coagulation cascade during travel through the pump.

The qualitative thrombotic behavior of the pumps is quite remarkable. Embolus is extremely common, and likely contributes to the high risk of EXCOR stroke. In addition, it is rare that one section begins to thrombose alone, and often multiple sections germinate thrombosis together. This is perhaps due to an elevation in the coaguable state of the patients blood. The difference in section performance is also interesting. The fact that some sections are much worse than others point to issues with flow potentiated thrombogenicity, since the material surfaces are controlled for. It is also of note that spikes in thrombotic behavior rarely cause pump changes.

The marked difference in pump behavior of Pt 4 vs Pt 1-3 could be easily attributed to pump size or flow rate, but at this point this information is unavailable to us, and the root cause remains a mystery. In the future, a more in depth analysis of patient-related data, such as flow, pump size, and incidence of deleterious events would be of great use.

CHAPTER 4

IN VITRO SIMULATION OF DEVICE THROMBOSIS

4.1 Background

As we have established long-term perfusion methods as described in Chapter 2, we set out to recreate thrombosis directly in devices. We began with the ECMO connectors and Sorin Revolution centrifugal pump so that we could compare with the data and samples we have collected as detailed in Chapter 3. Then we ran a novel pulsatile pump in a preclinical preliminary *in vitro* test.

There is a great need for improved guidance of device design and device testing that incorporates flow, surfaces, and clinically relevant endpoints. Thus, the establishment of a reliable method to recreate, and therefore explore ways to prevent, bulk device thrombosis *in vitro* opens up new ways to approach device design.

4.1.1 ECMO Connectors

Through collection and analysis of clinical ECMO circuits, we have identified the tubing connectors as a major contributory source of thrombosis in ECMO. This study is detailed in Chapter 3. Briefly, for patients with cardiopulmonary failure, extracorporeal membrane oxygenation (ECMO) offers mechanical life support. The majority of ECMO patients are pediatric and neonatal ($\leq$ 30 days old), though the adult patient population has surged since 2009 due to H1N1 infection and has remained steady [69]. ECMO presents clinical challenges as it is burdened by both thrombotic and hemorrhagic complications [69, 81, 82]. Study of ECMO is difficult and is often limited to a case by case procedure. Potential bench-top models are limited by time and volume. We have developed an *in vitro* system that addresses these problems with a recirculating, high-volume system that can run exper-

iments for 24 hours and longer. Here we offer an *in vitro* loop demonstrating cabability to mimic ECMO connector thrombosis.

4.1.2 Sorin Revolution

While we were collecting clinical ECMO circuits, there was a change from roller pumps (COBE Century) to centrifugal pumps (Sorin Revolution). The Sorin Revolution has a stainless steel bearing shaft. In 100% of clinical circuits collected, the shaft exhibited thrombus coverage, and in some cases, large thrombus grew from this nidus into the pump. Collection and analysis of these circuits is detailed in Chapter 3. Here we also present *in vitro* recreation of a centrifugal pump circuit and validate it by similarity to clinical results.

4.2 Methods

The methods here are largely similar to those discussed in detail in Chapter 2. These methods will be briefly described here.

4.2.1 Perfusion

Whole porcine blood was collected from a local abattoir via direct collection of blood from the aorta into a clean container. The blood was immediately transferred into a jar with anticoagulant to provide a final concentration of 3.5 U/mL heparin. The blood was further treated with glucose (4.4 mmol/L), Sigma-Aldrich, Saint Louis, MO), L-glutamine (2 mmol/L), Sigma-Aldrich), and an antibiotic/antimycotic (10 mL/L, Gibco).

The whole blood was circulated in a mock loop. The loop design was dependent on the device of interest.

ECMO Connectors

Tubing and connectors were ordered from Medtronic (Minneapolis, MN). Bypass pumps (Century, Mesa, AZ) were supplied by our colleagues at Childrens Hospital of Atlanta at

Egleston. Heparinized porcine blood collected from a local abattoir was used. Circuit volumes were in the range of 150 300 mL. Heparin was dosed 6 and 12 hours after collection to maintain a concentration of 3.5 U/mL. Three ECMO connectors were assembled in series, with ports for access and pressure relief.

Circuits were perfused at a flow rate of 500 mL/min. After 24 hours, the circuit was drained of blood and inspected.

Sorin Revolution

The centrifugal pump loop required allocation of resistance to ensure clinically relevant pump performance. The circuit therefore consisted of a Sorin Revolution centrifugal pump, bladder (Better-Bladder, Circulatory Technology Inc.), two sizes of ECMO tubing to provide said resistance, connectors (Medtronic), and a pressure transducer. The total volume of the loop was 350 mL. The pump was set to 2000 rpm, and the circuit pressure was set to 80-90 mm Hg. On average the circuit flow rate corresponded to 2.4 lpm with the pump set to 2000 rpm. Heparin was dosed every 12 hours to maintain the bolus concentration. At 6 hours, 12, hours, and 24 hours during circulation, the pump was briefly stopped and examined for thrombus formation by inclusion of an air bubble, which was shifted over the area of interest. After examination for thrombus formation, the air bubble was removed from the circuit. After 48 hours of perfusion, the system was drained and examined for adherent thrombi. Location of thrombi was recorded, and samples were preserved in formalin.

4.2.2 Histology

Any samples of interest were preserved in 10% formalin. Samples were embedded, sectioned, and stained with Carstairs' stain in order to differentiate between fibrin and platelets, and to compare to histology of clinical samples.

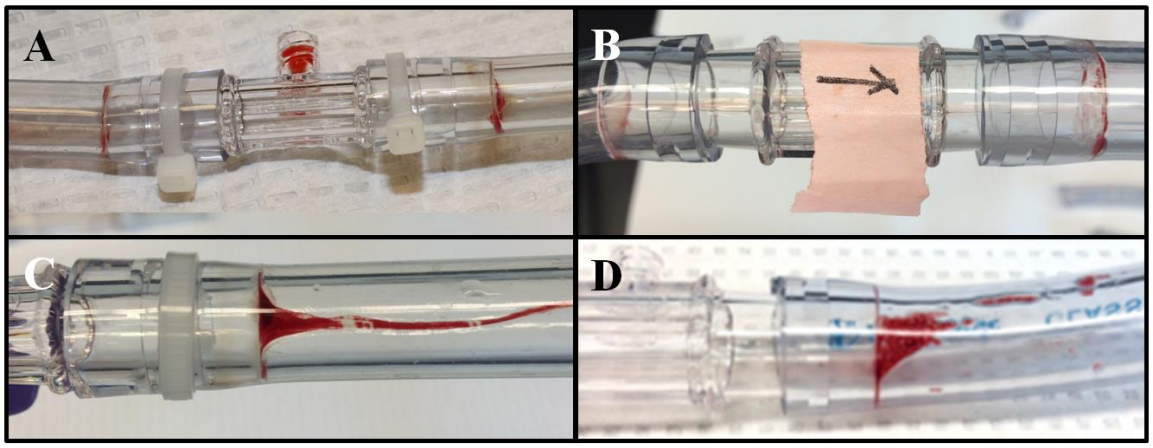

Figure 4.1: Clinical and *in vitro* thrombus sample comparison. A: Typical clinical TCJ thrombus. B: thrombus observed at TCJs after *in vitro* perfusion. C: Example of growth from a clinical TCJ. D: Growth was also observed *in vitro*.

4.3 Results

4.3.1 ECMO Connectors

Clots formed at the junctions formed by the tubing and the connectors (27/18, 150%, p=0.0239) (Fig 4.1). These clots were found to be fibrin rich, which is consistent with the composition of ECMO clots (Fig 4.2).

4.3.2 Sorin Revolution

Large-scale thrombus formed in all of the *in vitro* centrifugal pumps after circulation for 48 hours (n=5, 100%) (Fig 5). The stainless steel bearing from this experimental loop was covered with thrombus in all cases after 24 hours (n=2). The thrombus then extended from that point and grew more extensive over the next 24 hours. After 48 hours of perfusion, the thrombus extended to cover the tops of the vanes at the pump head inlet. The gross appearance of the thrombus in the experimental pump heads was similar to those found in the clinical pumps (Fig 5). Histological analysis of the *in vitro* thrombus revealed a strikingly similar predominance of blue indicating a predominance of platelet-based thrombus (Fig 6). In both clinical circuits and *in vitro* circuits, the thrombus was adherent. In the *in vitro*

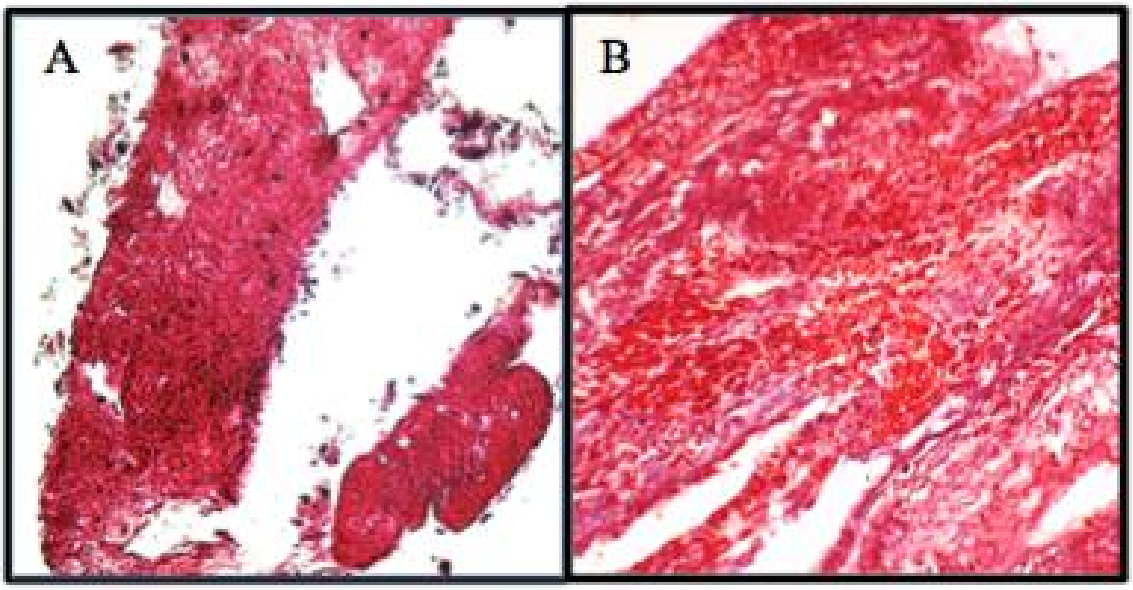

Figure 4.2: A: *In vitro* sample histology. B: Clinical sample histology. Carstairs stains red blood cells yellow to clear, fibrin red, muscle deep red, collagen bright blue, and platelets blue-gray to navy.

circuit, no embolization was observed.

4.4 Discussion

Ensuring clinical relevance of *in vitro* device assays is a current challenge in the biomedical engineering research field. Here we have demonstrated methods capable of simulation of device thrombosis that exhibits gross morphological and histological validation with clinical samples.

In the case of the ECMO connectors, a simplified loop potentiated thrombosis only at the TCJ, and not in the rest of the tubing of the circuit. The location, gross morphology, and histology were all in accordance with clinical samples.

In the case of the Sorin Revolution, we were able to recreate the large-scale thrombus via perfusion of whole porcine blood in a recirculating loop for 48 hrs. The macroscopic experimental thrombus matched the location and composition of the clinical thrombus. The *in vitro* experiment allowed us to observe thrombus as uniformly present at the shaft within

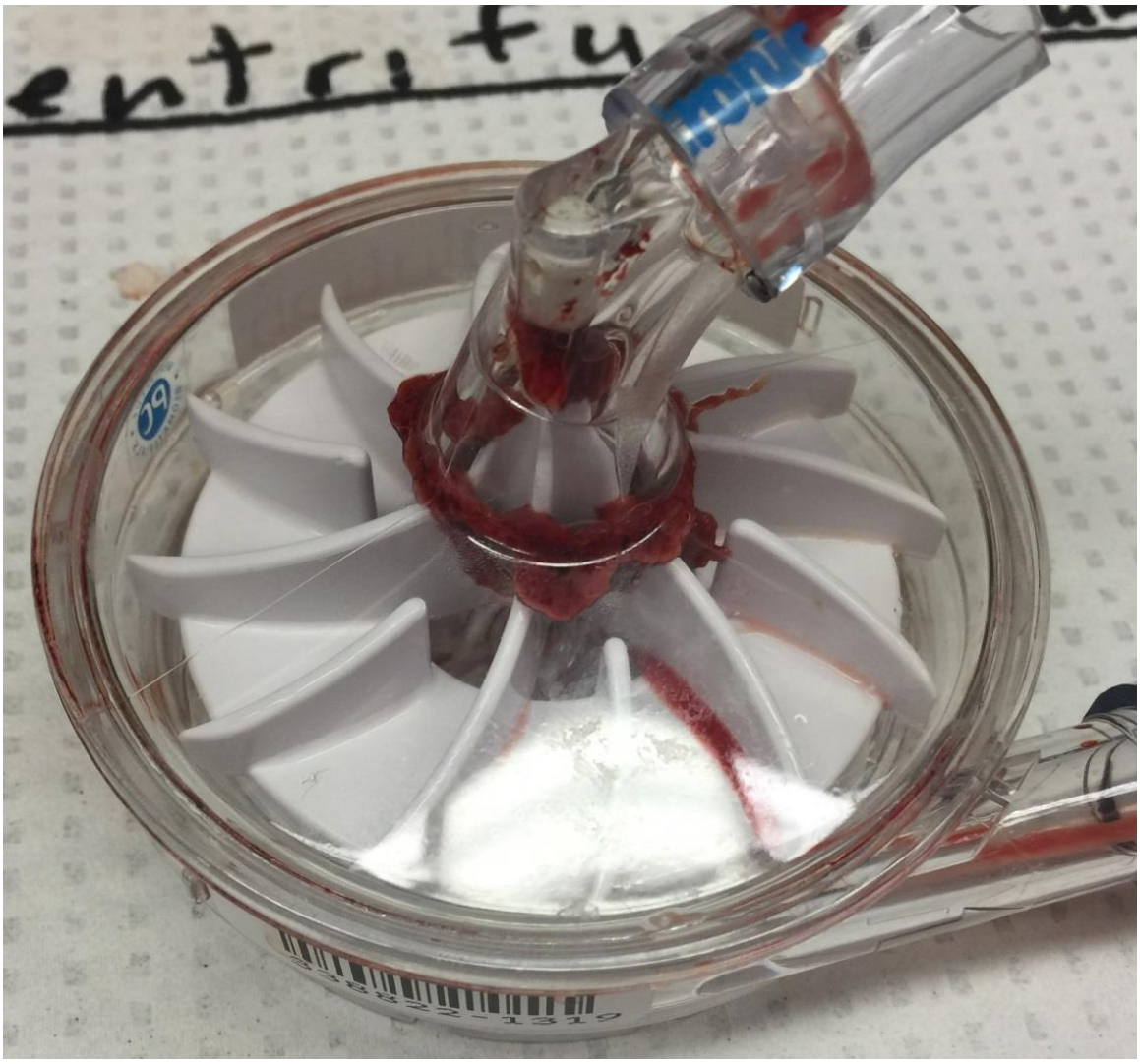

Figure 4.3: *In vitro* centrifugal pump thrombus grows from the shaft into the pump and is morphologically similar to clinical pump thrombus.

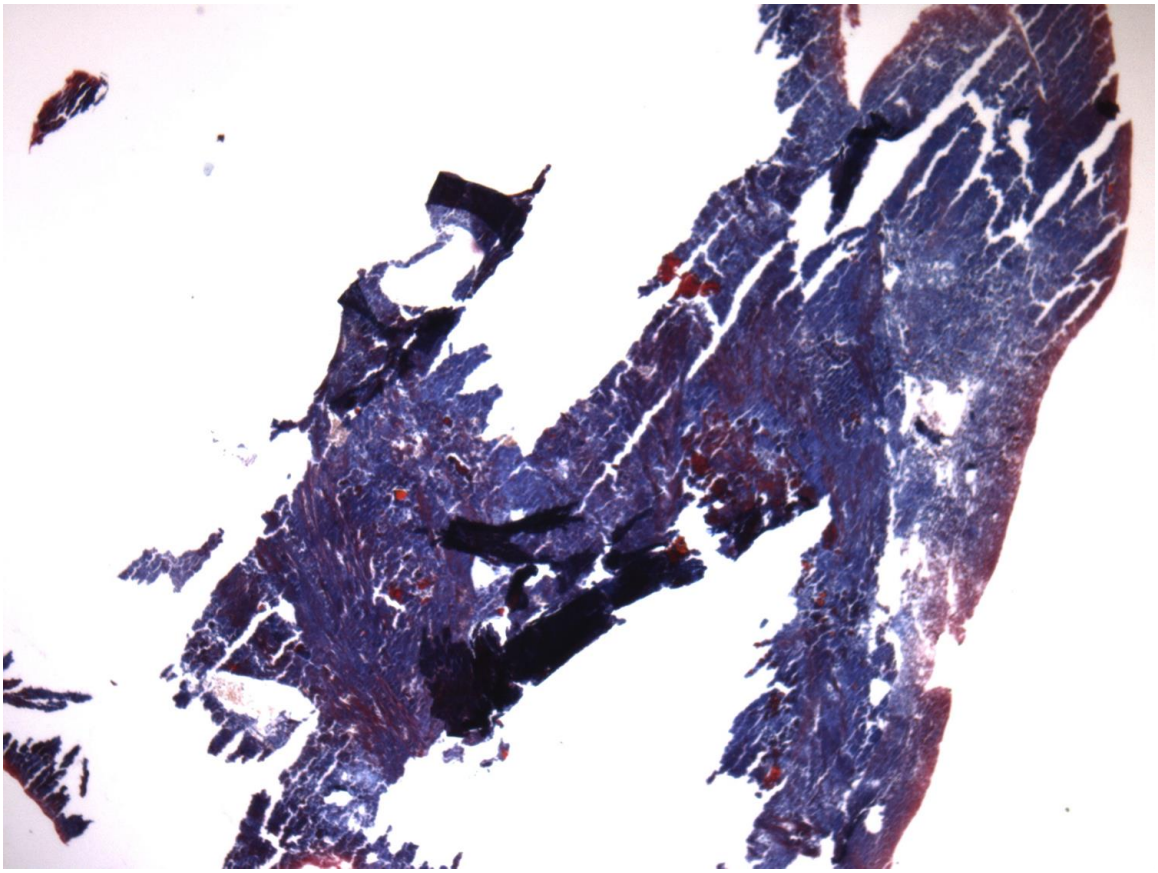

Figure 4.4: *In vitro* pump thrombus histology. Carstairs stains red blood cells yellow to clear, fibrin red, muscle deep red, collagen bright blue, and platelets blue-gray to navy. This image is at 10x magnification. Thrombi were of mixed composition of platelets and fibrin in distinct regions. In this image, 88% of pixels are blue and 12% of pixels are red.

24 hours that grew in extent over the inlet in the next 24 hours.

This system can be used to develop potential preventative methods for ECMO thrombosis and centrifugal pump thrombosis. Furthermore, since it is a high-volume recirculating system that can be run for an extensive period of time, this assay could be used to assess other blood-contact medical devices in an *in vitro* setting, as well as to test the thrombogenicity of novel devices, serving a crucial role in the progression of device design.

CHAPTER 5

DEVICE REDESIGN FOR IMPROVED THROMBOGENICITY

5.1 ECMO Connector Prototype

5.1.1 Introduction

Flexible tubing is commonly used for fluid transport in a wide variety of applications. Connectors for flexible tubing facilitate construction of tubing lengths and loops and can provide access to the fluid. Currently, flexible tubing connectors require expansion of the tubing around the connector, causing diameter changes.

Extracorporeal membrane oxygenation (ECMO) is a form of life support and consists of a flexible tubing circuit connected by such connectors. Clotting in the circuit is a burdensome clinical problem and connectors have long been recognized as a contributing source. As discussed in Chapter 3, we noticed that the sudden expansions and contractions created by the connectors potentiated thrombus formation. In Chapter 1, we tested the materials at these expansions and contractions across low, physiological, and high shear regimes and identified that the tubing material ranked high for low-shear thrombogenicity. We subsequently hypothesize that the elimination of the low-shear PVC exposure steps would greatly reduce thrombus formation in the circuit, and that it would be advantageous to procure a connector that prevents diameter changes and ensures smooth surfaces.

We have created two iterations of a prototype that removes the low-shear regime and tested them against the existing connector. The first version is a hollow acrylic tube that allows for connection of two ends of tubing. The tubing is secured via glue. This prototype provides no connector lumen, so while it demonstrates the proof-of-concept, it would not solve clinical challenges need to have a port for drug infusion. for access to blood. The second prototype has a lumen and the tubing is inserted and secured with glue so that it is

flush against the lumen edge. This solves the problem of the need for access, however rapid prototyping methods introduce potential thrombotic challenges such as rough surfaces.

We tested the first iteration of the prototype with our long-term recirculating *in vitro* methods that are known to simulate ECMO connector thrombosis as detailed in Chapter 4. We have also tested the second prototype against the current connector in a flow visualization model.

5.1.2 Methods

Prototype Creation

Input from clinicians and consideration of constraints led to an objectives list for the connector prototype:

Attributes List:

1. The connector should not potentiate thrombus
   1.1 The connector should not cause zones of shear extrema
   1.2 The connector should not employ known thrombogenic materials
      1.2.1 The connector should not introduce new materials into contact with blood
2. The connector should be safe
   2.1 The connector should not separate under application of extreme force
   2.2 The connector should be nontoxic
3. The connector should be able to be used in the clinic
   3.1 The joinging of the tubing and connector should be able to be done by clinical staff on site in the event of an emergent patient complication
      3.1.2 The joining of the tubing and connector should require very few steps
   3.2 The connector should allow for access to blood via a female Luer Lock
   3.3 The connector should facilitate circuit assembly
      3.3.1 The connector should be available in multiple inner diameter sizes in ac-

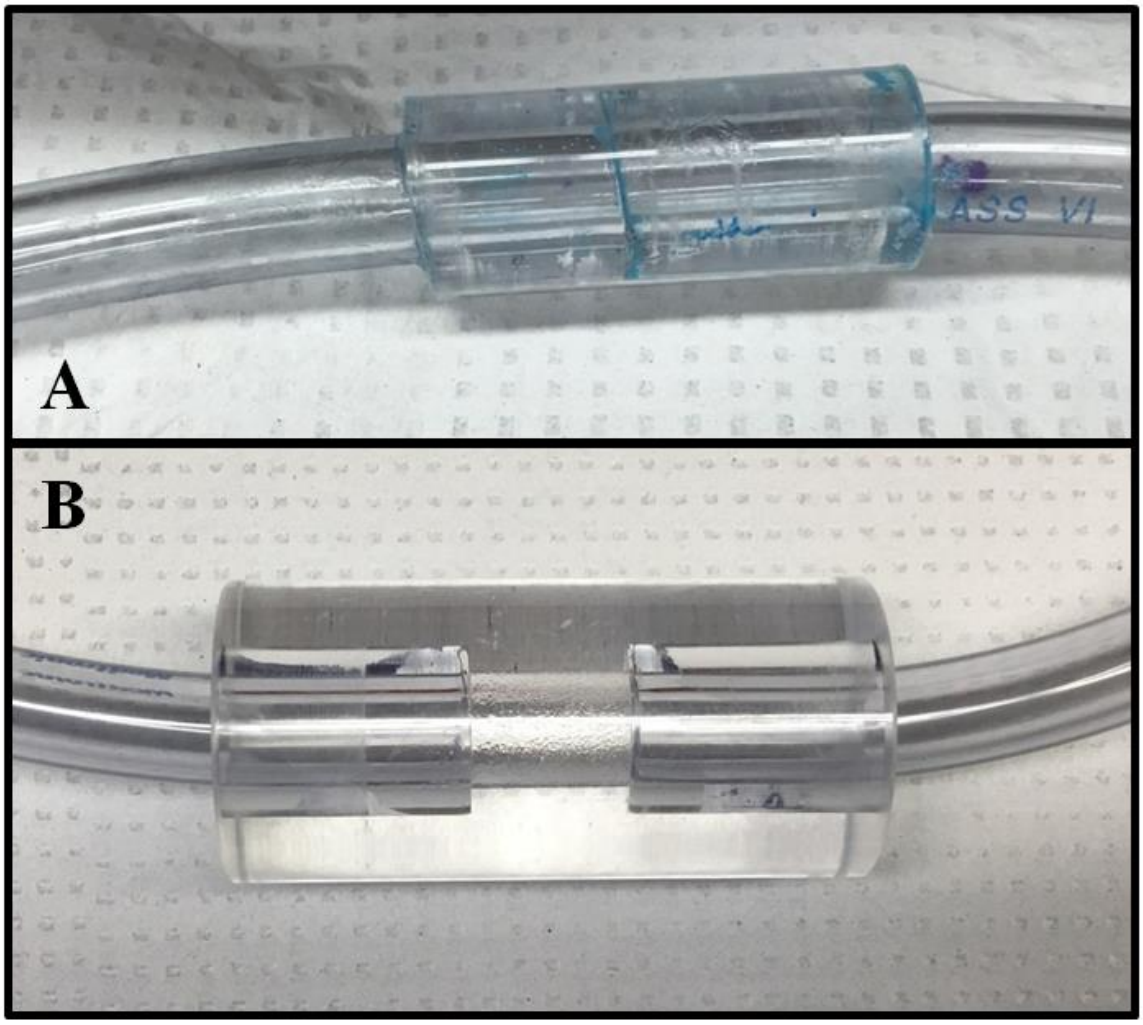

Figure 5.1: Prototypes. A: Straight tube prototype with the tubing ends butting up against each other. B: Connector with lumen.

cordance with existing medical devices

3.3.2 The connector should be available in an expansion that introduces a non-thrombogenic inner diameter change

3.3.3 The connector should be available in an equal "Y" connection to facilitate joining three separate tubing segments of equal inner diameter.

Solid acrylic tubes were machined in order to accomodate the desired interior diameter(s) (ID). The prototypes are shown in Fig 5.1.

Thrombogenicty Study via 96-hour Perfusion

Whole porcine blood was collected into light heparinization (3.5 U/mL) and treated with glucose, L-glutamine, and an antibiotic/antimycotic solution, as described Chapter 1, to ensure blood health during long-term perfusion. Prototype connectors were perfused in series. A control circuit with the current connector model was also perfused in series with the same blood sample. Portions of the circuit tubing was submerged in a water bath at 37 °C to maintain loop temperature. The loop flow rate was 500 mL/min and loops were run for 96 hours total, with replacement with fresh blood ocurring at 48 hrs as discussed in Chapter 1 to account for both adsorption and thrombosis.

Flow Visualization Studies

A loop with a single straight 3/8" connector was assembled and filled with water and perfused via a roller pump. A syringe filled with red dye was attached to a flat needle head and the needle was bored into the tubing upstream of the connector to facilitate dye entry. The flow rate of the loop was 500 mL/min.

5.1.3 Results

Thrombogenicity Study

After 96 hours of perfusion, proof-of-concept prototype connectors were thrombus-free, while control connectors had typical thrombus formation at the connector junctions (Fig 5.2).

Flow Visualization Studies

The CFD of the TCJ discussed in Chapter 3 revealed low shear rates and zones of recirculation created by the connector edge expansion. The connector prototypes eliminate this region.

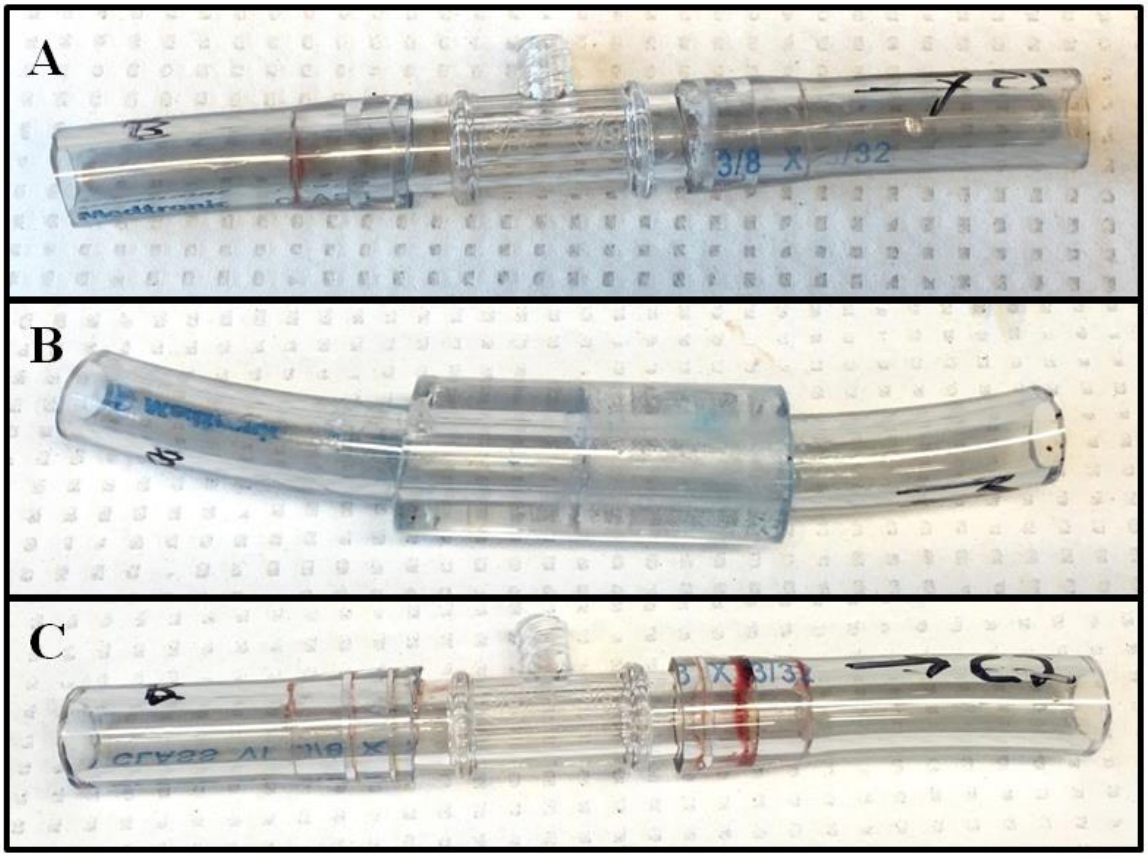

Figure 5.2: ECMO Conenctor prototype perfusion results. A,C: Current connector devices that were perfused in series with the prototype exhbiting typical TCJ thrombus. B: Connector prototype.

Flow visualization via dye confirmed the circulation at the edges of the current connector device (Fig 5.3). The prototype eliminated these discontinuities (Fig 5.3).

5.1.4 Discussion

ECMO connectors are known potentiators of thrombosis as we found in Chapter 3. The current connectors create a discontinuity on both the upstream and downstream sides. Thrombus growth directly co-locates with these discontinuities. In order to prevent thrombosis, we sought to eliminate these discontinuities.

Here we tested two versions of a prototype that both provide a continuous, smooth surface throughout the entirety of the connector. The first prototype connector serves as a proof of concept and demonstrated the feasibility of the approach. The second prototype allows for access to blood, addressing a clinical design constraint, and eliminates the discontinuities.

5.2 Polyvinyl Alcohol as Novel Graft Material

5.2.1 Introduction

Graft thrombosis remains a major complication in the field of surgical vascular reconstruction [97]. Thrombosis results in direct failure of the graft and puts the patient at risk for deleterious consequences. Early thrombosis (1 to 30 days) occurs in 2%-20% of grafts (depending on location) and is likely due to surgical errors or complications [97]. Late thrombosis ($>$ 2 years) occurs at a rate as high as 80% for distal placement.

PTFE and Dacron are the most commonly used synthetic graft materials. Meta-analysis of large-scale randomized comparison studies in various anatomical locations has shown no advantage of one material over the other [98]. All synthetic small diameter grafts (6 mm or less) eventually thrombose [99], and despite decades of research, novel replacement technologies such as cell-lined grafts are still in development. Our results in Chapter 1 predict these outcomes as well, with PTFE ranking high as nonthrombogenic at low shear

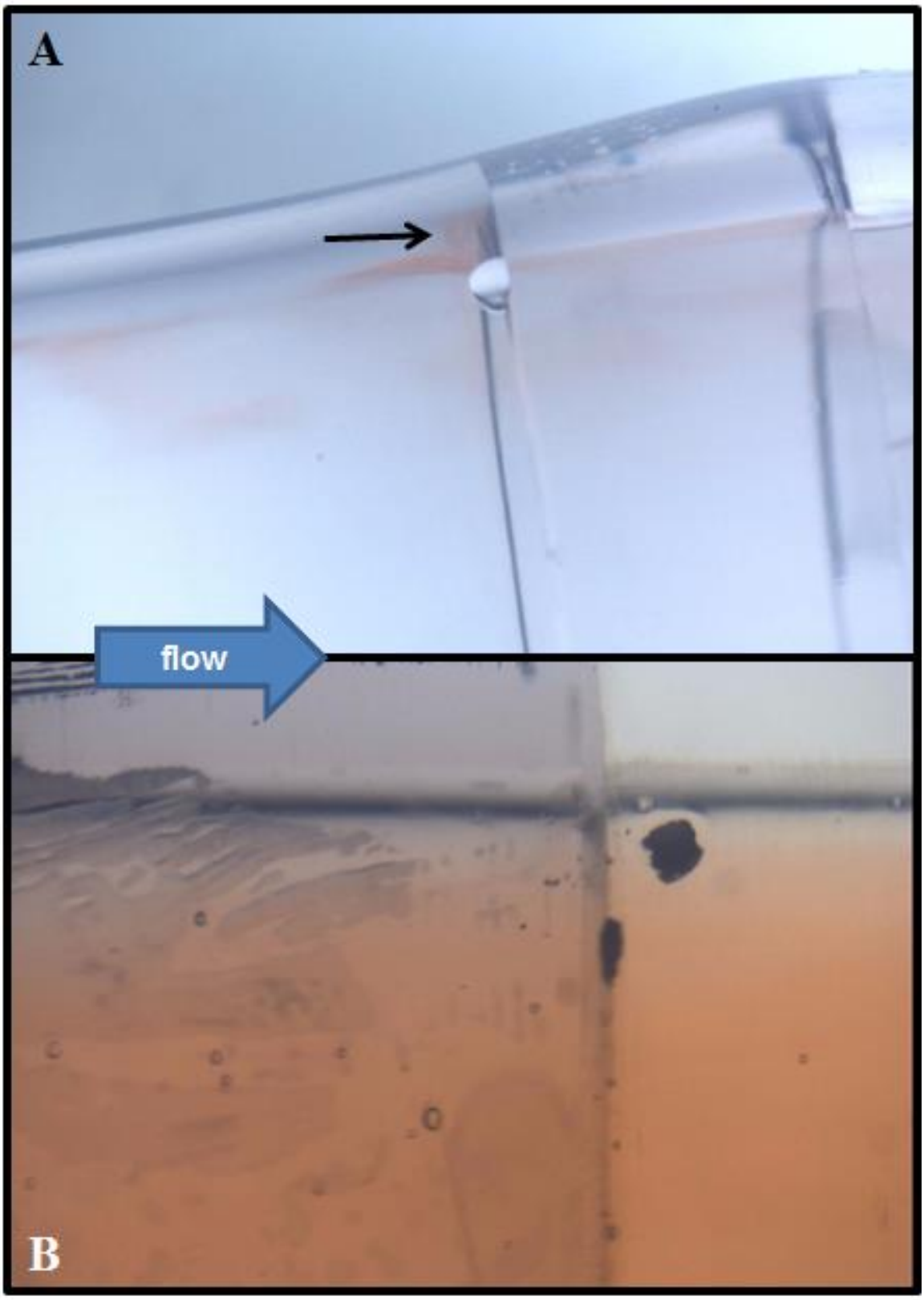

Figure 5.3: Flow visualization. A: Recirculation observed at the upstream edge of the existing connector. B: No discontinuities are observed at the edge of the prototype.

rates, but both PTFE and Dacron ranking highly thrombogenic at high shear rates.

Polyvinyl alcohol (PVA) has been extensively used and studied in the blood-contacting surface field. Hydrogels are generally thought to be biocompatible due to their high water content and soft flexibility [100]. Their mechanical weakness excludes them from ubiquitous applications, but the hydrogel has potential use as a graft material.

Here we use our *in vitro* perfusion loop to compare the thrombogencitiy of PVA with the Dacron and PTFE with an endpoint of macroscopic graft thrombosis after 48 hours of perfusion.

5.2.2 Methods

PVA tubes with inner diameters of 5 mm and 10 mm were sutured into PVC tubes (ID 3/8 or) with 6-0 prolene. Suture holes were sealed from the outside with clear silicon caulk. Care was taken to ensure no risk of contact of caulk with blood. PTFE grafts of 6 mm inner diameter and Dacron grafts of 10 mm inner diameter were also sutured into PVC tubes and circuits were constructed with PVA and either Dacron or PTFE in series (Fig 5.4) and perfused with a roller pump. The larger diameter loop (n = 3) with PVA and Dacron was perfused with wall shear rates of approximately 170 s^{-1} (n=2) and 980 s^{-1} (n=1). The smaller diameter loop (n = 2) was perfused with wall shear rates of approximately 1080 s^{-1}.

Whole porcine blood was collected from a local abattoir via direct collection of blood from the aorta into a clean container. The blood was immediately transferred into a jar with anticoagulant to provide a final concentration of 3.5 U/mL heparin. The blood was further treated with glucose (4.4 mmol/L), Sigma-Aldrich, Saint Louis, MO), L-glutamine (2 mmol/L), Sigma-Aldrich), and an antibiotic/antimycotic (10 mL/L, Gibco).

Post perfusion, the grafts were excised, splayed, and photographed. Any thrombi were preserved in 10% formalin. Histological analysis was done using Carstairs stain.

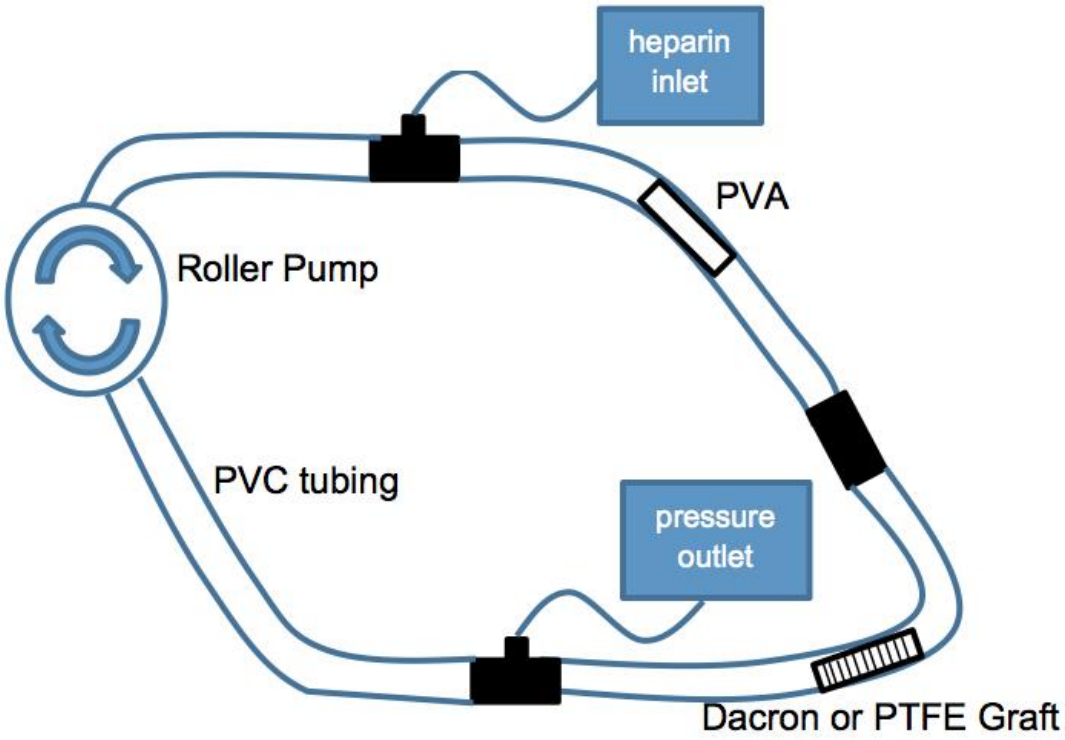

Figure 5.4: Loop setup. PVA, Dacron, and PTFE grafts were sutured into PVC tubing. Heparin was added every 12 hours to maintain the low level initial dose of 3.5 U/mL. A syringe was attached downstream of the grafts to allow for pressure increases in case of graft occlusion.

5.2.3 Results

The higher shear rate Dacron graft formed extensive thrombus while the PVA was clear of bulk thrombus (Fig 5.5). The PVA was slightly smaller in diameter than the surrounding tube and therefore obtained a red color due to the surrounding blood. Dacron grafts also had the same diameter mismatch. Blood did not continually flow past the graft, but filled the space between the graft and the tube. The lower shear Dacron graft did not occlude, but had some thrombus growth, and in one case an annular thrombus formed (Fig 6). The PVA again was relatively clean (Fig 5.6).

The PTFE grafts formed extensive thrombus (Fig 5.7). The PVA grafts in series remained clean (Fig 5.7). There was a better matchup of the PVA-PVC diameters and the PVA at this size was not reddened by blood.

The histological analysis of Dacron and PTFE clots revealed mixed composition of thrombus of both fibrin and platelets.

5.2.4 Discussion

PVA grafts demonstrated improved thrombogenicity over Dacron and PTFE grafts after 48 hours of perfusion in series at low and moderately high physiologic shear rates on the basis of bulk thrombus formation. As expected based on clinical experience, the Dacron graft performed worse at elevated shear rates, and 6 mm PTFE grafts were also highly thrombogenic.

The mixed composition of the thrombi is interesting and perhaps suggests a role of the material surface in platelet and fibrinogen recruitment regardless of shear regime. The annulus formed in the Dacron loop at shears considered too low for vWF unfolding and platelet aggregation [53, 57] yet exhibits high platelet content. This could be due to the recruitment of platelets to the Dacron surface. Alternatively, fibrinous clot could deposit first, then change the shear rate of the environment, potentiating high-shear platelet thrombosis.

Limitations of this study include low power replicates, possible effects of sutures, and

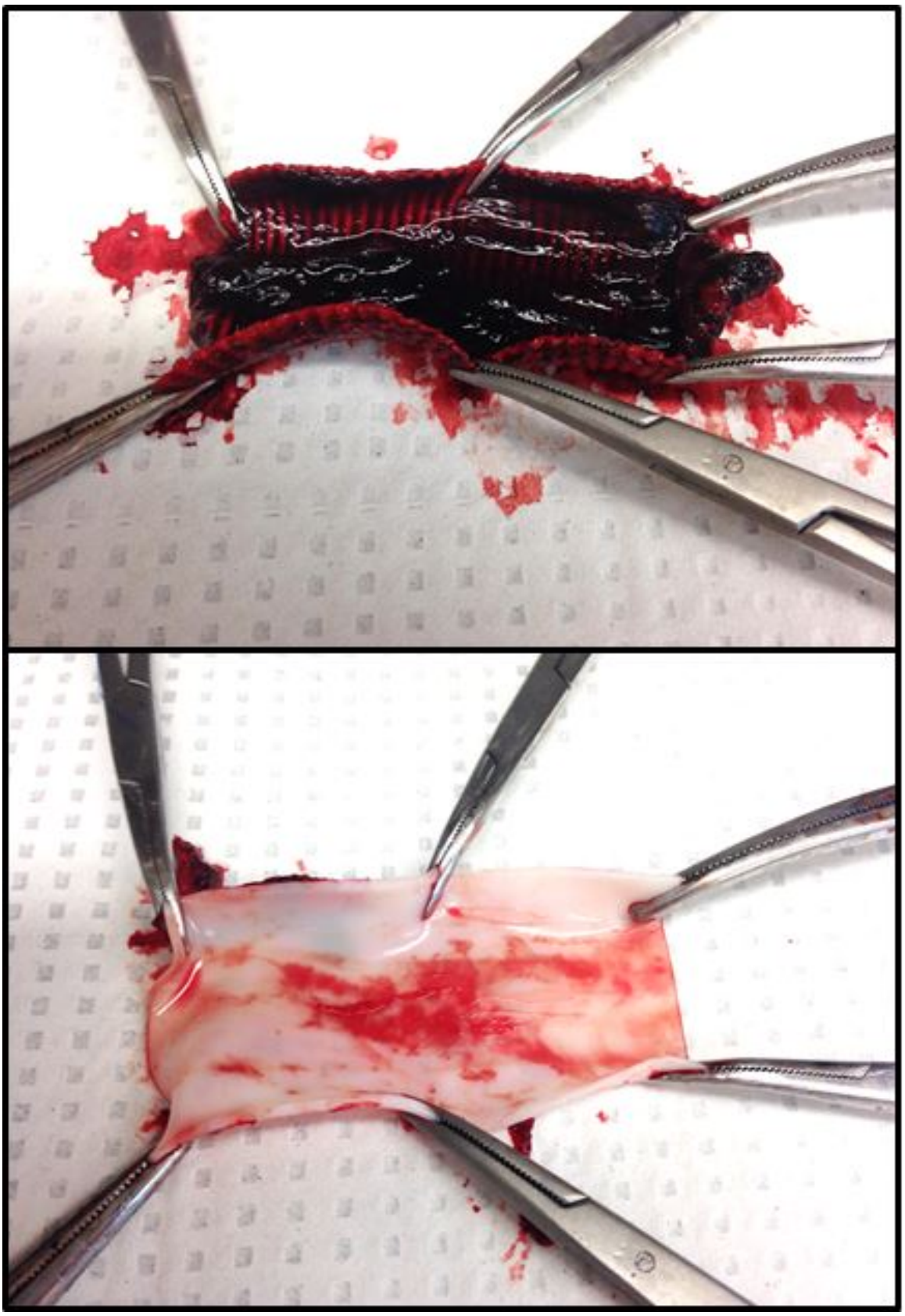

Figure 5.5: Dacron (top) and PVA (bottom) after 48 hours of perfusion with a wall shear rate of 980 s^{-1}.

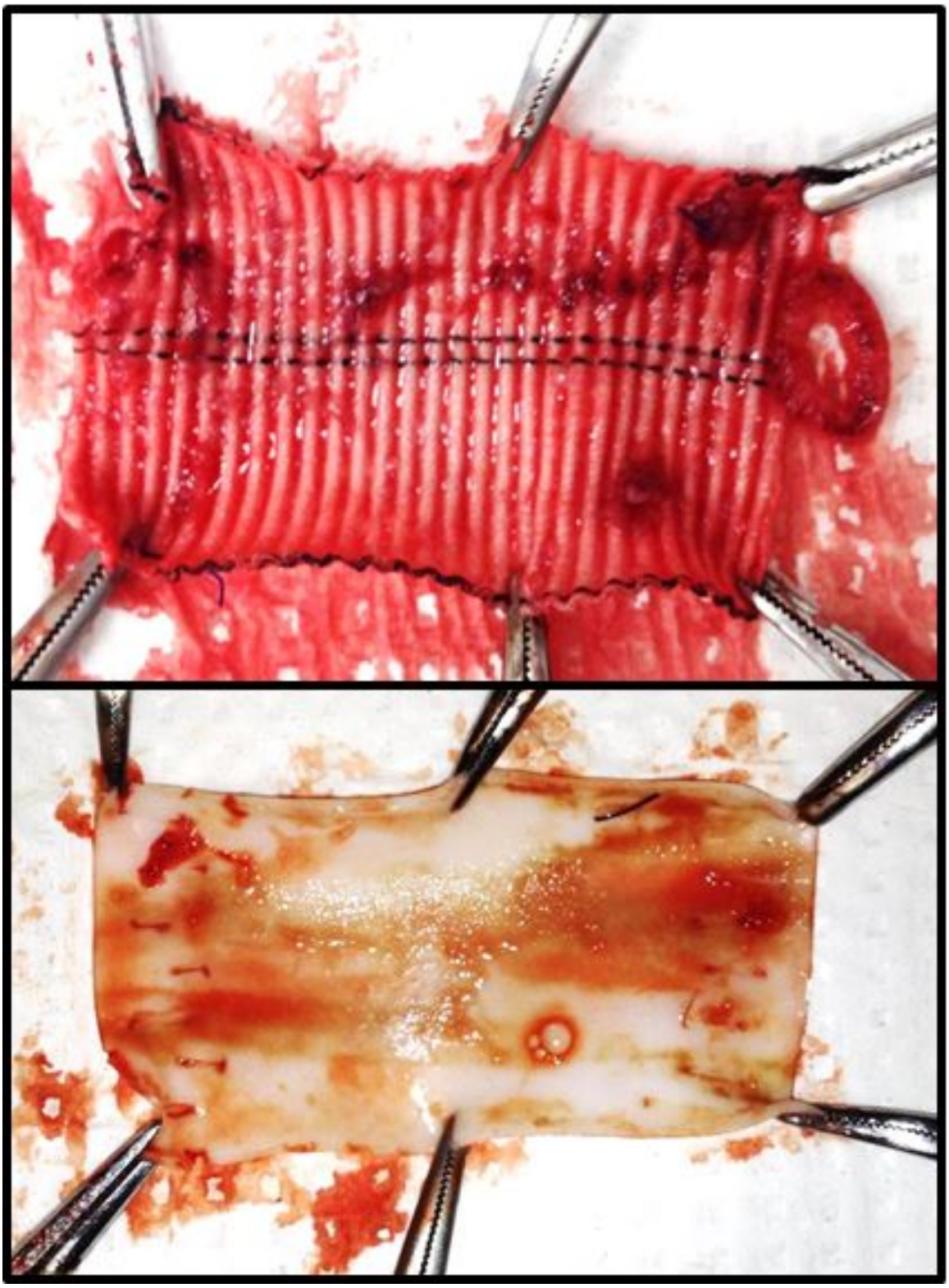

Figure 5.6: Dacron (top) and PVA (bottom) after 48 hours of perfusion with a wall shear rate of 170 s^{-1}

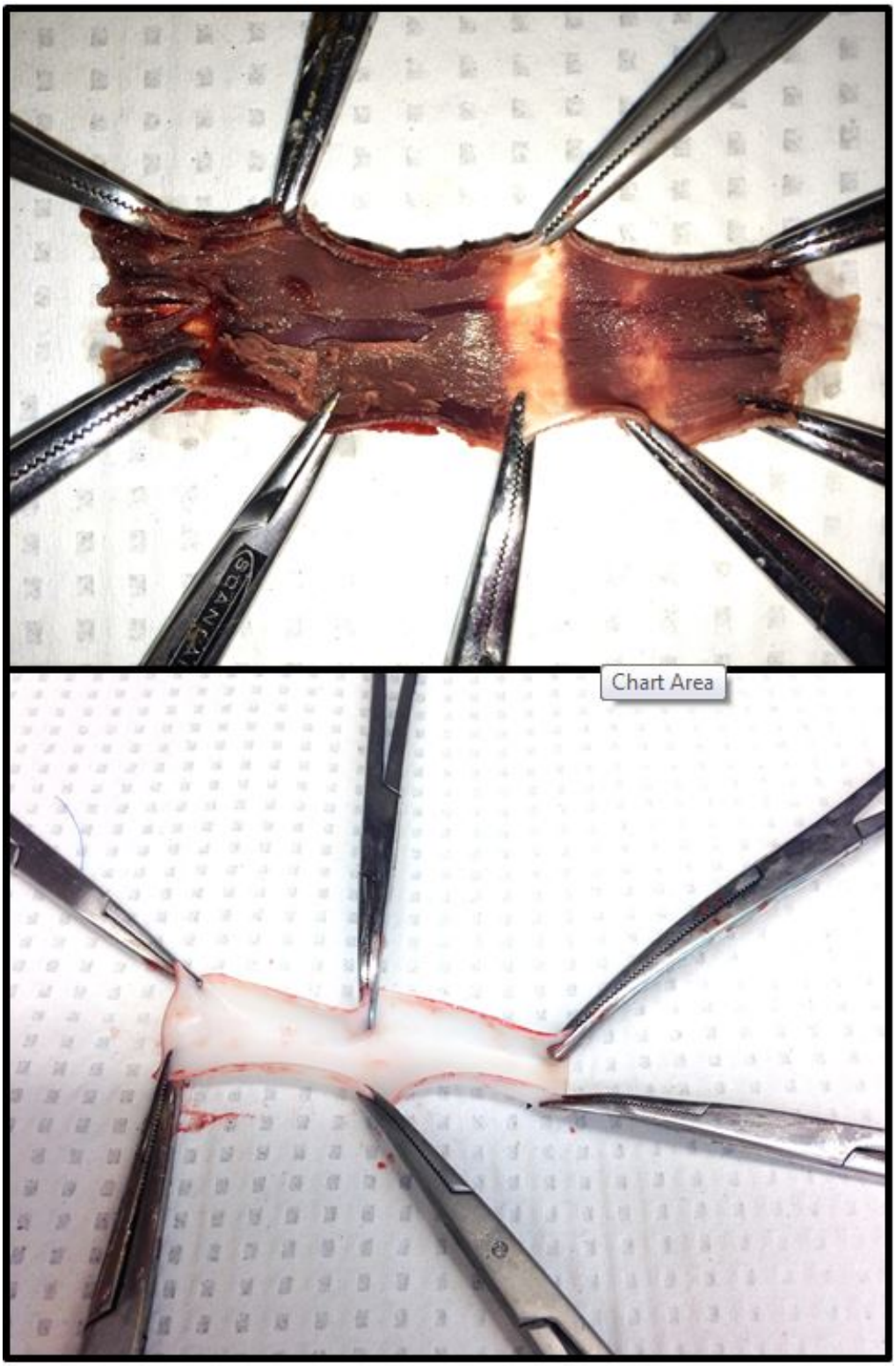

Figure 5.7: PTFE (top) and PVA (bottom) after 48 hours of perfusion with a wall shear rate of 1080 s^{-1}.

no capture of emboli.

PVA was less thrombogenic than Dacron and PTFE with a bulk thrombosis endpoint. These results therefore ultimately promote PVA as a vascular graft material.

CHAPTER 6
CONCLUSIONS

6.0.1 Results

In this thesis, we have attacked the problem of blood-contacting medical devices from multiple avenues.

We designed and perfused flow chambers for 96 hours to elucidate the effects of material surface and shear rate on bulk thrombogenicity. From these results, we developed a thrombogenicity ranking and were able to make recommendations for device design. We also found no relationship among the currently used assays for thrombogenicity and the bulk thrombogenic performance of a material. The histological analysis revealed mixed platelet and fibrinous composition regardless of shear rate.

We investigated three cases of clinical device thrombosis in 1) ECMO circuits, 2) a centrifugal pump, and 3) a pediatric VAD. Thrombotic incidence was our endpoint to assess thrombogenicity which provided useful information regarding the thrombotic mechanism.

We used CFD Analysis in the case of the ECMO circuit and centrifugal pump to confirm our mechanistic hypotheses. We were also able to make recommendations for clinical management of thrombosis in these devices.

We simulated device thrombosis *in vitro* and validated our results against our clinical analysis. We were able to form thrombus morphologically and histologically similar to thrombosis in ECMO circuits and a centrifugal pump.

We proposed novel devices to correct for thrombogenic issues in 1) ECMO connectors and 2) vascular grafts. We validated these prototypes to show superiority *in vitro*.

These results are summarized below:

· Use of a perfusion system to evaluate thrombosis on device materials and comparison of

the performance of these materials relative to each other

· Histological analysis of bulk thrombi revealing mixed platelet and fibrinous composition regardless of shear rate

· Analysis of clinical thrombosis in 1) ECMO circuits, 2) the Sorin Revolution centrifugal pump and 3) Berlin Heart EXCOR pediatric VAD on the basis of macroscopic thrombus formation

· CFD analysis of areas of thrombotic germination in ECMO circuits and the Sorin Revolution

· Development of a system for *in vitro* simulation of device thrombosis validated against clinical samples

· Proposal and prototyping of novel devices validated *in vitro*

6.0.2 Contributions

The main contributions of this work are elucidated below.

We have shown shear-dependency of relative thrombogenicity performance of a selection of device materials in a perfusion system. Our results suggest that it is necessary to consider flow regime when examining material thrombogenicity. We have also shown that the adsorption process and bulk thrombosis are separate entities, both requiring substantial lengths of time (!¿24 and !¿6 hours, respectively) to occur from whole blood. These results suggest that shorter assessments of thrombogenicity, and especially thrombosis alone, are insufficient. The histological analysis demonstrated thrombi with mixed composition of platelet-rich and fibrinous sections, which contradicts the idea of two distinct mechanisms of thrombosis producing “red” fibrinous clots or platelet-rich “white” clots.

Our clinical analysis examined current devices with an endpoint of macroscopic thrombosis, which does not currently exist in the field for ECMO circuits, centrifugal pumps, or

Berlin Hearts. The analysis revealed certain thrombogenic areas responsible for the majority of the thrombosis in the device, suggesting that more careful consideration of materials and shear regime interactions could greatly improve device design and thrombogenic outcomes.

We developed *in vitro* perfusion methods to simulate device thrombosis. We successfully mimicked both centrifugal pump and ECMO circuit thrombosis. These methods pave the way for *in vitro* device thrombogenicity assessment and novel device design.

We developed and tested prototypes for two devices by destroying thrombotic mechanisms identified by our studies. The ECMO connector prototype is nonthrombogenic vs. the current device as tested in our *in vitro* perfusion loop. PVA shows promise as a graft material vs. existing synthetics as demonstrated by low levels of bulk thrombus formation in PVA grafts alone.

These contributions are summarized below:

· Demonstration of differences in bulk thrombosis formation of materials across shear regimes

· Recommendations for device design and clinical management from a thrombogenicity ranking

· Discovery of material surfaces overriding classical “red” and “white” clot mechanisms

· Identification of specific thrombogenic areas and elucidation of thrombotic behavior in ECMO circuits, the Sorin Revolution, and the Berlin Heart EXCOR

· Hypothesis and validation of thrombotic mechanisms in ECMO circuits and the Sorin Revolution

· Validated *in vitro* simulation of device thrombosis

· Device design and *in vitro* validation

6.0.3 Limitations

In our studies we have largely ignored the nuances of adsorption and focused primarily on the end result of large-scale thrombus formation. There are many finer details to be explored on the adsorption side of the mechanism, such as surface properties and initial deposition. These can all be tied to bulk thrombosis in our system to produce a clinically and scientifically relevant outcome.

The endpoint of bulk thrombosis also ignores potential downstream effects that could be undesirable in a patient. For example, PVA is known to have high propensity for platelet activation and to cause platelet consumption [28]. The endpoint of bulk thrombosis is therefore not always necessarily consistent with other biocompatibility endpoints, which while potentially problematic, is an interesting inconsistency.

In addition, we always employ the use of heparin, which is clinically relevant, but limits the common pathway of coagulation. We do not test other anticoagulants or antiplatelet agents and do not use untreated blood.

6.0.4 Comparison with Other Systems

Over the decades of material research, other rankings have been proposed and comparison with our results is a useful exercise. In 1969, Mason et al. ranked 58 materials using an *in vitro* assay evaluation based on platelet activation and coagulation activation under stagnant conditions [101]. They divided the materials in the three categories of "good", "intermediate and "poor. Our results have some agreement, as under low shear stainless steel was good and Dacron was worse, but also some disagreement with silicone being in the middle of his ranking. Note that these assays were drawn into silicone-coated glass, which is different from our shear studies at longer time points.

Sanak et al in 2010 looked at 8 materials and compared polymers and metals [102]. The endpoint was platelet adhesion after 5 minutes of 1000 s^{-1} shear rate exposure. Metals were the worst, silicone was the best, and the polymers fell in between. We have good

agreement with these results, as stainless steel was the worst at high shear, and silicone was the second best.

Recently, Hanson wrote a chapter in a biomaterials book discussing general material performance [103]. He stated that overall rankings are not possible, and suggested that device design should be selected for based on mechanical requirements, and that material selection for compatibility should then be taken from previous clinical experience. He states that polymers are typically acceptable for use, metals tend to be thrombogenic, and PTFE is better than Dacron. Our ranking has partial agreement in that bulk thrombosis outcome depends on shear rate provides some insight into the complexity of the problem, and that a single general overarching ranking system without the inclusion of shear would not be meaningful. Other rankings show a dependence of adsorption on shear as well as differences between ranking of surfaces [43, 44]. While we lack information to directly equate or extrapolate from static adsorption studies, there is at least agreement here that surface order rankings vary depending on the assay.

Some adsorption studies have indicated a need for shear consideration [43, 44] and we confirm this need for thrombogenicity evaluation. Our material-dependent macroscale findings after 96 hours of perfusion are extensions of mechanisms occurring at the surface interaction level, and while we lack information describing the transition from surface to macroscale thrombus growth, we observe some parallels. It has been shown that the conformation of adsorbed protein over the concentration influences downstream procoagulant activity, and that the conformation is modified by the surface [12, 22, 23, 24, 34], which is likely a contributing factor to our finding that bulk thrombus formation on materials differs. Shear rate has also been demonstrated to modify initial adsorption and adhesion processes [43, 44], which could account for our finding that shear regime modulates the relative bulk thrombus formation performance of surfaces. Flow has long been included as a contributing factor to thrombogenicity, but has been rarely explored [10, 45]. Here we do not contradict classical surface studies, but highlight the need for the inclusion of

this parameter for applicability to the device setting. Our effects of shear rate on a relatvie bulk thrombus formation on material surfaces highlights the clinical limited applicability of no-flow surfaces studies. Coagulation cascade crosstalk with immune response has also long been reported and is an important consideration for biocompatibility [10, 30, 31, 42]. In addition, the response is modulated by the material surface [36]. Our finding of immune cells uniformly distributed through some samples and differences among surfaces fits with these previous surface findings.

The histology from our studies contradicts classical "red" and "white" thrombus formation at low and high shear rates on biological surfaces [53, 55], and suggests large, propogating effects of the immune response. The large presence of platelets at low shear regimes implies an alternative mechanism of platelet capture, and perhaps one mediated by leukocytes. The intertwining of the coagulation cascade and the complement cascade [10, 26, 27], and the ability of the complement cascade to induce leukocyte activation [104], leads to the possilibilty of the complement as a contributing mechanism to bulk device thrombosis. This also confirms the suggestions of previous authors of the possilibilty of an anti-inflammatory as an inhibitor of device thrombosis.

6.0.5 Future Directions

In Chapter 2, we tested materials across shear rates over the course of 96 hours with an endpoint of bulk thrombus formation. There are many more materials to explore in this setup to further develop a thrombogenicity ranking, both currently in use and on the horizon. Such materials include: polycarbonate, titanium, polyurethanes, and PVA. The histological results of these studies reveal mixed composition of thrombi with both platelet-rich and fibrinous regions. It would be of additional interest to apply anticoagulants, anti-inflammatory agents, and antiplatelet agents to the system to confirm prevention of thrombus formation.

In Chapter 3, we analyzed thrombogenicity of devices currently in use. There are also

many more devices in dire need of thrombogenicity analysis by inspection of macroscopic thrombus formation. Many devices are difficult or impossible to examine during use due to opaque surfaces, masking by blood, or position of the device. However, all devices could benefit from post-processing evaluation if preserved and handled properly. These findings lead us to discovery of thrombotic mechanisms intiated by the device. It would be especially of use to compare other centrifugal pumps that lack a stainless steel bearing to the Sorin Revolution.

In Chapter 4, we developed *in vitro* methods for device thrombosis simulation. The reliability of replication in our loop lends itself nicely to investigation of improvements to existing devices and novel device design, the latter which we begin in Chapter 5. However, there are endless devices to test *in vitro*, both to explore thrombogenic mechanisms as well as to continue to validate our methods.

In Chapter 5, we tested two novel approaches to devices. There is much more work to be done to progress to the point of clinical uses. The connector prototypes will next be made by injection molding with the inclusion of all clinical design constraints and tested in the *in vitro* system. The device will ultimately need to be tested in an *in vivo* setting to demonstrate non-inferiority at a minimum. The PVA will also need an *in vivo* validation.

REFERENCES

[1] I. H. Jaffer, J. Hirsh, and J. I. Weitx, "Medical device-induced thrombosis: What causes it and how can we prevent it?" *Journal of Thrombosis and Haemostasis*, vol. 13, no. 71, S72–S81, 2015.

[2] S. Susen, A. Rauch, E. Van Belle, A. Vincentelli, and P. J. Lenting, "Circulatory support devices: Fundamental aspects and clinical management of bleeding and thrombosis," *Journal of Thrombosis and Haemostasis*, vol. 13, no. 10, pp. 1757–1767, 2015.

[3] D. Basmadjian, M. V. Sefton, and S. A. Baldwin, "Coagulation biomaterials in flowing blood: Some theoretical considerations," *Biomaterials*, vol. 18, no. 23, pp. 1511–1522, 1997.

[4] C. Sperling, M. Fischer, M. F. Maitz, and C. Werner, "Blood coagulation on biomaterials requires the combination of distinct activation processes," *Biomaterials*, vol. 30, no. 27, pp. 4447 –4456, 2009.

[5] S. R. Schmidt, H. Waldeck, and W. J. Kao, *Protein adsopriton to biomaterials in d. a. puleo and r. bizios (eds.), biological interactions on surface materials: Understanding and controlling protein, cell, and tissue responses*. New York City: Springer, 2009.

[6] W. G. Pitt, K. Park, and S. L. Cooper, "Sequential protein adsorption and thrombus deposition on polymeric biomaterials," *Journal of Colloid and Interface Science*, vol. 111, no. 2, pp. 343 –362, 1986.

[7] S. Forti, L. Lunelli, C. D. Volpe, S. Siboni, L. Pasquardini, A. Lui, R. Canteri, L. Vanzetti, C. Potrich, M. Vinante, C. Pederzolli, and M. Anderle, "Hemocompatibility of pyrolytic carbon in comparison with other biomaterials," *Diamond and Related Materials*, vol. 20, no. 56, pp. 762 –769, 2011.

[8] K. Ekdahl, J. Lambris, H Elwing, D Ricklin, P. Nilsson, Y Teramura, I. Nicholls, and B Nilsson, "Innate immunity activation on biomaterial surfaces: A mechanistic model and coping strategies," *Advanced Drug Delivery Review*, vol. 63, pp. 1042–1050, 2011.

[9] E. Vogler and C. Siedlecki, "Contact activation of blood plasma coagulation," *Biomaterials*, vol. 30, pp. 1857–1869, 2009.

[10] M. Gorbet and M. Sefton, "Contact activation of blood plasma coagulation," *Biomaterials*, vol. 25, pp. 5681–5703, 2004.

[11] D Basmadijan, M. Sefton, and S. Baldwin, "Direct observation of von willebrand factor elongation and fiber formation on collagen during acute whole blood exposure to pathological flow," *Biomaterials*, vol. 18, pp. 1511–1522, 1997.

[12] P Thevenot, W Hu, and L Tang, "Surface chemistry influence implant biocompantibility," *Current Topics in Medicinal Chemistry*, vol. 8, no. 4, pp. 270–280, 2008.

[13] J. Anderson, T. Bonefield, and N. Ziats, "Protein adsorption and cellular adhesion and activation on biomedical polymers," *International Journal of Artificial Organs*, vol. 13, pp. 375–382, 1990.

[14] N Nath, J Hyun, H Ma, and A Chilkoti, "Surface engineering strategies for control of protein and cell interactions," *Surface Science*, vol. 570, pp. 98–110, 2004.

[15] M Shen, I Garcia, R. Maier, and T. Horbett, "Effects of adsorbed protein and surface chemistry on foreign body giant cell formation, tumor necrosis factor alpha release, and pro-coagulant activity of monocytes," *Journal of Biomedical Material Research*, vol. 70A, pp. 533–541, 2004.

[16] J. Grunkemeier, W. Tsai, and T. Horbett, "Co-adsorbed fibrinogen and von willebrand factor augment platelet procoagulant activity and spreading," *Journal of Biomaterials Science, Polymer Edition*, vol. 12, pp. 1–20, 2001.

[17] T. Lenk, T. Horbett, B. Ratner, and K. Chittur, "Infrared spectroscopic studies of time-dependent changes in fibrinogen adsorbed to polyurethanes," *Langmuir*, vol. 7, pp. 1755–1764, 1991.

[18] W. Hu, J. Eaton, and L Tang, "Molecular basis of biomaterial-mediated foreign body reactions," *Blood*, vol. 98, pp. 1231–1238, 2001.

[19] K. Evans-Nguyen, R. Fuierer, B. Fitchett, L. Tolles, J. Conboy, and M. Schoenfisch, "Changes in adsorbed fibrinogen upon conversion to fibrin," *Langmuir*, vol. 22, pp. 5115–5121, 2006.

[20] J. Andrade, V. Hlady, and R. Van Wagenen, "Effects of plasma protein adsorption on protein conformation and activity," *Pure Appl Chem*, vol. 56, pp. 1345–1350, 1984.

[21] M Dadsetan, J. Jones, A Hiltner, and J. Anderson, "Surface chemistry mediates adhesive structure, cytoskeletal organization, and fusion of macrophages," *Journal of Biomedical Material Research*, vol. 71A, pp. 439–448, 2004.

[22] L Tang and W Hu, "Molecular determinants of biocompatibility," *Expert Review of Medical Devices*, vol. 2, pp. 493–500, 2005.

[23] C. Wilson, R. Clegg, D. Leavesley, and M. Pearcy, "Mediation of biomaterial-cell interactions by adsorbed protein: A review," *Tissue Engineering*, vol. 11, pp. 1–18, 2005.

[24] T. Horbett and K. Lew, "Residence timne effects on monoclonal antibody binding to adsorbed fibrinogen," *Journal of Biomaterials Science Polymer Edition*, vol. 6, pp. 15–33, 1994.

[25] M Misoph, S Schwender, and J Babin-Ebell, "Response of the cellular immune system to cardiopulmonary bypass is independent of the applied pump tube and the use of heparin-coated surfaces," *Thoracic Cardiovascular Surgery*, vol. 46, pp. 222–227, 1998.

[26] M. Blajchman and A. Ozge-Anwar, "The role of the complement system hemostasis," *Progressive Hematology*, vol. 14, pp. 149–182, 1986.

[27] R. Johnson, "Complement activation during extracorporeal therapy: Biochemistry, cell biology and clinical relevance," *Nephrology Dialysis Transplantation*, vol. 9, pp. 36–45, 1994.

[28] C. Gemmel, "Flow cytometric evaluation of material-induced platelet and complement activation," *Journal of Biomaterials Science, Polymer Edition*, vol. 11, pp. 1197–1210, 2000.

[29] A. Engberg, P. Nilsson, S Huang, K Fromell, O. Hamad, T. Mollnes, J. Rosengren-Holmberg, K Sandholm, Y Teramura, I. Nicholls, B Nilsson, and K Ekdahl, "Prediction of inflammatory reponses induced by biomaterialsin contact with human blood using protein fingerprint from plasma," *Biomaterials*, vol. 36, pp. 55–65, 2015.

[30] J Wettero, P Tengvall, and T Bengtsson, "Platelets stimulated by igg-coated surfaces bind and activate neutrophils through a selectin-dependent pathway," *Biomaterials*, vol. 24, pp. 1559–1573, 2003.

[31] M. Gorbet and M. Sefton, "Material-induced tissue factor expression but not cd11b upregulation depends on the presence of platelets," *Journal of Biomedical Materials Research*, vol. 67A, pp. 792–800, 2003.

[32] J. Grunkemeier, W. Tsai, M. Alexander, D. Caster, and T. Horbett, "Platelet adhesion and procoagulant activity induced by contact with radiofrequency glow discharge roles of adsorbed fibrinogen and vwf," *Journal of Biomedical Materials Research*, vol. 51, pp. 669–679, 2000.

[33] W. Tsai, J. Grunkemeier, C. McFarland, and T. Horbett, "Platelet adhesion and procoagulant activity induced by contact with radiofrequency glow discharge roles of adsorbed fibrinogen and vwf," *Journal of Biomedical Materials Research*, vol. 60, pp. 348–359, 2002.

[34] W. Tsai, J. Grunkemeier, and T. Horbett, "Variations in the ability of adsorbed fibrinogen to mediate platelet adhesion to polystyrene-bases materials: A multivariate statistical analysis of antibody binding to the platelet binding sites of fibrinogen," *Journal of Biomedical Materials Research*, vol. 67A, pp. 1255–1268, 2003.

[35] M Shen and T. Horbett, "The effects of surface chemistry and adsorbed proteins on monocyte/macrophage adhesion to chemically modified polystyrene surfaces," *Journal of Biomedical Materials Research*, vol. 5, pp. 336–345, 2001.

[36] M Shen, I Garcia, R. Maier, and T. Horbett, "Effects of adsorbed proteins and surface chemistry on foreign body giant cell formation, tumor necrosis factor alpha release and procoagulant activity of monocytes," *Journal of Biomedical Materials Research*, vol. 70A, pp. 533–541, 2004.

[37] M. Gorbet and M. Sefton, "Leukocyte activation and leukocyte procoagulant activities after blood contact with polystyrene and polyethylene glycol-immobilized polystyrene beads," *Journal of Laboratory and Clinical Medicine*, vol. 137, pp. 345–355, 2001.

[38] M. Sefton, C. Gemmel, and G. MB, "What really is blood compatibility?" *Journal of Biomaterials Science, Polymer Edition*, vol. 11, pp. 1165–1182, 2000.

[39] M. Sefton, A Sawyer, M Gorbet, J. Black, E Cheng, C Gemmell, and E Pottinger-Cooper, "Does surface chemistry affect thrombogenicity of surface modified polymers?" *Journal of Biomedical Materials Research*, vol. 55, pp. 447–459, 2001.

[40] A. Engberg, J. Rosengren-Holmberg, H Chen, B Nilsson, J. Lambris, I. Nicholls, and K. Ekdahl, "Blood protein-polymer adsorption: Implications for understanding complement-mediated hemoincompatibility," *Journal of Biomedical Materials Research Part A*, vol. 97, pp. 74–84, 2011.

[41] S Huang, A. Engberg, N Jonsson, K Sandholm, I. Nicholls, T. Mollnes, K Fromell, B Nilsson, and K. Ekdahl, "Reciprocal relationship[p between contact and complement system activation on artificial polymers exposed to whole human blood," *Biomaterials*, vol. 77, pp. 111–119, 2016.

[42] C Speth, G Rambach, R Wurzner, C Lass-Florl, H Kozarcanin, O. Hamad, B Nilsson, and K. Ekdahl, "Reciprocal relationship[p between contact and complement system activation on artificial polymers exposed to whole human blood," *Molecular Immunology*, vol. 67, pp. 108–118, 2015.

[43] M Otto, A Franzen, T Hansen, and C. Kirkpatrick, "Modification of human platelet adhesion on biomaterial surfaces by protein preadsorption under static and flow conditions," *Journal of Materials Science: Materials in Medicine*, vol. 15, pp. 35–42, 2004.

[44] V Balasubramanian and S. Slack, "The effect of fluid shear and co-adsorbed proteins on the stability of immobilized fibrinogen and subsequent platelet interactions," *Journals of Biomaterials Science, Polymer Edition*, vol. 16, pp. 543–561, 2002.

[45] B. Ratner, "Blood compatibility a perspective," *Journals of Biomaterials Science, Polymer Edition*, vol. 11, pp. 1107–1119, 2000.

[46] H. Al-Khaffaf and D. Charlesworth, "Albumin-coated vascular prostheses: A five-year follow-up," *Journal of Vascular Surgery*, vol. 23, pp. 686–690, 1996.

[47] Y. Marois, N. Chakf, R. Guidoin, R. C. Duhamel, R. Roy, M. Marois, M. W. King, and Y. Douville, "An albumin-coated polyester arterial graft: In vivo assessment of biocompatibility and healing characteristics," *Biomaterials*, vol. 17, no. 1, pp. 3 –14, 1996.

[48] Y.-H. Kim, C. W. Lee, M.-K. Hong, S.-W. Park, S.-J. Tahk, J.-Y. Yang, S. Saito, T. Santoso, L. Quan, J. Ge, N. J. Weissman, A. J. Lansky, G. S. Mintz, and S.-J. Park, "Randomized comparison of carbon ionimplanted stent versus bare metal stent in coronary artery disease: The asian pacific multicenter arthos stent study (pass) trial," *American Heart Journal*, vol. 149, no. 2, pp. 336 –341, 2005.

[49] P. B. Sick, O. Brosteanu, M. Ulrich, H. Thiele, J. Niebauer, I. Busch, and G. Schuler, "Prospective randomized comparison of early and late results of a carbonized stent versus a high-grade stainless steel stent of identical design: The prevention of recurrent venous thromboembolism (prevent) trial," *American Heart Journal*, vol. 149, no. 4, pp. 681 –688, 2005.

[50] P. B. Sick, G. Gotz, U. Kalnins, A. Erglis, R. Bonan, W. Aengevaeren, D. Elsner, B. Lauer, M. Woinke, O. Brosteanu, and G. Schuler, "Comparison of early and late results of a carbofilm-coated stent versus a pure high-grade stainless steel stent (the carbostent-trial)," *The American Journal of Cardiology*, vol. 93, no. 11, pp. 1351–1356, 2004.

[51] A. L. Lewis, L. A. Tolhurst, and P. W. Stratford, "Analysis of a phosphorylcholine-based polymer coating on a coronary stent pre- and post-implantation," *Biomaterials*, vol. 23, pp. 1697–1706, 2002.

[52] M. Calli, A. Bartorelli, F. Bedogni, N. DeCesare, S. Klugmann, K. Maiello, F. Miccoli, T. Moccetti, M. Onofri, V. Paolillo, R. Pirisi, P. Presbitero, P. Sganzerla,

M. Viecca, S. Zerboni, and G. Lanteri, "Italian biodivysio open registry biodivysio pc-coated stent): Study of clinical outcomes of the implant of a pc-coated coronary stent," *Journal of Invasive Cardiology*, vol. 12, pp. 452–450, 2000.

[53] A. Para, D. Bark, A. Lin, and D. Ku, "Rapid platelet accumulation leading to thrombotic occlusion," *Annals of Biomedical Engineering*, vol. 39, no. 7, pp. 1961–1971, 2011.

[54] Y Ikeda, M Handa, K Kawano, T Kamata, M Murata, Y Araki, H Anbo, Y Kawai, K Watanabe, and I Itagaki, "The role of von willebrand factor and fibrinogen in platelet aggregation under varying shear stress.," *The Journal of Clinical Investigation*, vol. 87, no. 4, pp. 1234–1240, 1991.

[55] Y. Cadroy, T. A. Horbett, and S. R. Hanson, "Discrimination between platelet-mediated and coagulation-mediated mechanisms in a model of complex thrombus formation in vivo," *Journal of Laboratory and Clinical Medicine*, vol. 113, no. 4, pp. 436–438, 1989.

[56] S. J. E., "Biochemistry and genetics of von willebrand factor," *Annual Review of Biochemistry*, vol. 67, pp. 395–424, 1998.

[57] S. W. Schneider, S. Nuschele, A. Wixforth, C. Gorzelanny, A. Alexander-Katz, R. R. Netz, and M. F. Schneider, "Shear-induced unfolding triggers adhesion of von willebrand factor fibers," *Proceedings of the National Academy of Sciences*, vol. 104, no. 19, pp. 7899–7903, 2007.

[58] P. J. Wellings and D. N. Ku, "Mechanisms of platelet capture under very high shear," *Cardiovascular Engineering and Technology*, vol. 3, no. 2, pp. 161–170, 2012.

[59] T. Colace and S. Diamond, "Direct observation of von willebrand factor elongation and fiber formation on collagen during acute whole blood exposure to pathological flow," *Arteriosclerosis and Thrombosis Vascular Biology*, vol. 33, pp. 105–113, 2013.

[60] W. R. Wagner and J. A. Hubbell, "Local thrombin synthesis and fibrin formation in an in vitro thrombosis model result in platelet recruitment and thrombus stabilization on collagen in heparinized blood," *Journal of laboratory and clinical medicine*, vol. 116, no. 5, pp. 636–50, 1990.

[61] H. J. A. and M. L. V., "Technique for visualization and analysis of mural thrombogenesis," *Review of Scientific Instruments*, vol. 57, pp. 892–897, 1986.

[62] M. J. Eppihimer, N. Sushkova, J. L. Grimbsby, N. Efimova, W. Kair, S. LArson, B. Forsyth, B. A. Huibregtse, K. D. Dawkins, G. J. Wilson, and J. F. Granada, "Impact

of stent surface on thrombogenicity and vascular healing: A comparative analysis of metallic and polymeric surfaces," *Circulation: Cardiovascular Interventions*, vol. 6, pp. 370–377, 2013.

[63] K. Kolandaivelu, R. Swaminathan, W. J. Gibson, V. B. Kolachalama, K. Nguyen-Ehrenreich, V. L. Giddings, L. Coleman, G. K. Wong, and E. R. Edelman, "Stent thrombogenicity early in high-risk interventional settings is driven by stent design and deployment and protected by polymer-drug coatings," *Circulation*, vol. 123, no. 13, pp. 1400–1409, 2011.

[64] S. Krajewski, B. Neumann, J. Kurz, N. Perle, M. Avci-Adali, G. Cattaneo, and H. Wendel, "Preclinical evaluation of the thrombogenicity and endothelialization of bare metal and surface-coated neurovascular stents," *American Journal of Neuroradiology*, vol. 36, no. 1, pp. 133–139, 2015. eprint: `http://www.ajnr.org/content/36/1/133.full.pdf+html`.

[65] K. Grove, S. Deline, S. Schatz T. aznd Howard, D. Porter, and M. Smith, "Thrombogenicity testing of medical devices in a minimally heparinized ovine blood-loop," *Journal of Medical Devices*, vol. 10, pp. 1–18, 2017.

[66] L. Zydney, "Cross-flow membrane plasmapheresis; an analysis of flux and hemolysis," PhD thesis, Massachusetts Instituite of Technology, 1985.

[67] H. C. Han, S. Marita, and D. N. Ku, "Changes of opening angle in hypertensive and hypotensive arteries in 3-day organ culture," *Journal of Biomechanics*, vol. 39, pp. 2410–2418, 2005.

[68] T. Thiagarajan, R. Barbaro, P. Rycus, D. McMullan, S. Conrad, J. Fortenberry, and M. Paden, "Extracorporeal life support organization registry international report 2016," *American Society for Artificial Internal Organs*, vol. 63, 2017.

[69] M. L. Paden, S. A. Conrad, P. T. Rycus, R. R. Thiagarajan, and E. Registry, "Extracorporeal life suuport organization registry report 2012," *Journal of the American Society of Artificial Internal Organs*, vol. 59, pp. 202–210, 2013.

[70] K. C. Carstairs, "The identification of platelets and platelet antigens in histological sections," *Journal of Pathology and Bacteriology*, vol. 90, pp. 225–231, 1965.

[71] H. J. Weiss, V. T. Turitto, and H. R. Baumgartner, "Role of shear rate and platelets in promoting fibrin formation on rabbit subendothelium. studies utilizing patients with quantitative and qualitative platelet defects," *Journal of Clinical Investigation*, vol. 78, pp. 1072–1078, 1986.

[72] R. D. Guy, A. K. Fogelson, and J. P. Keener, "Fibrin gel formation in a shear flow," *Mathematical Medicine and Biology*, vol. 24, pp. 111–130, 2007.

[73] B. Urlesberger, G. Zobel, W. Zenz, M. Kuttnig-Haim, U. Maurer, F. Reiterer, M. Riccabona, D. Dacar, S. Gallistl, B. Leschnik, and W. Muntean, "Activation of the clotting system during extracorporeal membrane oxygenation in term newborn infants," *The Journal of Pediatrics*, vol. 129, pp. 264–268, 2001.

[74] P. Arnold, S. Jackson, J. Wallis, J. Smith, D. Bolton, and S. Haynes, "Coagulation factor activity during neonatal extra-corporeal membrane oxygenation," *Intensive Care Medicine*, vol. 27, pp. 1395–1400, 2001.

[75] K. Lehle, A. Philipp, O. Gleich, A. Holzamer, T. Muler, T. Bein, and C. Schmid, "Efficiency in extracorporeal membrane oxygenation-cellular deposits on polymethylpentene membranes increase resistance to blood flow and reduce gas exchange capacity," *Journal of the American Society of Artificial Internal Organs*, vol. 54, pp. 612–617, 2008.

[76] M. B. Gorbet and M. V. Sefton, "Biomaterial-associated thrombosis: Roles of coagulation factors, complement, platelets and leukocytes," *Biomaterials*, vol. 25, pp. 5681–5703, 2004.

[77] J. Hirsh, S. S. Anand, J. L. Halperin, and V. Fuster, "Mechanism of action and pharmacology of unfractionated heparin," *Arteriosclerosis, Thrombosis, and Vascular Biology*, vol. 21, pp. 1094–1096, 2001.

[78] C. Dornia, A. Philipp, S. Bauer, M. Lubnow, T. Muller, K. Lehle, C. Schmid, R. Muller-Wille, P. Wiggermann, C. Stroszczynski, and A. G. Schreyer, "Analysis of thrombotic deposits in extracorporeal membrane oxygenators by multidetector computer tomography," *Journal of the American Society of Artificial Internal Organs*, vol. 60, pp. 652–656, 2014.

[79] L. B. Leverett, J. D. Hellums, C. Alfrey, and E. C. Lynch, "Red blood cell damage by shear stress," *Biophysical Journal*, vol. 12, pp. 257–273, 2011.

[80] S. Hastings, D. Ku, S Wagoner, K. Maher, and S Deshpande, "Sources of circuit thromobsis in pediatric extracorporeal membrane oxygenation," *American Society for Artificial Internal Organs*, vol. 63, pp. 86–92, 2017.

[81] N. M. Haines, P. T. Rycus, J. Zwischenberger, R. H. Bartlett, and A. Undar, "Extracorporeal life support registry report 2008: Neonatal and pediatric cardiac cases," *Journal of the American Society of Artificial Internal Organs*, vol. 55, pp. 111–116, 2009.

[82] I. Halaweish, A. Cole, E. Cooley, W. R. Lynch, and J. W. Haft, "Roller and centrifugal pumps: A retrospective comparison of bleeding complications in extracorporeal membrane oxygenation," *Journal of the American Society of Artificial Internal Organs*, vol. 61, pp. 496–501, 2015.

[83] S. Lawon, C. Ellis, K. Butler, C. McRobb, and B. Mejak, "Neonatal extracorporeal membrane oxygenation devices, techniques and team roles: 2011 survey results of the united states' extracorporeal life support organization centers," *The Journal of ExtraCorporeal Technology*, vol. 43, pp. 236–244, 2011.

[84] J. Byrnes, W. McKamie, C. Swearingen, P. Prodhan, A. Bhutta, R. Jaquiss, M. Imamura, and R. Fiser, "Hemolysis during cardiac extracorporeal membrane oxygenation: A case-control comparison of roller pumps and centrifugal pumps in a pediatric population," *Journal of the American Society of Artificial Internal Organs*, vol. 57, pp. 456–61, 2011.

[85] L. Lequier, S. B. Horton, D. M. McMullan, and R. H. Bartlett, "Extracorporeal membrane oxygenation circuitry," *Pediatric Critical Care Medicine*, vol. 14, S7–S12, 2013.

[86] S. Bottrell, M. Bennett, S. Augustin, C. Thuys, B. Schultz, A. Horton, and S. Horton, "A comparison study of haemolysis production in three contemporary centrifugal pumps," *Perfusion*, vol. 29, pp. 411–416, 2014.

[87] A. P. Thiara, T. N. Hoel, F. Kristiansen, M. H. Karlsen, A. E. Fiane, and J. L. Svennevig, "Evaluation of oxygenators and centrifugal pumps for long-term pediatric extracorporeal membrane oxygenation," *Perfusion*, vol. 22, pp. 323–326, 2007.

[88] V. Tchantchaleishvili, F. Sagebin, R. E. Ross, W. Hallinan, K. Q. Schwarz, and H. T. Massey, "Evaluation and treatment of pump thrombosis and hemolysis," *Annals of Cardiothoracic Surgery*, vol. 3, pp. 490–495, 2014.

[89] B. R. Alevriadou, J. L. Moake, N. A. Turner, Z. M. Ruggeri, B. J. Folie, M. D. Phillips, A. B. Schreiber, M. E. Hrinda, and L. V. McIntire, "Real-time analysis of shear-dependent thrombus formation and its blockade by inhibitors of von willebrand factor binding to platelets," *Blood*, vol. 81, no. 5, pp. 1263–1276, 1993.

[90] L. Badimon and J. J. Badimon, "Mechanisms of arterial thrombosis in nonparallel streamlines: Platelet thrombi grow on the apex of stenotic severely injured vessel wall. experimental study in the pig model," *Journal of Clinical Investigation*, vol. 84, pp. 1134–1144, 1989.

[91] R. Barstad, P Kierulf, and K. Sakariassen, "Collagen induced thrombus formation at the apex of eccentric stenoses–a time course study with non-anticoagulated human blood," *Thrombosis and haemostasis*, vol. 75, no. 4, pp. 685–692, 1996.

[92] S. Hastings, S. Deshpande, S Wagoner, K. Maher, and D. Ku, "Sources of circuit thromobsis in pediatric extracorporeal membrane oxygenation," *International Journal of Artificial Organs*, vol. 39, pp. 200–204, 2016.

[93] C. Almond, D. Morales, E. Blackstone, M. Turrentine, M Imamura, M. Massicotte, L. Jordan, E. Devaney, C Ravishankar, K. Kanter, W Holman, R Kroslowitz, C Tjossem, L Thuita, G. Cohen, H Buchholz, J. St. Louis, K Nguyen, R. Niebler, H. Walters, B Reemtsen, P. Wearden, O Reinhartz, K. Guleserian, M. Mitchell, M. Bleiweis, C. Canter, and T Humpl, "Berlin heart excor pediatric ventricular assist device for bridge to heart transplantation in us children," *Circulation*, vol. 127, pp. 1702–1711, 2013.

[94] D Mah, T. Singh, R. Thiagarajan, K Gauvreau, G. Piercey, E. Blume, F Fynn-Thompson, and C. Almond, "Incidence and risk factors for mortality in infants awainting heart transplantation in the usa," *Journal of Heart and Lung Transplantation*, vol. 28, pp. 1292–1298, 2009.

[95] D. Morales, F Zafar, J. Rossano, J. Salazar, J. Jefferies, D. Graves, J. Heinle, and C. Fraser, "Use of ventricular assist devices in children across the united states: Analysis of 7.5 million pediatric hospitalizations," *Annals of Thoracic Surgery*, vol. 90, pp. 1313–1318, 2010.

[96] Y Fan, Y. Weng, M Huebler, J Cowger, D Morales, N Franz, Y. Xiao, E Potapov, and R Hetzer, "Predictors of in-hospital mortality in children after long-term ventricular assist device insertion," *Journal of the American College of Cardiology*, vol. 58, pp. 1183–1190, 2011.

[97] G. Zelenock, T. Huber, L. Messina, A. Lumsden, and G. Moneta, *Mastery of vascular and endovascular surgery*. Philadelphia: Lippincott Williams & Wilkins, 2005.

[98] S Roll, J Muller-Nordohrn, T Keil, H Scholz, D Eidt, W Greiner, and S. Willich, "Dacron vs. ptfe as bypass materials in peripheral vascular surgery - systematic review and meta-analysis," *BMC Surgery*, vol. 8, pp. 1–8, 2008.

[99] W. Burkel, "The challenge of small diameter vascular grafts," *Medical Progress Through Technology*, vol. 14, pp. 165–175, 1988.

[100] C. Sharma and M Szycher, *Blooc compatible materials and devices: Perspectives towards the 21st century*. Boca Raton: CRC Press, 1990.

[101] R. Mason, D. Scarborough, S. Saba, K. Brinkhous, L. Ikenberry, J. Kearney, and H. Clark, "Thrombogenicity of some biomedical materials: Platelet-interface reactions," *Journal of Biomedical Materials Research Part A*, vol. 3, pp. 615–644, 1969.

[102] M Sanak, B Jakiela, and W Wegrzyn, "Assessment of hemocompatibility of materials with arterial blood flow by platelet functional tests," *Bulletin of the Polish Academy of Sciences, Technical Sciences*, vol. 58, pp. 317–322, 2010.

[103] H. SR, *Blood-material interactions*. Berlin: Springer, 2013.

[104] S Schmidt, G Haase, E Csomor, R Lutticken, and H Peltroche-Llacsahuanga, "Inhibitor of complement, compstain, prevents polymer-mediated mac-1 up-regulation of human neutrophils independent of biomaterial type tested," *Journal of Biomedical Materials Research*, vol. 66A, pp. 491–499, 2003.